

ORGANIC CHEMISTRY

General method for iron-catalyzed multicomponent radical cascades–cross-couplings

Lei Liu^{1†}, Maria Camila Aguilera^{2†}, Wes Lee¹, Cassandra R. Youshaw¹, Michael L. Neidig^{2*}, Osvaldo Gutierrez^{1,3*}

Transition metal-catalyzed cross-coupling reactions are some of the most widely used methods in chemical synthesis. However, despite notable advantages of iron (Fe) as a potentially cheaper, more abundant, and less toxic transition metal catalyst, its practical application in multicomponent cross-couplings remains largely unsuccessful. We demonstrate 1,2-bis(dicyclohexylphosphino)ethane Fe-catalyzed coupling of α -boryl radicals (generated from selective radical addition to vinyl boronates) with Grignard reagents. Then, we extended the scope of these radical cascades by developing a general and broadly applicable Fe-catalyzed multicomponent annulation–cross-coupling protocol that engages a wide range of π -systems and permits the practical synthesis of cyclic fluorinated compounds. Mechanistic studies are consistent with a bisarylated Fe(II) species being responsible for alkyl radical generation to initiate catalysis, while carbon-carbon bond formation proceeds between a monoarylated Fe(II) center and a transient alkyl radical.

Organoboron compounds are valuable and highly versatile reagents widely used in modern organic synthesis (1). In particular, the use of organoboron reagents in palladium-catalyzed Suzuki–Miyaura couplings is one of the top five most used reactions in drug discovery (2). Photoredox catalysis has further expanded the utility of alkyl organoboron compounds as versatile radical precursors for numerous transformations (3). More recently, vinyl organoboron reagents have been used as effective lynchpins in three-component nickel- and metallaphotoredox-catalyzed cross-coupling reactions, leading to alkyl boryl scaffolds primed for further functionalization (4–9). Despite these efforts, the equivalent iron (Fe)-catalyzed transformation remains highly desirable in pharmaceutical research because of Fe's low cost, abundance, and potential for distinct and complementary modes of reactivity.

Fe-catalyzed cross-couplings have enabled the union of diverse carbon (C)-centered radicals and organometallic partners (Fig. 1A). However, although organoboron reagents have found utility in Fe-catalyzed two-component cross-couplings (Suzuki–Miyaura), application in multicomponent cross-couplings remains an elusive transformation (Fig. 1B) (10–15). Here, we report the successful realization of Fe-catalyzed cross-coupling of α -boryl radicals (generated from selective radical addition to vinyl boronates) with Grignard reagents to form dicarbofunctionalized compounds (Fig. 1C). Furthermore, to address a long-standing

challenge in multicomponent cross-couplings, we report a general Fe-catalyzed multicomponent annulation–cross-coupling (MAC) protocol that facilitates the practical synthesis of tetrafluoroethylene-containing carbocycles and derivatives, which were previously difficult to make (16). Last, spectroscopy experiments [in situ Mössbauer, electron paramagnetic resonance (EPR), and x-ray crystallography], density functional theory (DFT), and radical probes shed light on the mechanism of this transformation.

Development of a three-component coupling reaction

On the basis of our recently reported studies on Fe-catalyzed radical cross-couplings (17–21), we hypothesized that the electron-deficient nature of vinyl boronates and the rapid kinetics observed in the Fe-catalyzed Kumada cross-couplings could be coupled to engage transient α -boryl radicals in selective three-component radical cross-couplings (22–24). In this vein, we first tested the proposed three-component radical cross-coupling using a sterically hindered alkyl halide under the slow addition of aryl Grignard nucleophile to avoid competing two-component cross-coupling and biaryl formation. After extensive experimentation, we identified FeCl₃ (10 mol %) in combination with 1,2-bis(dicyclohexylphosphino)ethane **L1** (20 mol %) as an effective catalytic system that engages α -boryl radicals, presumably through regioselective Giese addition of *tert*-butyl radical to vinyl boronate **2a**, to form the desired product **4a** in 90% yield (tables S1 and S2). In contrast to existing nickel systems, the reaction proceeded in <1 hour at low temperatures. Precatalysts with weakly coordinating triflate or acetate groups diminished the efficiency of the system, whereas halides or acetylacetonate counterions had minor effect on

the yields (table S2, entries 1 to 6). Furthermore, 1,2-bis(dicyclohexylphosphino)ethane **L1** was a distinctly effective ligand (table S2, entries 7 to 13). Control experiments demonstrated that both the ligand and Fe salt are crucial for the reaction to proceed (table S2, entries 17 to 19). Both alkyl iodides and bromides provided the desired product under these conditions (~90% yield), although diminished yields were observed with alkyl chlorides (table S2, entries 20 and 21).

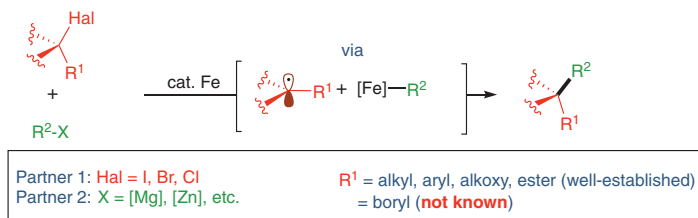
Encouraged by these findings, we turned our attention to studying the generality of the three-component radical cascade transformation. As shown in Fig. 2, we observed a wide range of organomagnesium compounds to be suitable cross-coupling partners with alkyl α -boryl radicals. In particular, difunctionalization of vinyl boronates proceeded with good yields and excellent regioselectivity with mono- and disubstituted aryl Grignard nucleophiles that varied in electron density at the para- and meta positions (**4a** to **4q**) as well as (hetero)aryl nucleophiles (**4r**). Furthermore, in contrast to nickel and metallaphotoredox catalytic systems, this protocol is compatible with alkenyl and alkynyl nucleophiles, albeit with lower yields observed for the latter (**4s** to **4w**). However, ortho-substituted aryl Grignard reagents were less efficient, presumably because of increased steric demand (**4y**). Having established the reactivity with sp- and sp²-hybridized Grignard nucleophiles, we next probed the alkyl halide scope (Fig. 2, bottom). A range of tertiary acyclic and cyclic aliphatic electrophiles afforded the desired products with good yields (**4a'** to **4f'**). Secondary alkyl halides (**4g'**) and tertiary alkyl halides bearing aryl or heteroatom substituents also formed the desired products (**4f'** and **4h'**). Last, we identified tertiary α -bromo esters as competent substrates, leading to **4i'** bearing both an ester and alkyl boron as versatile synthetic handles for further diversification. Despite substantial advances in the synthesis of organofluorinated compounds (25), selective and catalytic C(sp³)-CF₂R bond formation remains challenging (26) and is exceedingly rare in Fe-catalyzed cross-couplings (27–31). Seeking to expand the alkyl radical scope, we investigated whether this protocol could provide direct access to versatile fluorinated alkyl boron compounds. As shown in Fig. 2, bottom, a wide range of fluoroalkyl radical precursors—including those containing alkyl, ester, silyl, heteroaryl, phenoxy, perfluoroalkyl, and protected aldehydes—proved compatible partners, which led to the desired 1,2-alkylfluorinated-aryl organoboron products (**4j'** to **4p'**) in good to excellent yield. The distinctive properties of C–F bonds (32–35), versatility of the alkyl boron bond, and practicality of this method are anticipated to provide rapid access to valuable fluoroalkyl boron building blocks for synthetic applications.

¹Department of Chemistry and Biochemistry, University of Maryland, College Park, MD 20742, USA. ²Department of Chemistry, University of Rochester, Rochester, NY 14627, USA. ³Department of Chemistry, Texas A&M University, College Station, TX 77843, USA.

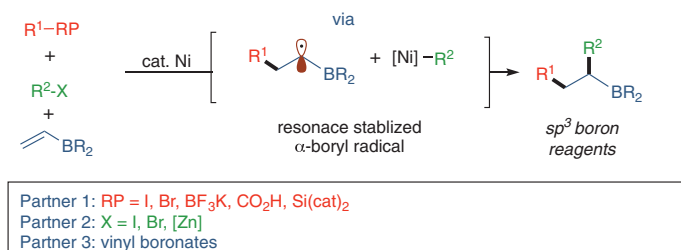
*Corresponding author. Email: og.labs@tamu.edu (O.G.); michael.neidig@rochester.edu (M.L.N.)

†These authors contributed equally to this work.

A Fe-catalyzed cross-coupling of C-center radicals



B Strategies for multicomponent transition metal-catalyzed cross-coupling of α -boryl radicals



C Fe-catalyzed multicomponent radical cascade-cross-couplings (this work)

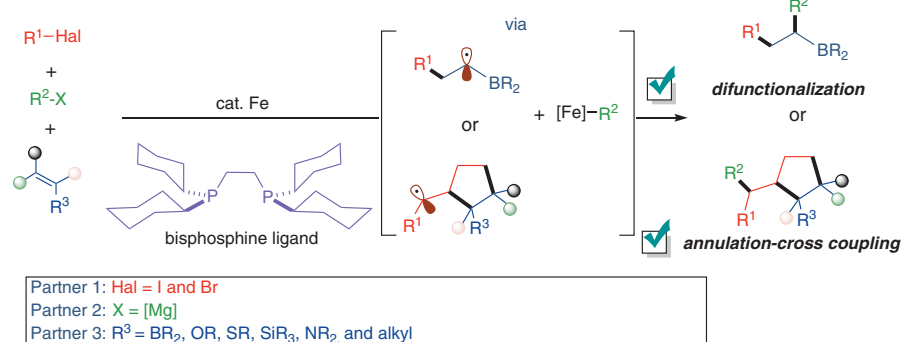


Fig. 1. Metal-catalyzed cross-coupling of α -boryl radicals. (A) Established methods for Fe-catalyzed C–C cross-coupling with alkyl radicals. (B) Current strategies for three-component trapping of α -boryl radicals. (C) Our report on the use of bisphosphine-iron complexes to promote radical cascade-cross-coupling reactions.

Extension to MACs

With the aim of expanding the applications of multicomponent radical cross-couplings, we turned our attention to alkyl halides with pendant alkenes as bifunctional coupling partners (36). Despite the utility of radical-based cyclization cascades and transition metal-catalyzed intramolecular cyclization-arylation in organic synthesis (37), the analogous intermolecular three-component radical cycloaddition-arylations have proven unexpectedly elusive. Furthermore, although incorporating CF₃, C₂F₅, and perfluoroalkyl alkyl groups in pharmaceutical research is common, practical and general synthetic methods for incorporation of the tetrafluoroethylene (-CF₂-CF₂-) moiety into cyclic compounds remains a challenge (16, 38). We hypothesized that 4-bromo-3,3,4,4-tetrafluoro-1-butene **1s'**, which is commercially available and safe to handle, could serve as a general and practical lynchpin for the construction of tetrafluoroethylene-containing carbocycles that were previously hard to make.

Similar conditions to those used for the three-component radical cross-coupling led to the MAC product **5a**, albeit in low yields because of competitive formation of dicarbofunctionalization product **4s'** (Fig. 3A). After screening of conditions, we found that by lowering the iron concentration and changing the catalyst-to-ligand ratio, we could shut down the dicarbofunctionalization pathway and increase yield of the annulation product **5a**. Presumably, lower catalyst concentration allows for more efficient 5-*exo* cyclization, leading to **int-2**, which in turn can undergo radical cross-coupling to form the annulation product (Fig. 3B).

With optimized conditions in hand, we next explored the generality with respect to alkene (Fig. 3C). Overall, a broad range of olefinic partners (**2a** to **2j**) (table S5) were found to be competent partners that lead to tetrafluoroethylene-containing drug-like scaffolds in one synthetic step. In particular, as shown in Fig. 3C, in addition to boron-substituted alkenes (**2a** and **2b**), vinyl silanes (**2c**), ketene

acetals (**2d**), ethers (**2e** and **2v**), thioenols (**2f**), and enamines (**2g** and **2w**) were compatible. Furthermore, four-, five-, and six-membered (hetero)carbocycles bearing exo-cyclic alkenes (**2j** to **2r**) formed the corresponding spirocyclic compounds in good yields. We did not observe erosion of stereochemistry when using the enantiopure exo-methylene-containing pyrrolidine **2m** that led to the corresponding annulation-arylation product **5m**, as characterized by means of x-ray crystallography. In addition, this method allowed the gram-scale synthesis of spirocyclic compound **5p**, a derivative of sequeempervirin A (39), and fused bicyclic (hetero)cyclic structures, starting from the corresponding di- and trisubstituted cyclic (hetero)alkenes with good yields and modest to high regio- and diastereoselectivity (**2s** to **2x**). Acyclic olefins bearing alkyl chains with pendant functional groups—including aryl (**2z**), primary chloride (**2za**), alkene (**2zb**), alkyl boryl (**2zc**), unprotected alcohol (**2zd**) and amine (**2ze**), and alkyl ester (**2zf**)—were also competent partners. Tetrasubstituted alkenes and terminal alkynes also yielded the desired annulation-arylation products (**5zg**, **5zh**, **5zi**, and **5zj**), albeit in lower yields. To demonstrate potential for late-stage modification of bioactive compounds, we applied this protocol to natural products that bear alkene groups (**5zk** to **5zo**). We also explored the alkyl radical scope and found that other radical precursors could participate in the annulation (**5zp** to **5zu**).

We next explored the reaction scope of the nucleophile (Fig. 3D). In general, we found that para-substituted electron-rich and electron-poor aryl Grignard reagents formed the desired products (**5zv** to **5zza**). In addition, we found good yields across the board with aryl magnesium nucleophiles that bear electron-withdrawing groups (**5zza**, **5zzb**, **5zzf**, and **5zzg**); sterically hindered systems (**5zcc**, **5zcd**, **5zce**, and **5zzi**), including those bearing C(sp²)-Cl bonds for further functionalization; (hetero)aryls (**5zzk** and **5zll**); and vinyl Grignard reagents (**5zzm** and **5znn**).

Mechanistic studies

To elucidate the mechanism of this multicomponent iron-catalyzed cross-coupling, we used a combined spectroscopic, structural, computational, and organic synthetic approach. First, to provide direct insight into the iron intermediates involved in catalysis and enable the identification of the key iron species that initiates radical generation, we applied freeze-trapped 80 K ⁵⁷Fe Mössbauer and 10 K EPR spectroscopies, combined with single-crystal x-ray crystallography. For these spectroscopic studies, ⁵⁷FeBr₂ was used as the starting Fe salt because it was a more accessible ⁵⁷Fe source, and it performed similarly to FeCl₃ under catalytic conditions. Two equivalents of **L1** (dcype) were

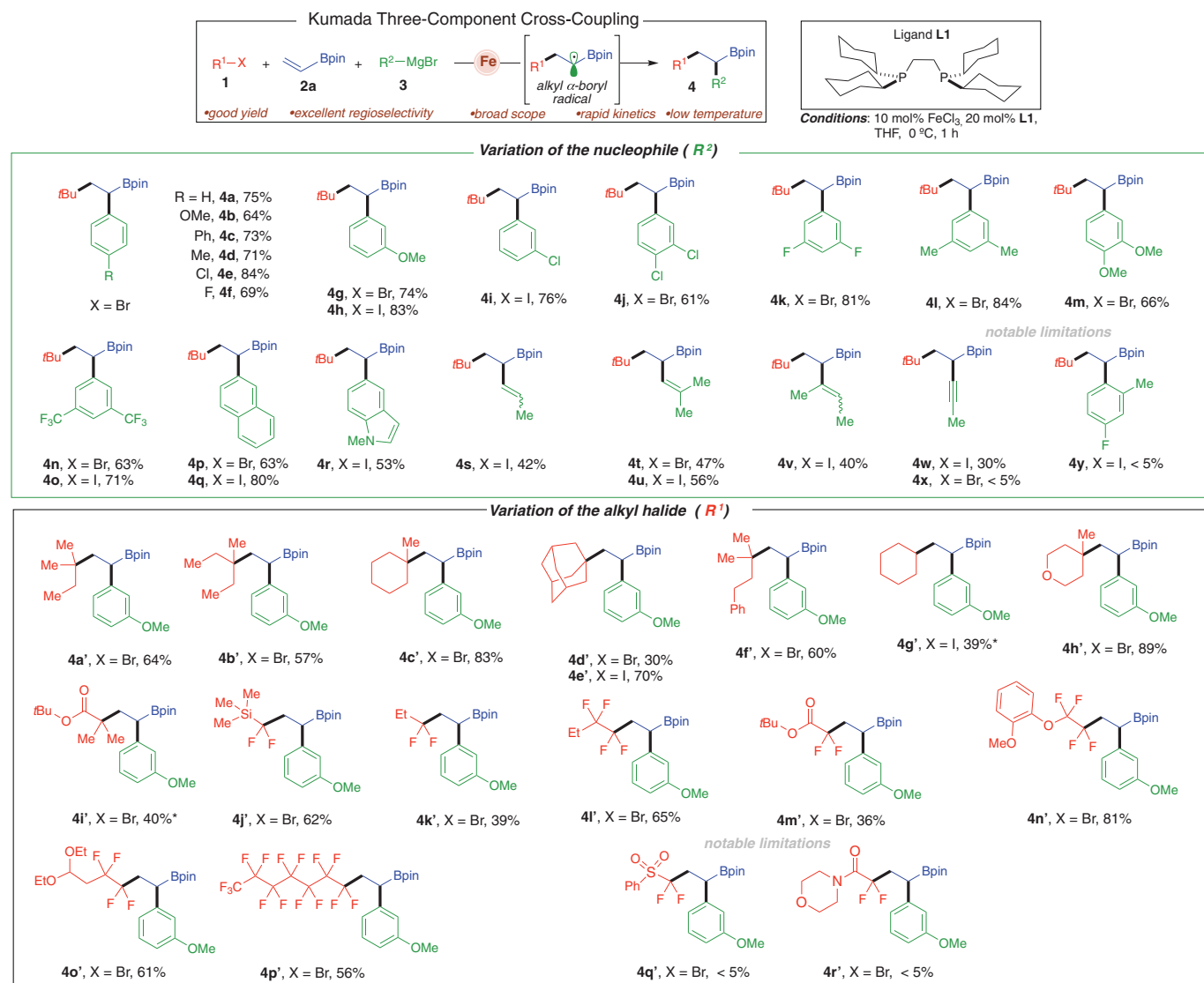


Fig. 2. Reaction scope of three-component dicarbofunctionalization of vinyl boronates by using bisphosphine-iron complexes as catalysts.

Reactions were carried out on a 0.20-mmol scale at 0 °C for 1 hour, performed with **1** (2.0 equiv), **2a** (1.0 equiv), Grignard reagent **3** (2.0 equiv)

with THF (0.2 ml). Grignard reagent **3** was added dropwise by means of a syringe pump over 1 hour, isolated yield. ***1** (5.0 equiv), Grignard **3** (5.5 equiv), and **3h**. Bpin, boronic acid pinacol ester; Me, methyl; Ph, phenyl; tBu, *tert*-butyl.

combined with $^{57}\text{FeBr}_2$ in tetrahydrofuran (THF) for 10 min at 0 °C, after which the solution was freeze-trapped in liquid N_2 ; an 80 K Mössbauer spectrum then revealed the formation of a single Fe species ($\delta = 0.72$ mm/s and $|\Delta E_Q| = 3.21$ mm/s, where δ is the isomer shift and $|\Delta E_Q|$ is the quadrupole splitting) (table S6), which was later isolated and characterized by x-ray crystallography and Evans method nuclear magnetic resonance (NMR) as the high-spin Fe(II) dihalide complex $\text{Fe}(\text{dcype})\text{Br}_2$ (**1**) [effective magnetic moment (μ_{eff}) = 5.2(1), $\delta = 0.73$ mm/s, and $|\Delta E_Q| = 3.13$ mm/s for isolated material; numbers in parentheses indicate standard deviation] (Fig. 4A). The reaction of **1** with 1 equiv of the aryl Grignard reagent 3-methoxyphenyl magnesium bromide at 0 °C

resulted in the formation of a single Fe species with Mössbauer parameters of $\delta = 0.51$ mm/s and $|\Delta E_Q| = 2.49$ mm/s, which is consistent with previously reported monoarylated Fe(II) bisphosphine complexes (Fig. 4A) (**4o**, **4l**). X-ray crystallography combined with Evans method NMR confirmed this species as the distorted tetrahedral, monoaryl high-spin Fe(II) complex $\text{Fe}(\text{dcype})\text{BrAr}$ (Ar, 3-MeOC₆H₄) [μ_{eff} = 5.0(2), $\delta = 0.52$ mm/s, and $|\Delta E_Q| = 2.45$ mm/s for isolated material] (**2**).

Addition of a second equivalent of aryl Grignard reagent led to a color change of the solution from pale to brilliant yellow over the course of 1 min, which further evolved to dark green over 5 min. At that point, freeze-trapped Mössbauer spectroscopy indicated the formation

of two new iron species, **3** and **4**, corresponding to 50 and 10% of the total Fe concentration, respectively (Fig. 4A). At a shorter reaction time (1 min), only 25% of species **2** had been converted to **3** without any formation of **4**. Further experiments revealed that species **4** could be accessed in higher amounts if excess aryl Grignard reagent is added (fig. S4A). This observation suggested the possible identity of **4** as a reduced Fe species, which was subsequently confirmed with x-ray crystallography to be $(\text{dcype})\text{Fe}^{\text{I}}\eta^6\text{-}[3,3'-(\text{OMe})_2\text{-1,1'-(C}_6\text{H}_4)_2]$ (Fig. 4A and fig. S4B). The identification of this Fe(0) complex suggested that **3** was likely an Fe(II) bisaryl species formed before reductive elimination ($\delta = 0.23$ mm/s and $|\Delta E_Q| = 4.35$ mm/s). This assignment was subsequently

confirmed with crystallographic analysis as the bisarylated species Fe(dcype)Ar₂ (**3**), in which the large increase in the quadrupole splitting of **3** is consistent with the distorted square planar geometry of this Fe(II) complex. Although crystals of **3** repeatedly decayed over the course of the data collection, which limited the quality of the structure, the atomic assignments, overall geometry, connectivity, and identification of this complex are unambiguous. The product **3** was too thermally unstable for further characterization. However, literature precedent for $S = 1$ distorted square planar Fe phosphine compounds bearing two mesityl ligands, including their comparable Mössbauer parameters to **3**, supports assignment of **3** as an intermediate-spin ($S = 1$) Fe(II) complex (41, 42). This molecular geometry is atypical for bisaryl-Fe(II)-bisphosphines beyond mesityl complexes, which suggests an increased donor strength for **L1** that results from the cyclohexyl substituents. In addition, the identification of **4** indicates that **3** undergoes a two-electron reduction pathway similar to that previously observed in Fe(II)-SciOPP species (SciOPP, 1,2-bis[3,5-di(*tert*-butyl)phenyl]phosphino)benzene (40). Although all stoichiometric reactions were performed with an excess of **L1**, as prescribed for the catalytic reaction, all the iron species identified in situ contained only one bisphosphine per iron center.

We proceeded to evaluate the reactivity of the identified, transmetalated Fe(II)-aryl-bisphosphine species toward electrophile (2-iodo-2-methylpropane) to determine their potential for radical initiation in catalysis. Pseudo-single-turnover studies for the reaction of monoarylated species **2** (generated in situ) with an excess of 2-iodo-2-methylpropane (20 equiv) in the presence of vinyl boronic acid pinacol ester indicated that **2** is reactive toward electrophile at an observed rate (k_{obs}) of $\sim 0.04 \text{ min}^{-1}$ (figs. S5 and S6), which resulted in three-component product formation. However, the observed rate of reaction is far too slow to be catalytically relevant, including the initial radical generation, considering the average turnover frequency during catalysis ($\sim 0.17 \text{ min}^{-1}$). Conversely, Mössbauer spectroscopic studies indicated that **3** is highly reactive toward electrophile. The reaction of a mixture of **2** and **3** (generated in situ after 1 min) with excess 2-iodo-2-methylpropane (20 equiv) leads to the complete consumption of species **3** within 25 s with concomitant generation of complex **1**, whereas the complex **2** in solution does not react with electrophile, which is consistent with its aforementioned slow reactivity (Fig. 4B). However, when a similar reaction is performed in the presence of vinyl boronic acid pinacol ester, species **2** is also consumed (fig. S7), which suggests a likely recombination of the

secondary radical (formed after addition of the tertiary radical to the alkene) with **2** to generate product (further insights are available in the supplementary materials, materials and methods). Although complex **4** was also found to be highly reactive toward excess electrophile (20 equiv) (fig. S8), only undesired side products, including the two-component coupling of the electrophile and alkene, were observed to form, which is consistent with the lack of the aryl component required to form the three-component product. Furthermore, the reaction of the bisarylated species **3** with electrophile is faster ($< 25 \text{ s}$) than its transformation to complex **4** ($> 1 \text{ min}$); thus, **4** is unlikely to be generated in any substantial amount under catalytic conditions, which is consistent with no observation of **4** during catalysis. However, formation of **4** is more facile when only 1 equiv of **L1** is used (fig. S9), providing one possible role of excess ligand in achieving optimal yields in catalysis, although other roles of the excess phosphine, such as coordination to magnesium cations, cannot be excluded (43). Overall, these reactivity studies identify the distorted square planar bisarylated Fe(II) complex **3** as the key iron species responsible for the initial radical formation with the alkyl electrophile, which is required as the first step to initiate catalysis. Details about the nature of C–C bond formation were studied by means of DFT calculations.

We bolstered these stoichiometric studies with in situ iron speciation studies during catalysis: 80 K Mössbauer and 10 K EPR spectroscopy experiments were carried out on freeze-trapped reaction samples at various time points throughout the catalytic reaction (10, 30, and 50 min) (fig. S10). The distribution of species during catalysis consisted of $\sim 48\%$ **1** and $\sim 52\%$ **2** by Mössbauer spectroscopy; no EPR active species were observed. The presence of **2** in such large quantities during catalysis is consistent with the previous observation that **2** reacts slowly with electrophile. Complex **3** being undetectable during catalysis is also consistent with the prior observation of its rapid reactivity toward electrophile.

We next considered the success of **L1** as the supporting ligand because other related bisphosphines resulted in substantially decreased product formation. To understand this effect, we compared the distribution of species formed under catalytically relevant conditions with tetraethyl ligand **L3**. The Mössbauer spectrum of the freeze-trapped solution after reaction of $^{57}\text{FeBr}_2$ with 2 equiv of **L3** [1,2-bis(diethylphosphino)ethane (depe)] at 0°C shows the formation of a single Fe species ($\delta = 0.47 \text{ mm/s}$ and $|\Delta E_{\text{Q}}| = 1.51 \text{ mm/s}$), which corresponds to the previously reported, distorted octahedral Fe(II) complex Fe(depe)₂Br₂

(**5**) (fig. S11) (44). Complex **5** also preferentially forms over the 1:1 **L3**:Fe complex, even when only 1 equiv of **L3** is used (fig. S12). Reaction of **5** with aryl Grignard (1 or 2 equiv) at 0°C led to a color change from brilliant yellow-green to orange within 5 min. Freeze-trapped Mössbauer spectroscopy indicated the formation of a single new Fe species **6** ($\delta = 0.30 \text{ mm/s}$ and $|\Delta E_{\text{Q}}| = 0.27 \text{ mm/s}$) (fig. S13), even at extended reaction times, with the reduced isomer shift (relative to complex **5**) and small quadrupole splitting consistent with a distorted octahedral, arylated low-spin Fe(II) complex, as expected for the transmetalation of **5** with aryl Grignard reagent (40). Combined with additional reaction data at room temperature (fig. S13), this species is assigned to the monoarylated complex Fe(depe)₂BrAr. Reaction of **6** with 20 equiv of 2-iodo-2-methylpropane resulted in no consumption of this coordinatively saturated iron species, even at extended time points (20 min), which indicates limited or no reactivity toward electrophile (fig. S14). The observed slow transmetalation of **5** and lack of reactivity of **6** described above are consistent with their presence as the major Fe species in solution during catalysis (fig. S15). In the presence of excess nucleophile, a $S = 1/2$ Fe species could also be observed (fig. S16), which likely corresponds to a five-coordinate Fe(depe)₂X complex (X = Br or Ar), consistent with previously reported Fe(I) complexes formed as a result of the reaction of Fe-bisphosphines with aryl Grignard reagents (44, 45). A coordinatively saturated, bisarylated Fe(depe)₂Ar₂ complex may also form in situ before reduction to Fe(I), although this species could not be unambiguously observed. The reduced Fe(I) species was found to be reactive toward electrophile in the presence of alkene (fig. S17), but the formation of only side products, including the two-component coupling of the electrophile and alkene, was observed, which is consistent with this Fe(I) species being unproductive for catalysis. Overall, these observations are consistent with the poor catalytic performance when using **L3** and highlight the importance of steric effects on the bisphosphine ligands in promoting the formation of coordinatively unsaturated Fe(II) species capable of initiating the radical formation as well as undergoing recombination to generate the desired product selectively.

Next, using vinyl cyclopropane as radical probe **2zp** (Fig. 5A), we observed the 1,5-dicarbonyl functionalization product **4'** and no annulation product **5'** to be consistent with faster alkyl radical ring opening ($k \sim 10^7 \text{ s}^{-1}$) than radical 5-*exo* cyclization ($k \sim 10^5 \text{ s}^{-1}$) and arylation ($k \sim 10^4 \text{ s}^{-1}$) (19, 46). In addition, consistent with the intermediacy of the alkyl radical, we also observed stereoconvergence in

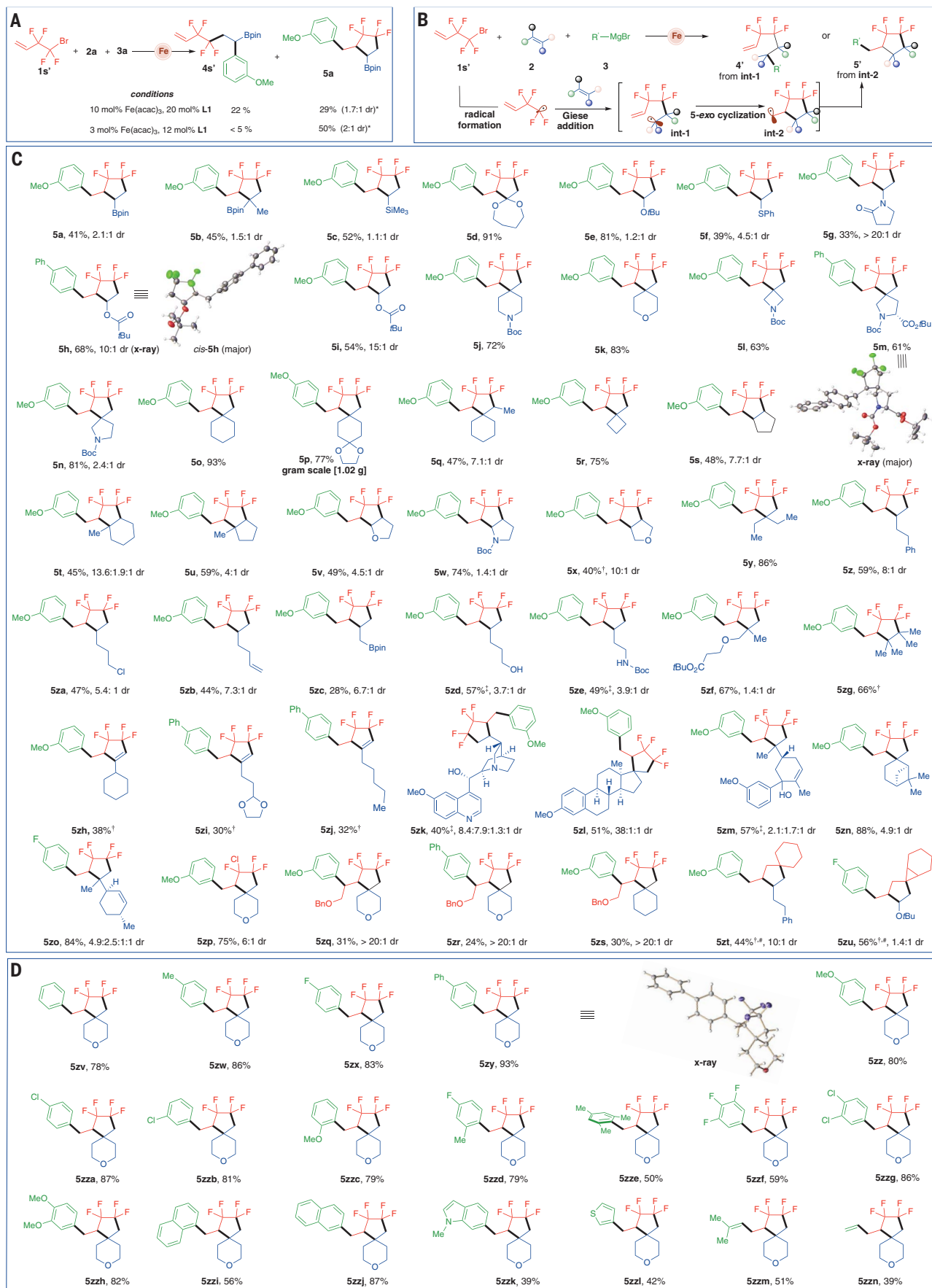


Fig. 3. Reaction scope of three-component annulation-arylation reaction sequence catalyzed by bisphosphine-iron catalysts. Reactions were carried out on a 0.20-mmol scale at 0°C for 1 hour, performed with **1** (1.0 equiv), **2** (1.5 equiv) Grignard reagent **3** (2.0 equiv), Fe(acac)₃ (3 mol %), and **L1** (12 mol %) with THF (0.2 ml). Grignard reagent **3** was added dropwise via a syringe pump over 1 hour. Reported yields and dr are from isolated yields. acac, acetylacetonate; Boc, *tert*-Butyloxycarbonyl; dr, diastereomeric ratio. *¹H NMR yield with CH₂Br₂ as internal standard. †Alkene or alkyne (14 equiv). ‡Grignard **3** (3.0 equiv). #No additional solvent.

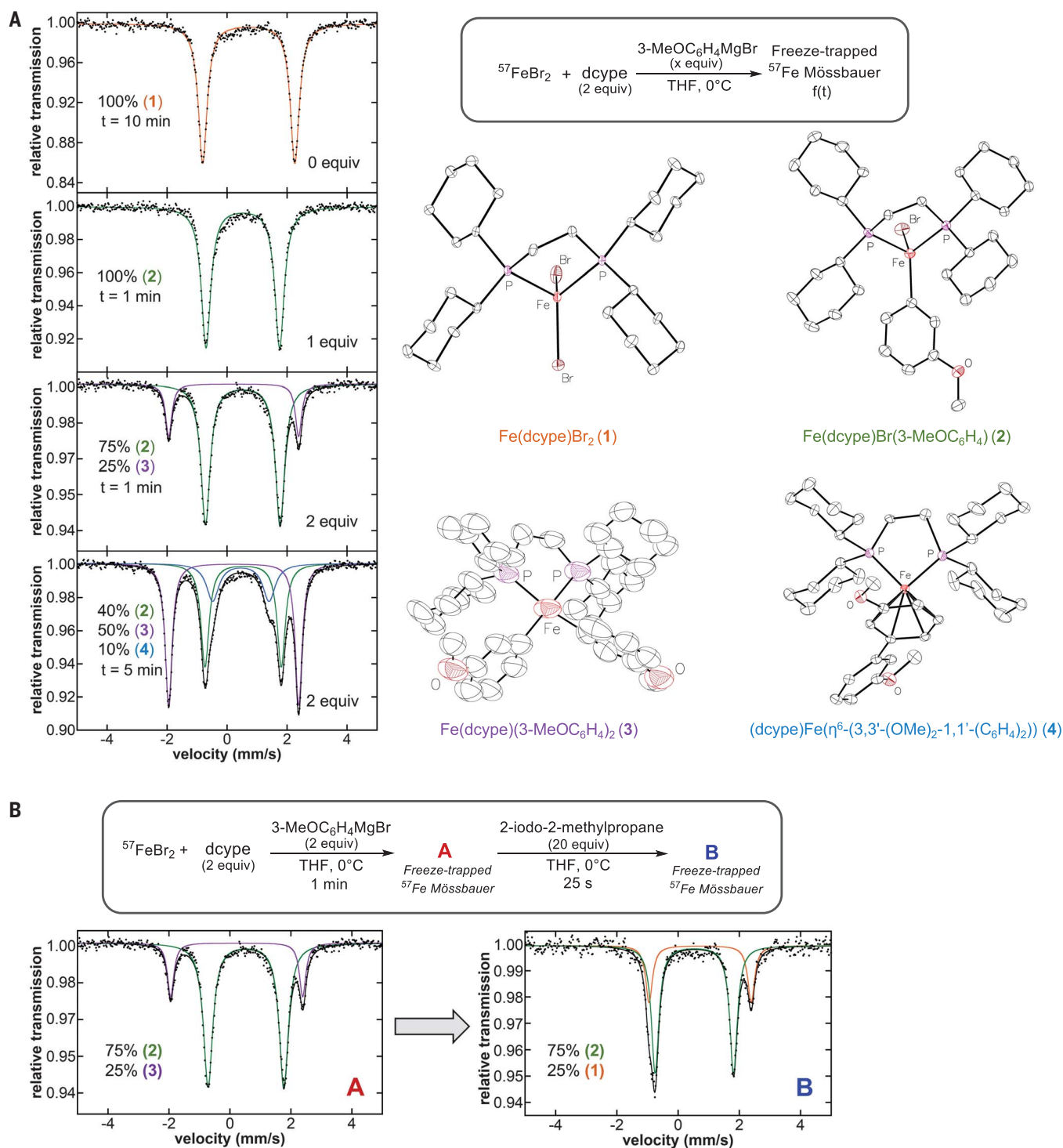
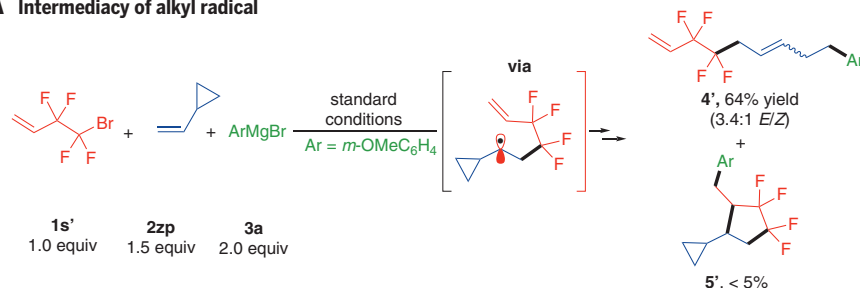
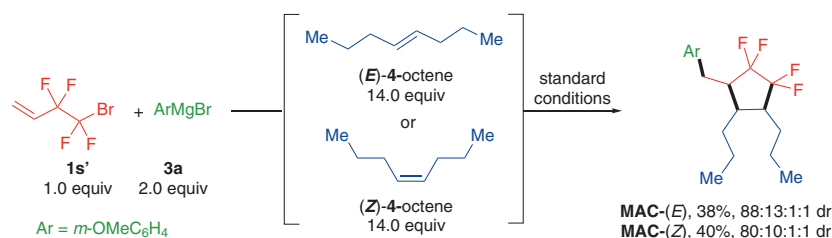


Fig. 4. Freeze-trapped 80 K Mössbauer spectra of stoichiometric reactions. (A) ⁵⁷FeBr₂, 2 equiv of **L1**, and various equivalents of 3-MeOC₆H₄MgBr (left). Combining SC-XRD and Mössbauer studies of crystalline material, the individual components were assigned as Fe(dcype)Br₂ (**1**) (orange), Fe(dcype)Br(3-MeOC₆H₄) (**2**) (green), Fe(dcype)(3-MeOC₆H₄)₂ (**3**) (purple), and (dcype)Fe[η⁶-[3,3'-(OMe)₂-1,1'-(C₆H₄)₂]] (**4**) (blue). Thermal ellipsoids are shown at 50% probability. (B) The freeze-trapped 80 K Mössbauer spectrum of the in situ formed iron species upon reaction of ⁵⁷FeBr₂ and 2 equiv of **L1**, with 2 equiv of 3-MeOC₆H₄MgBr for 1 min (left) and following subsequent reaction with 2-iodo-2-methylpropane for 25 s (right).

A Intermediacy of alkyl radical



B Stereoconvergence via alkyl radical C-C bond rotation



C Nature of carbon-carbon bond formation

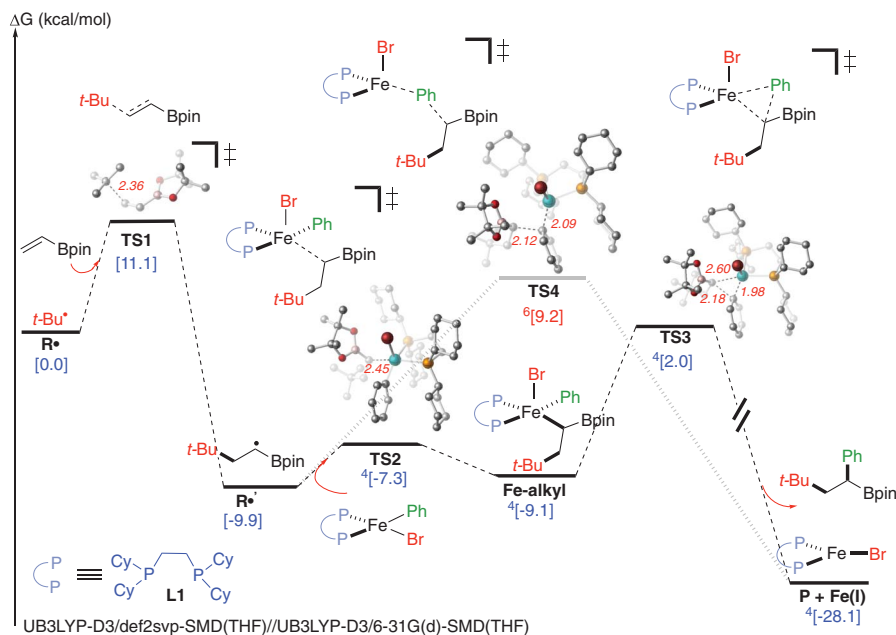


Fig. 5. Experimental and DFT calculations insights into the mechanism. (A and B) Standard conditions were carried out on a 0.20-mmol scale at 0°C; Grignard reagent **3a** was added dropwise by means of a syringe pump over 1 hour. Reported yields and dr are from isolated yields. (C) Computed lowest-energy pathway for the Fe-catalyzed multicompartment radical cascade cross-coupling reaction leading to dicarbofunctionalization of vinyl boronates. TS, transition state structure.

the three-component annulation, leading to the same product outcome by using either *E* or *Z* 4-octene, which suggests rapid equilibration (through sigma-bond rotation) before 5-*exo* radical cyclization-arylation (Fig. 5B). Last, to gain insight into the nature of the C-C bond formation, we turned to DFT calculations, which supported initial radical formation from an intermediate-spin distorted square planar bisarylated Fe(II) species through halogen

abstraction (barrier, ~20 kcal/mol), which led to Fe(III) and tertiary radical (fig. S19). In turn, as shown in Fig. 5C, radical addition to vinyl boronate is predicted to be fast (barrier, ~11 kcal/mol) and irreversible, leading to α -boryl radical R^\bullet . Then, this radical can rapidly and reversibly add (barrier, ~2.6 kcal/mol) to the corresponding high-spin distorted tetrahedral, monoarylated Fe(II) species, which leads to a distorted square pyramidal Fe(III)-

alkyl intermediate. Subsequent irreversible reductive elimination by means of quartet spin state leads to the desired product and Fe(I) species, which can then restart the catalytic cycle (17, 47). We also located the competing outer-sphere C-C forming transition state, but this pathway is less likely because of a much higher barrier (~19 kcal/mol) in comparison with the inner-sphere stepwise C-C bond formation (Fig. 5C, **TS4**). (Further mechanistic discussion and alternative pathways are provided in fig. S22.)

Overall, we anticipate that the method disclosed here will provide a practical and general route to functionalization of electron-rich and electron-deficient alkenes with various alkyl and hetero-substituents and application to late-stage functionalization of bioactive molecules.

REFERENCES AND NOTES

- E. Fernández, A. Whiting, *Synthesis and Application of Organoboron Compounds* (Springer, 2015).
- J. P. Wolfe, R. A. Singer, B. H. Yang, S. L. Buchwald, *J. Am. Chem. Soc.* **121**, 9550–9561 (1999).
- J. C. Tellis, D. N. Primer, G. A. Molander, *Science* **345**, 433–436 (2014).
- M. W. Campbell, J. S. Compton, C. B. Kelly, G. A. Molander, *J. Am. Chem. Soc.* **141**, 20069–20078 (2019).
- A. García-Domínguez, R. Mondal, C. Nevado, *Angew. Chem. Int. Ed.* **58**, 12286–12290 (2019).
- R. S. Mega, V. K. Duong, A. Noble, V. K. Aggarwal, *Angew. Chem. Int. Ed.* **59**, 4375–4379 (2020).
- S.-Z. Sun, Y. Duan, R. S. Mega, R. J. Somerville, R. Martin, *Angew. Chem. Int. Ed.* **59**, 4370–4374 (2020).
- M. Chierchia, P. Xu, G. J. Lovinger, J. P. Morken, *Angew. Chem. Int. Ed.* **58**, 14245–14249 (2019).
- X.-X. Wang, X. Lu, S.-J. He, Y. Fu, *Chem. Sci.* **11**, 7950–7956 (2020).
- T. Hatakeyama *et al.*, *J. Am. Chem. Soc.* **132**, 10674–10676 (2010).
- H. M. O'Brien *et al.*, *Nat. Catal.* **1**, 429–437 (2018).
- M. P. Crockett, A. S. Wong, B. Li, J. A. Byers, *Angew. Chem. Int. Ed.* **59**, 5392–5397 (2020).
- R. B. Bedford *et al.*, *Organometallics* **33**, 5940–5943 (2014).
- N. Kumar, R. R. Reddy, N. Eghbarieh, A. Masarwa, *Chem. Commun.* **56**, 13–25 (2020).
- J. C. Lo *et al.*, *J. Am. Chem. Soc.* **139**, 2484–2503 (2017).
- J. Václavík, I. Klímánková, A. Budinská, P. Beier, *Eur. J. Org. Chem.* **2018**, 3554–3593 (2018).
- W. Lee, J. Zhou, O. Gutierrez, *J. Am. Chem. Soc.* **139**, 16126–16133 (2017).
- L. Liu, W. Lee, M. Yuan, O. Gutierrez, *Comments Inorg. Chem.* **38**, 210–237 (2018).
- L. Liu, W. Lee, J. Zhou, S. Bandyopadhyay, O. Gutierrez, *Tetrahedron* **75**, 129–136 (2019).
- L. Liu *et al.*, *Chem. Sci.* **11**, 3146–3151 (2020).
- L. Liu *et al.*, *Chem. Sci.* **11**, 8301–8305 (2020).
- M. L. Neidig *et al.*, *Acc. Chem. Res.* **52**, 140–150 (2019).
- J. D. Sears, P. G. N. Neate, M. L. Neidig, *J. Am. Chem. Soc.* **140**, 11872–11883 (2018).
- D. G. Hall, Structure, properties, and preparation of boronic acid derivatives: in *Boronic acids* (Wiley, 2005), chap. 1, pp. 1–133.
- M.-C. Belhomme, T. Besset, T. Poisson, X. Pannecoucke, *Chemistry* **21**, 12836–12865 (2015).
- L. An, C. Xu, X. Zhang, *Nat. Commun.* **8**, 1460 (2017).
- L. An, Y.-L. Xiao, S. Zhang, X. Zhang, *Angew. Chem. Int. Ed.* **57**, 6921–6925 (2018).
- X. X. Rong, H.-Q. Pan, W. R. Dolbier Jr., B. E. Smart, *J. Am. Chem. Soc.* **116**, 4521–4522 (1994).
- J. Derosa, O. Apollinar, T. Kang, V. T. Tran, K. M. Engle, *Chem. Sci.* **11**, 4287–4296 (2020).
- D. V. Avila *et al.*, *J. Am. Chem. Soc.* **116**, 99–104 (1994).
- X. Lin, F. Zheng, F.-L. Qing, *Organometallics* **31**, 1578–1582 (2012).
- D. O'Hagan, *Chem. Soc. Rev.* **37**, 308–319 (2008).
- K. Müller, C. Faeh, F. Diederich, *Science* **317**, 1881–1886 (2007).
- S. Purser, P. R. Moore, S. Swallow, V. Gouverneur, *Chem. Soc. Rev.* **37**, 320–330 (2008).

35. M. A. Miller, E. M. Sletten, *ChemBioChem* **21**, 3451–3462 (2020).
36. J. Boström, D. G. Brown, R. J. Young, G. M. Keserü, *Nat. Rev. Drug Discov.* **17**, 709–727 (2018).
37. A. Studer, D. P. Curran, *Angew. Chem. Int. Ed.* **55**, 58–102 (2016).
38. L. Li *et al.*, *Angew. Chem. Int. Ed.* **56**, 9971–9975 (2017).
39. S. Maity, S. Ghosh, *Tetrahedron Lett.* **48**, 3355–3358 (2007).
40. S. L. Daifuku, J. L. Kneebone, B. E. R. Snyder, M. L. Neidig, *J. Am. Chem. Soc.* **137**, 11432–11444 (2015).
41. S. L. Daifuku, M. H. Al-Afyouni, B. E. R. Snyder, J. L. Kneebone, M. L. Neidig, *J. Am. Chem. Soc.* **136**, 9132–9143 (2014).
42. E. J. Hawrelak *et al.*, *Inorg. Chem.* **44**, 3103–3111 (2005).
43. A. M. Messinis *et al.*, *Nat. Catal.* **2**, 123–133 (2019).
44. D. J. Evans, R. A. Henderson, A. Hills, D. L. Hughes, K. E. Oglieve, *J. Chem. Soc., Dalton Trans.* (7): 1259–1265 (1992).
45. R. B. Bedford *et al.*, *Organometallics* **33**, 5767–5780 (2014).
46. M. Newcomb, in *Encyclopedia of Radicals in Chemistry, Biology and Materials*, C. Chatgililoglu and A. Studer, Eds. (Wiley, 2012).
47. A. K. Sharma *et al.*, *J. Am. Chem. Soc.* **139**, 16117–16125 (2017).

ACKNOWLEDGMENTS

We thank P. Y. Zavalij (University of Maryland) and W. W. Brennessel (University of Rochester) for help with x-ray diffraction and Y. Li (University of Maryland) for help with the high-resolution mass spectrometry. **Funding:** Funding was provided by the National Institutes of Health (grant R35GM137797 to O.G. and R01GM111480 to M.L.N.) and the National Science Foundation (CAREER 1751568 to O.G.). **Author contributions:** L.L. developed the method and performed DFT calculations, and M.C.A. carried out the mechanistic studies. W.L. carried out DFT calculations and chromatography. C.R.Y. performed materials preparation and chromatography. O.G. and M.L.N. directed the investigations and wrote the manuscript with revisions provided by the other authors. **Competing interests:**

The authors declare that they have no competing interests. **Data and materials availability:** Crystallographic data are available free of charge from the Cambridge Crystallographic Data Center under reference nos. CCDC-2085294, CCDC-2085295, CCDC-2085297, CCDC-2085565, CCDC-2085566, CCDC-2085567, and CCDC-2085568. All other data are available in the main text or the supplementary materials.

SUPPLEMENTARY MATERIALS

[science.org/doi/10.1126/science.abj6005](https://doi.org/10.1126/science.abj6005)
Materials and Methods
Supplementary Text
Figs. S1 to S22
Tables S1 to S13
References (48–69)

24 May 2021; accepted 9 August 2021
[10.1126/science.abj6005](https://doi.org/10.1126/science.abj6005)



General method for iron-catalyzed multicomponent radical cascades–cross-couplings

Lei Liu, Maria Camila Aguilera, Wes Lee, Cassandra R. Youshaw, Michael L. Neidig, and Osvaldo Gutierrez

Science, **374** (6566), .

DOI: 10.1126/science.abj6005

Iron links a trio

Iron holds particular appeal as a catalytic metal—it is safe and abundant, as well as a mainstay of enzymatic reactivity. Nonetheless, in synthetic construction of carbon-carbon bonds, modern chemists have largely had to rely on rarer metals such as palladium. Liu *et al.* now report that coordination of iron by a bulky chelating phosphine ligand enables efficient mutual coupling of three different reactants—an alkyl halide, an aryl Grignard, and an olefin—to form two carbon-carbon bonds (see the Perspective by Lefèvre). A combination of Mössbauer spectroscopy, crystallography, and computational simulations illuminates the mechanism. —JSY

View the article online

<https://www.science.org/doi/10.1126/science.abj6005>

Permissions

<https://www.science.org/help/reprints-and-permissions>

Use of this article is subject to the [Terms of service](#)

Science (ISSN) is published by the American Association for the Advancement of Science. 1200 New York Avenue NW, Washington, DC 20005. The title *Science* is a registered trademark of AAAS.

Copyright © 2021 The Authors, some rights reserved; exclusive licensee American Association for the Advancement of Science. No claim to original U.S. Government Works

On the Nature of C(sp³)–C(sp²) Bond Formation in Nickel-Catalyzed Tertiary Radical Cross-Couplings: A Case Study of Ni/Photoredox Catalytic Cross-Coupling of Alkyl Radicals and Aryl Halides

Mingbin Yuan,[‡] Zhihui Song,[‡] Shorouk O. Badir, Gary A. Molander,^{*} and Osvaldo Gutierrez^{*}

Cite This: *J. Am. Chem. Soc.* 2020, 142, 7225–7234

Read Online

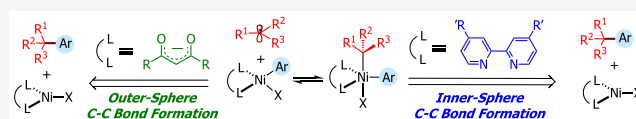
ACCESS |

Metrics & More

Article Recommendations

Supporting Information

ABSTRACT: The merger of photoredox and nickel catalysis has enabled the construction of quaternary centers. However, the mechanism, role of the ligand, and effect of the spin state for this transformation and related Ni-catalyzed cross-couplings involving tertiary alkyl radicals in combination with bipyridine and diketonate ligands remain unknown. Several mechanisms have been proposed, all invoking a key Ni(III) species prior to undergoing irreversible inner-sphere reductive elimination. In this work, we have used open-shell dispersion-corrected DFT calculations, quasi-classical dynamics calculations, and experiments to study in detail the mechanism of carbon–carbon bond formation in Ni bipyridine- and diketonate-based catalytic systems. These calculations revealed that access to high spin states (e.g., triplet spin state tetrahedral Ni(II) species) is critical for effective radical cross-coupling of tertiary alkyl radicals. Further, these calculations revealed a disparate mechanism for the C–C bond formation. Specifically, contrary to the neutral Ni-bipyridyl system, diketonate ligands lead directly to the corresponding tertiary radical cross-coupling products via an outer-sphere reductive elimination step via triplet spin state from the Ni(III) intermediates. Implications to related Ni-catalyzed radical cross-couplings and the design of new transformations are discussed.



INTRODUCTION

Nickel-catalyzed cross-coupling reactions (CCRs) have emerged as powerful synthetic methods for the mild and selective construction of carbon–carbon bonds.¹ Although C(sp²)–C(sp²) couplings are highly reliable and well-established,² significant limitations are often encountered in the application of sp³-hybridized reagents, particularly in the installation of quaternary centers.³ Notable examples are from reports by the Glorius⁴ and Biscoe⁵ groups that used a Ni-based catalyst with N-heterocyclic carbene (NHC) ligands to perform C(sp²)–C(sp³) cross-couplings between aryl bromides and tertiary alkyl Grignard nucleophiles (Scheme 1A). Fu employed a nickel/bipyridine system for the cross-coupling between unactivated alkyl bromides and organoboron compounds.⁶ Gong used a monodentate pyridine as ligand in combination with a nickel system for the reductive coupling between aryl halides and tertiary alkyl halides,⁷ while Watson utilized a Ni/phosphine system for the cross-coupling between tertiary benzylic acetates and organoboron compounds.⁸ More recently, the Molander group disclosed the first dual photoredox–Ni catalytic strategy for the cross-coupling between potassium tertiary alkyltrifluoroborates and aryl bromides (Scheme 1B).⁹ Notably, the bidentate bipyridyl-based ligand (4,4-di-*tert*-butyl-2,2-bipyridine; dtbbpy), which has proven effective in the dual photoredox–Ni-catalyzed cross-coupling of secondary alkylboron reagents, was ineffective with acyclic tertiary alkyltrifluoroborates in this case. On the other hand, *anionic* diketonate-based *bidentate* ligands

(e.g., 2,2,6,6-tetramethyl-3,5-heptanedionate, TMHD, and acetylacetonate, acac) yielded the desired cross-coupling products between *acyclic* tertiary organoboron reagents and a wide range of electron-poor and electron-neutral aryl bromides. In this context, Baran reported the use of an anionic TMHD ligand in the nickel-catalyzed radical C(sp²)–C(sp³) cross-coupling between *tertiary* alkyl redox-active esters and arylzinc reagents, while Shenvi reported a dual Mn/Ni(acac)₂ system to form all-carbon arylated quaternary centers from tertiary radical precursors.¹⁰

However, although the evidence for the presence of radical intermediates in these systems is strong,¹¹ the mechanism, effect of ligand (neutral versus anionic), and molecular-level understanding of the key C(sp²)–C(sp³) bond-forming step remain poorly understood. The use of quantum mechanical calculations to investigate the mechanisms, electronic properties, and dynamics of transition metal complexes has led to a deeper understanding of the molecular-level interactions controlling reactivity and selectivity in complex catalytic cycles.^{12–17} Herein, quantum mechanical calculations were used to address the following questions: (1) What is the effect

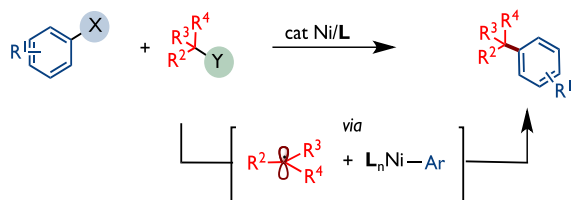
Received: March 3, 2020

Published: March 20, 2020

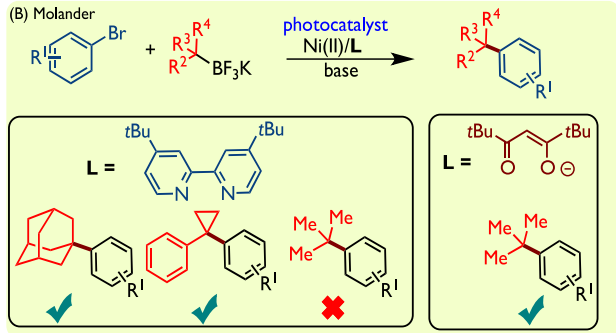


Scheme 1. Methods for the Construction of All-Carbon Quaternary Centers via Ni-Catalyzed Cross-Couplings between Tertiary Alkyl Precursors and Aryl Halides

(A) Glorius, Biscoe, Fu, Gong, and Baran



(B) Molander



of anionic diketonate-based ligands versus neutral bipyridine ligands in the commonly proposed Ni(0)/Ni(I)/Ni(III) and Ni(0)/Ni(II)/Ni(III) pathways.¹⁷ (2) What are the factors responsible for the distinct reactivity of 2° vs 3° alkyl radicals in the Ni-bipyridine system? (3) What is the role of spin state of the purported Ni complexes and the nature of C(sp²)-C(sp³) bond formation in the nickel radical cross-couplings? (4) What is the lifetime of the Ni(III) intermediate prior to undergoing inner-sphere reductive elimination and dynamic effects on radical dissociation/rebound? In this article, we report a comprehensive computational study of the mechanism of Ni-catalyzed CCRs between aryl halides and tertiary alkyl radicals using both neutral (dtbbpy) and anionic (TMHD) ligands with broad implications to related Ni-catalyzed radical cross-couplings involving tertiary alkyl radicals as reported by Fu, Baran, and others.^{6,9–11,18}

RESULTS AND DISCUSSION

Methods. All optimizations were performed without restrictions using open-shell, dispersion-corrected DFT (with guess = mix keyword) using THF with the CPCM implicit solvation model [noted as UB3LYP-D3/def2-SVP-CPCM-(THF)] as implemented in Gaussian 09 (see Supporting Information for complete reference). Dispersion correction with Becke–Johnson damping (with EmpiricalDispersion = GD3BJ keyword) was also used to calculate the key pathway in the Ni-bipyridine system, and the results were consistent with those calculated with zero-damping (see Figure S9 in the Supporting Information for comparison of calculated results). Stability tests were conducted (with stable keyword) on all singlet species to confirm that the wave functions are stable as implemented in Gaussian 09, and all singlet species were identified as closed-shell except ¹F' and ¹G' based on S² values (shown in the Coordinates and Energetics section in the Supporting Information). Further, for comparison and to refine energetics, we also performed single-point energy calculations using a larger basis set (def2-TZVPP), different solvents used experimentally (DMA and THF), other

dispersion-corrected DFT functionals (e.g., UM06), and the DLPNO–CCSD(T) method (in ORCA; see Supporting Information for complete reference). These methods have been used extensively to rationalize and predict reactivity and selectivity in transition-metal-catalyzed transformations, including Ni-catalyzed cross-couplings.¹³ Overall, all methods lead to the same conclusions (see Supporting Information for details). For simplicity, only the energies obtained from UB3LYP-D3/def2-TZVPP-CPCM (DMA or THF) will be discussed here (see Figure S1 in the Supporting Information for energetics using other methods of the Ni-TMHD system). For all purported intermediates, we considered both low- and high-spin states (i.e., singlet/doublet and triplet/quartet) and performed a manual conformational search to identify the lowest energy structure (see Figure S2 in the Supporting Information). Initially, to reduce the computational cost, we modeled the 2,2,6,6-tetramethyl-3,5-heptanedionate ligand used experimentally (red; Scheme 1B) as acetylacetonate. Notably, the acac ligand has also enabled nickel-catalyzed cross-couplings with tertiary radicals albeit with lower yields, as demonstrated by us and Baran.^{9,10} Nonetheless, to validate our model, we also compared the lowest energy pathways using the much bulkier TMHD ligand. The calculated energy values and the obtained structures with the TMHD ligand are similar to those using the acac ligand (see Figure S15 in the Supporting Information).

Previously, we used open-shell DFT to investigate the mechanism of the dual photoredox/Ni-catalyzed cross-coupling between aryl bromides and *benzyl radicals*.¹⁷ Therein, we found that the energetically favored pathway, using neutral bipyridine and bisoxazoline ligands, proceeds via facile radical addition to Ni(0) followed by oxidative addition to the aryl halide to form a Ni(III) intermediate [i.e., Ni(0)/Ni(I)/Ni(III) mechanism]. Importantly, although based on the energetics, we could not rule out the Ni(0)/Ni(II)/Ni(III) pathway; we found that both pathways converged to a Ni(III) intermediate, which could undergo reversible radical dissociation/addition prior to undergoing irreversible (and stereo-determining) inner-sphere C(sp²)-C(sp³) bond formation. Based on these studies, we first explored the effect of an anionic ligand on the purported mechanisms for comparison (Figure 1).

Ni-TMHD Catalytic System with *tert*-Butyl Radical as Substrate. As shown in Figure 1 (red), in the absence (or low concentration) of alkyl radical, (acac)Ni(I)⋯substrate complex ²A could undergo *facile* oxidative addition via ²A-TS (overall barrier is only 4.6 kcal/mol), leading to a Ni(III) ²B intermediate (~11 kcal/mol downhill in energy). We also located a different, slightly higher energy conformation (²A'-TS) that permits direct oxidative addition from ²A', after isomerization from ²A to complex ²A', to form Ni(III) ²B (green-red). In turn, Ni(III) ²B will then undergo an internal reorganization from distorted tetrahedral to distorted square planar conformation, leading to Ni(III) ²C (uphill in energy by ~6 kcal/mol from ²B).¹⁹ The distorted square planar ²C is now poised to undergo facile radical “outer-sphere” cross-coupling with the tertiary alkyl radical. Specifically, in this geometry, the tertiary alkyl radical is energetically favored to complex, but not add, to the Ni center, leading to ³C-complex. Finally, this radical will then undergo a spin-selective (barrier is only 3.1 kcal/mol from ³C-complex) outer-sphere C(sp²)-C(sp³) bond formation (via triplet spin state ³C-TS), leading to the desired product and bromo Ni(acac) products (³P_A + *t*-

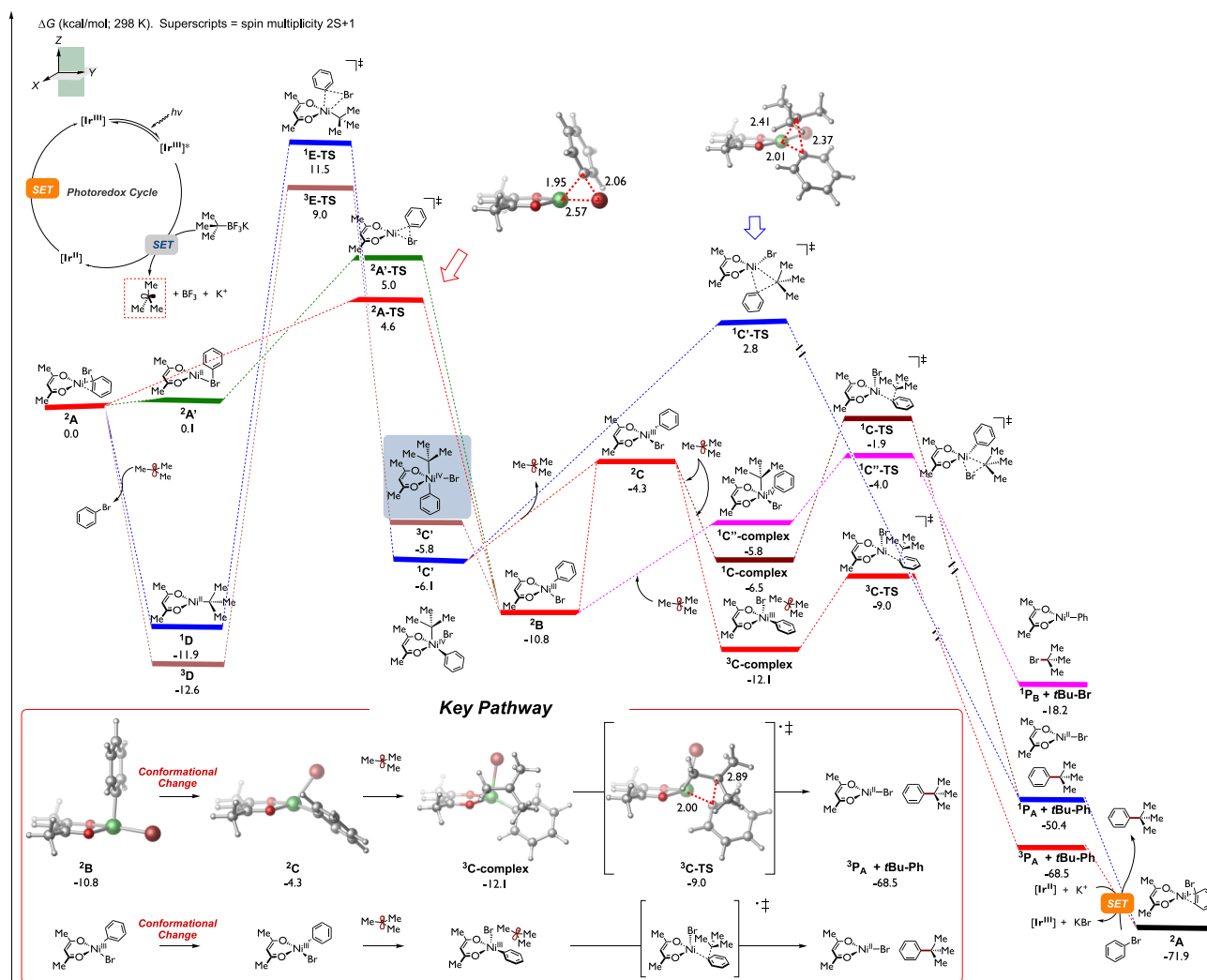


Figure 1. Calculated energetics of the Ni-catalyzed cross-coupling between *tert*-butyl radical and bromobenzene using anionic TMHD as ligand. Relative Gibbs free energy values were computed at the UB3LYP-D3/def2-TZVPP-CPCM(DMA)//UB3LYP-D3/def2-SVP-CPCM(THF) level.

Bu-Ph) downhill in energy by ~ 69 kcal/mol. $^3\text{P}_\text{A}$ will then undergo an energetically favorable single electron transfer (SET) with the photocatalyst ($[\text{Ir}^{\text{III}}] = [\text{Ir}\{\text{dFCF}_3\text{ppy}\}_2(\text{bpy})]^+$) to generate the nickel catalyst ^2A with concomitant formation of KBr complex to restart the transition metal catalytic cycle (see Figure S17 in the Supporting Information for details).

Notably, the outer-sphere radical coupling via the singlet spin state ($^1\text{C-TS}$) is found to be ~ 7 kcal/mol higher in energy than the calculated $^3\text{C-TS}$ and is thus not productive.¹⁴ We also explored alternative pathways initiated from radical addition to the phenyl bromide Ni(acac) complex ^2A , but all were found higher in energy. Specifically, as shown in Figure 1 (light brown), in the presence of alkyl radical, radical addition to ^2A and concomitant displacement of phenyl bromide could lead to singlet ^1D , which is exergonic by ~ 12 kcal/mol. The triplet spin state (^3D) is also favored by more than 12 kcal/mol. From ^3D , calculations predict a high-barrier (~ 22 kcal/mol) and rate-determining, oxidative addition via triplet spin state ($^3\text{E-TS}$), leading to $^3\text{C}'$. Unexpectedly, this $^3\text{C}'$ intermediate will then undergo barrierless tertiary radical dissociation, leading back to distorted tetrahedral ^2B , merging both pathways. Alternatively, $^3\text{C}'$ could undergo an intersystem crossing ($^3\text{C}' \rightarrow ^1\text{C}'$; not calculated) followed by radical

dissociation leading back to distorted square planar ^2C intermediate. Ultimately, both of these pathways will lead to triplet spin, outer-sphere $\text{C}(\text{sp}^2)\text{-C}(\text{sp}^3)$ bond formation (via $^3\text{C-TS}$). Based on prior computational studies by us and others,^{13–17} we also considered the possibility of the commonly proposed singlet spin state, inner-sphere reductive elimination ($^1\text{C}'\text{-TS}$) that can be directly accessed from $^1\text{C}'$. However, this pathway was found much higher in energy (~ 12 kcal/mol) than the triplet spin, outer-sphere $\text{C}(\text{sp}^2)\text{-C}(\text{sp}^3)$ bond formation, and thus this pathway, with an anionic diketonate ligand, can be ruled out. In addition, based on our prior work in Fe-catalyzed radical cross-couplings,²⁰ we also located (pink) the reductive elimination transition state ($^1\text{C}''\text{-TS}$) and the corresponding Ni-tertiary alkyl intermediate $^1\text{C}''\text{-complex}$, which leads to the formation of tertiary alkyl bromide (*t*-Bu-Br) and phenyl Ni(acac) ($^1\text{P}_\text{B}$). However, this pathway was also found to be higher in energy and thus unproductive. Nonetheless, akin to Ni(I)-Ar intermediates invoked in related cross-coupling reactions,⁶ in principle, LNi-Ph ($^1\text{P}_\text{B}$) could undergo oxidative addition to the tertiary alkyl bromide (reverse reaction, the barrier is only ~ 14 kcal/mol), leading to $^1\text{C}''\text{-complex}$. In turn, these complex computational results also predict radical dissociation to form distorted ^2B

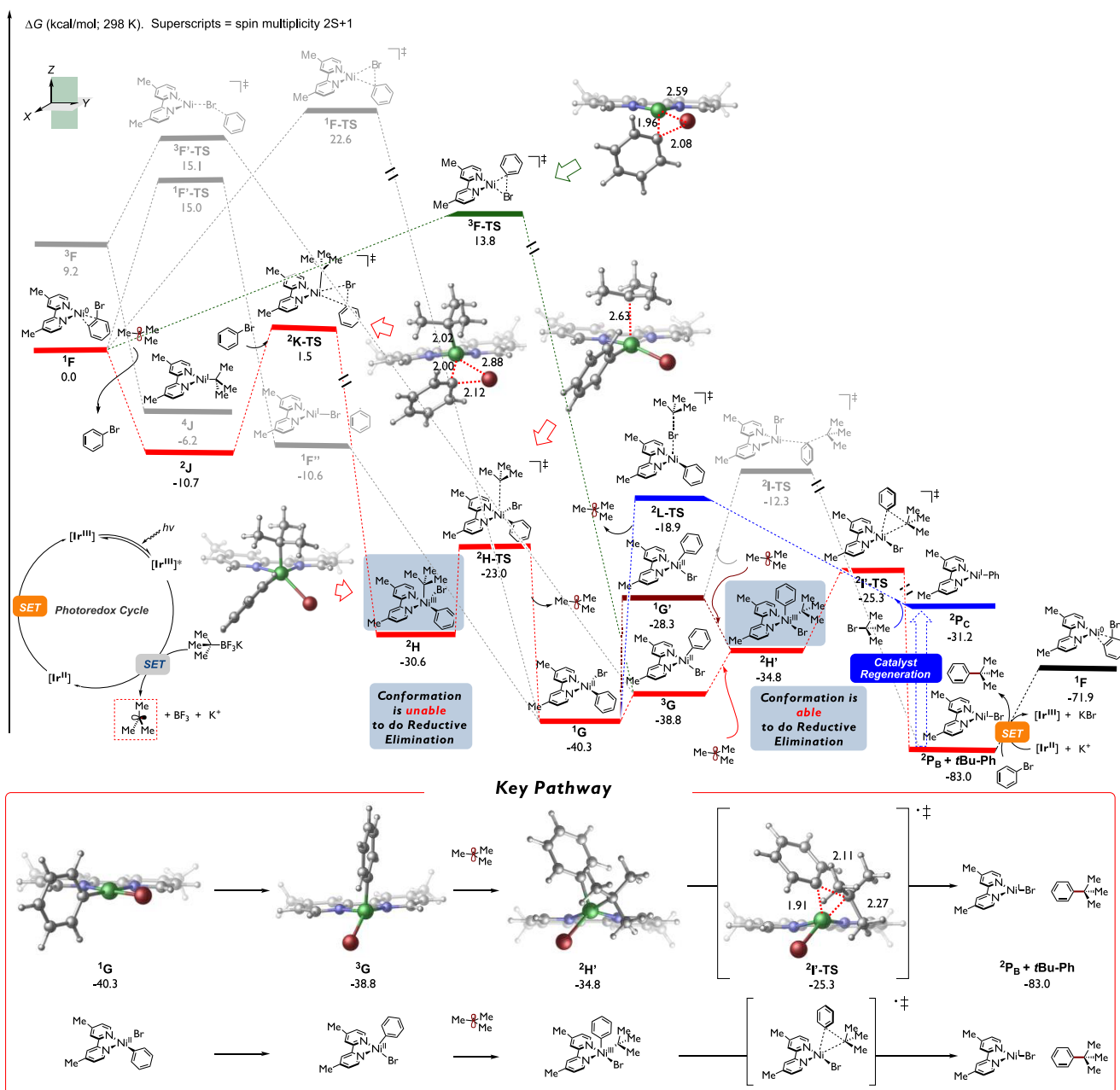


Figure 2. Calculated energetics of the Ni-catalyzed cross-coupling between *tert*-butyl radical and bromobenzene using neutral bipyridine as ligand. Relative Gibbs free energy values were computed at the UB3LYP-D3/def2-TZVPP-CPCM(THF)//UB3LYP-D3/def2-SVP-CPCM(THF) level of theory.

and, ultimately, lead to outer-sphere $C(sp^2)-C(sp^3)$ bond formation. Thus, independent of active nickel species (LNi, LNi-alkyl, or LNi-aryl; L = acac), these calculations revealed a new mechanistic manifold in which tertiary alkyl radicals involved in Ni-diketonate systems are predicted to proceed via outer-sphere $C(sp^2)-C(sp^3)$ bond formation via a triplet spin state. We also considered the likelihood of explicit DMA solvent coordinating to the key nickel species 2A or 2C and promoting ligand dissociation. However, calculations showed that the DMA solvent is unlikely to cause ligand dissociation during the transition metal catalytic cycle (see Figure S14 in the Supporting Information). Moreover, we also carried out experiments using excess TMHD anionic ligand (see Supporting Information). These results showed that excess TMHD ligand (50 and 100 mol %), which would

coordinatively saturate the nickel intermediates, has a minor effect on the efficiency of the system (*vide infra*). Finally, the electronic properties of the aryl bromide do not change the overall mechanistic conclusions (see Figure S3 in the Supporting Information).

Overall, as shown in Figure 1 (inset), the key findings from calculations are summarized as follows: For anionic diketonate-Ni systems involving tertiary alkyl radicals (i.e., as reported by Molander,⁹ Baran,^{10a} and Shenvi^{10b}) after oxidative addition from Ni(I) complex 2A , distorted tetrahedral Ni(III) species 2B can be formed, which requires a conformational change to form the distorted square planar 2C . Subsequently, 2C can form the triplet spin 3C -complex with a tertiary alkyl radical, followed by a triplet spin, outer-sphere $C(sp^2)-C(sp^3)$ bond-forming pathway via 3C -TS to generate the desired product

and bromo Ni(acac) ($^3P_A + t\text{-Bu-Ph}$). In sum, independent of mechanism, in the presence of tertiary alkyl radicals, these results strongly support a novel, low-barrier, spin-selective “outer-sphere” radical cross-coupling pathway via triplet spin state and, contrary to commonly proposed pathways, disfavor the formation of sterically hindered halo-aryl-alkyl-Ni intermediates using anionic ligands.²¹ These results could be applied to a wide range of experimental observations in which privileged anionic ligands, in combination with nickel complexes, allow radical cross-coupling with tertiary radical precursors.^{9,10}

Ni-Bipyridine Catalytic System with *t*-Bu Radical Substrate. Previously, neutral bipyridine ligands in combination with nickel as catalyst failed to undergo $C(sp^2)-C(sp^3)$ cross-couplings with acyclic tertiary radical under dual photoredox/nickel catalysis (Scheme 1B). Nonetheless, this bipyridyl-nickel system has found success for a wide range of Ni-catalyzed radical $C(sp^2)-C(sp^3)$ cross-couplings with secondary and cyclic tertiary alkyl radical precursors, and many groups, including ours,^{13c,17,22c} have taken advantage of this reactivity to promote selective dicarbofunctionalization of olefins.^{16,22} However, despite the widespread utility of the bipyridyl-nickel system in organic synthesis with tertiary alkyl radicals, the mechanism and, in particular, the nature of the critical C–C bond formation is not known. To gain insights from this divergent reactivity with tertiary alkyl radicals, we examined the competing reaction pathways (Figure 2, see Figure S4 in the Supporting Information for energetics using other methods).

Ni(0)/Ni(I)/Ni(III) Pathway. As with previous calculations, in the presence of alkyl radical, overall the lowest energy pathway (red) proceeds via barrierless *tert*-butyl radical addition to Ni(0), leading to Ni(I) intermediate 2J . In turn, Ni(I) 2J undergoes oxidative addition to aryl halide via $^2K\text{-TS}$; the overall barrier is ~ 12 kcal/mol from 2J , leading to Ni(III) intermediate 2H . However, despite numerous attempts, we were unable to locate the direct, inner-sphere reductive elimination from this isomer. Instead, we found a very low barrier tertiary alkyl radical dissociation (via $^2H\text{-TS}$) that leads to the formation of square planar Ni(II) intermediate 1G . This square planar aryl halide Ni(II) intermediate is favored to undergo an intersystem crossing/conformational change to form the tetrahedral, triplet spin state Ni(II) intermediate 3G . In turn, 3G is now poised to undergo radical addition to form Ni(III) intermediate $^2H'$ followed by inner-sphere reductive elimination (via $^2I'\text{-TS}$), leading to the desired products 2P_B and *t*-Bu-Ph, which is exergonic by 83 kcal/mol. After the $C(sp^2)-C(sp^3)$ bond-forming step, SET can occur between the bromo Ni species and the reduced Ir photocatalyst to regenerate the Ni(0) catalytic species 1F with concomitant formation of KBr complex and restart the transition metal catalytic cycle (see Figure S17 in the Supporting Information for details). Overall, catalyst regeneration is ~ 11 kcal/mol uphill in energy but, based on the free energy span, energetically favorable. Given the prevalence of proposed Ni(I)/Ni(III)/Ni(I) pathways by the community and the lack of understanding of the dynamic effects in nickel-catalyzed radical cross-coupling reactions, we conducted preliminary quasi-classical dynamics simulations on the transition state of oxidative addition $^2K\text{-TS}$ and that of reductive elimination $^2I'\text{-TS}$, respectively (see Figure S13 in the Supporting Information). Simulated results suggest that starting from $^2K\text{-TS}$ in the forward direction, 60% of the trajectories resulted

in the formation of a Ni(III) intermediate, while 40% formed the square planar Ni(II) intermediate and concomitant dissociation of *tert*-butyl radical. No cross-coupling product (*t*-Bu-Ph) was observed in any simulated trajectory (see Figure S13a in the Supporting Information for details). These observations support our static DFT calculations that the Ni(III) intermediate obtained from direct oxidative addition on the alkyl Ni(I) intermediate cannot undergo reductive elimination, but rather undergoes radical dissociation to generate the square planar Ni(II) intermediate 1G . On the other hand, within dynamics calculations propagated from $^2I'\text{-TS}$ in the reverse direction, all trajectories ended up in the Ni(III) intermediate without radical dissociation from the Ni center or structural rearrangement (see Figure S13b in the Supporting Information for details). This is also consistent with our assumption concerning the overall process because the radical addition to Ni involves a change of spin state of the Ni(II) species, while quasi-classical dynamics simulations only operate in a single spin state.²³ From a broader perspective, these results suggest a novel Ni(0)/Ni(I)/Ni(III)/Ni(II)/Ni(III)/Ni(I) pathway in bipyridine-nickel radical cross-couplings with tertiary alkyl radicals.

Ni(0)/Ni(II)/Ni(III) Pathway. In the absence (or low concentration) of a *tert*-butyl radical, Ni(0) could undergo oxidative addition via the triplet spin state ($^3F\text{-TS}$; green), leading directly to the productive tetrahedral, triplet spin state Ni(II) 3G intermediate, thus merging both Ni(0)/Ni(I)/Ni(III)/Ni(II) (red) and Ni(0)/Ni(II) (green) pathways. We also considered the possible outer-sphere C–C bond formation pathway between *tert*-butyl radical and Ni(II) intermediate, but the transition states of both the doublet ($^2I\text{-TS}$) and quartet spin state pathways ($^4I\text{-TS}$) are higher in energy compared to $^2I'\text{-TS}$ (see Figure S4 in the Supporting Information for details). Therefore, inner-sphere reductive elimination via Ni(III) intermediate $^2H'$ is preferred to that of the outer-sphere pathway from the Ni(II) intermediate in Ni-bipyridine catalytic systems.

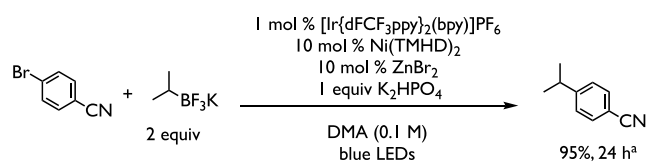
Ni(I)/Ni(II)/Ni(III) Pathway. Previously, alkyl halide activation by Ni(I) species (akin to 2P_C) have been proposed in a range of Ni-catalyzed cross-couplings.²⁴ As shown in Figure 2 (blue), in these cases, aryl bipyridine-Ni(I) could undergo halogen abstraction (via $^2L\text{-TS}$; barrier ~ 12 kcal/mol from 2P_C), leading to the Ni(II) 1G , thus also merging the cross-coupling cycles. Finally, Ni(II) 1G will need to undergo an isomerization/spin-crossing to form the productive tetrahedral Ni(II) 3G , which, after barrierless radical addition, will form the productive Ni(III) $^2H'$. Finally, inner-sphere reductive elimination (via $^2I'\text{-TS}$) will lead to the desired product and bromo Ni(I). From a broader perspective, although the pathway for catalyst regeneration from the bromo Ni(I) varies among nickel-catalyzed cross-coupling methods [e.g., it could undergo SET by photocatalyst or external reductant to form a Ni(0) 1F or, alternatively, could undergo transmetalation to form the Ni(I) $^2P_{C6}$], calculations show that these systems involving tertiary alkyl radicals share the same critical $C(sp^2)-C(sp^3)$ formation step! As an example, the phenyl bpy-Ni(I) species was proposed to be obtained via transmetalation in Fu's experiments.⁶ The overall key findings of these calculations are summarized as follows (Figure 2; inset): after singlet spin square planar Ni(II) species 1G forms, this species needs to undergo intersystem crossing/conformational change to generate the triplet spin tetrahedral 3G complex followed by tertiary alkyl radical addition to form Ni(III)

intermediate $^2\text{H}'$ (see Figure S6 in the Supporting Information for more detailed analysis). The requirement for the tetrahedral Ni(II) conformation to undergo Ni(II)/Ni(III) radical addition was also reported in a recent paper with a neutral bis(oxazoline) ligand, in which phenyl bromo Ni(II)-bis(oxazoline) is in a square planar geometry, while the radical adds to a tetrahedral phenyl bromo Ni(II) species.^{13e} Moreover, the results of our preliminary quasi-classical dynamics calculation are consistent with this suggested pathway (see Figure S7 and Figure S8 in the Supporting Information). Finally, $^2\text{H}'$ will undergo a doublet spin, inner-sphere reductive elimination pathway via $^2\text{I}'\text{-TS}$ to generate the desired C(sp²)-C(sp³) cross-coupling product and bromo Ni(bipyridine) ($^2\text{P}_\text{B} + t\text{-Bu-Ph}$).

Origin of the Difference in the C(sp²)-C(sp³) Bond-Forming Step in Ni-TMHD and Ni-Bipyridine Catalytic Systems. As shown above, independent of the operative catalytic active species, all pathways converge at the Ni(II) and tertiary radical. Thus, assuming facile intersystem crossing/conformational change, the barrier for inner-sphere tertiary radical C(sp²)-C(sp³) cross-coupling using the neutral bipyridine nickel system (~ 15 kcal/mol from ^1G) is much higher in energy than using an anionic diketonate nickel system (~ 4 kcal/mol). These relative barriers are consistent with the experiments that prevented the formation of the desired C(sp³)-C(sp²) bond using acyclic tertiary radicals under the Ni-bipyridyl/PC system.⁹ Moreover, the higher barrier could lead to unwanted side reactions with tertiary radicals such as H atom abstraction from the solvent, as observed by us.^{9,25} Further, in accord with experiments by Fu,⁶ switching to solvent systems with high bond dissociation energies (BDEs) (e.g., benzene) likely increases the barrier for H-abstraction and, in turn, allows favorable kinetics to promote C(sp³)-C(sp²) bond formation with tertiary alkyl radicals. The competence of alkyl radical undergoing H-abstraction (e.g., with solvent or other reagents) or C(sp³)-C(sp²) bond formation is not only seen in the Ni-bipyridine system in Fu's report⁶ but also observed in the Ni-TMHD(acac) system,¹⁰ suggesting that the H-abstraction reactions with alkyl radical are competing with C-C bond formation in related cross-coupling reactions and the efficiency of C-C bond formation (e.g., H-abstraction versus C-C cross-coupling) is likely system dependent.

On the other hand, the cross-coupling barrier for the diketonate-nickel system is only ~ 3 kcal/mol from the respective nickel complex and tertiary alkyl radical. Thus, we attribute the efficiency of Ni-diketonate systems with tertiary alkyl radicals under photocatalytic conditions^{9,10} to the nature of the outer-sphere C-C bond formation that avoids the formation of a high-energy, sterically congested aryl-alkyl-halo-Ni intermediate. Experiments using less sterically hindered secondary alkyltrifluoroborates also led to the desired product in 95% yield (Scheme 2). However, in contrast to tertiary alkyl

Scheme 2. Cross-Coupling of Secondary Alkyltrifluoroborates with Ni-TMHD



radicals, through DFT calculations we found that the favored pathway for less sterically hindered secondary alkyl radicals is via inner-sphere C-C bond formation with overall barriers for C-C bond formation of ~ 9 kcal/mol (see Figure S21 in the Supporting Information). Presumably, the less sterically hindered secondary alkyl radical (in contrast to the tertiary alkyl radical) does not pay a penalty to form the aryl-alkyl-halo-Ni species and can quickly undergo inner-sphere C-C bond formation. In contrast to the bipyridyl-Ni system, these results suggest that for acac/TMHD-Ni systems, the nature of the C-C bond formation and whether inner- or outer-sphere C(sp²)-C(sp³) is operative are dependent on the steric properties of the alkyl radical. Surprisingly, for cyclic tertiary systems, we found that this system did not undergo aryl substrate activation in the experiment, leading, after 24 h, to the recovered starting material (see Supporting Information). Although the reasons for lack of reactivity are not completely understood, computations showed that, if the cyclic radical were to engage with the nickel in the cross-coupling cycle, the formation of 1-bromoadamantane via inner-sphere C-Br bond formation is favored over C-C bond formation (see Figure S22 in the Supporting Information). However, because substoichiometric additives (e.g., LiBr, ZnBr₂, ZnCl₂) were found to influence the reactivity of substrates in the Ni-TMHD system where the bicyclic substrate (adamantyl-like) also failed,¹⁰ the exact reason for the failure of the adamantyl substrate remains unknown and is under exploration in our group.

To understand more fully the origins of the distinct reactivity (i.e., ligand effect on C-C bond formation), we conducted an activation strain-distortion/interaction analysis.²⁶ As shown in Table 1, comparing inner-sphere and

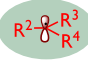
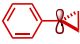

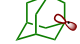
Table 1. Activation Strain-Distortion/Interaction Analysis of the C(sp²)-C(sp³) Bond Formation Step^a

| | | $\Delta E_{\text{activation}}$ (kcal/mol) | $\Delta E_{\text{distortion}}$ (kcal/mol) | $\Delta E_{\text{interaction}}$ (kcal/mol) |
|--------------|--------------|--|--|---|
| Outer-Sphere | | 19.1 | 28.6 | -9.6 |
| | | 12.2 | 17.1 | -4.9 |
| Inner-Sphere | | -3.9 | 41.0 | -44.9 |
| | | 2.7 | 16.0 | -14.0 |
| Outer-Sphere | | -13.3 | 18.4 | -31.7 |
| | Inner-Sphere | | -13.2 | 20.8 |

^aRelative electronic energy values were computed with respect to the separate corresponding phenyl-bromo-Ni-ligand species and *tert*-butyl radical at the UB3LYP-D3/def2-TZVPP//UB3LYP-D3/def2-SVP-CPCM(THF) level of theory.

outer-sphere C-C bond formation transition states in the Ni-bipyridine catalytic system (green background), the relative activation electronic energy of inner-sphere transfer is negative (-3.9 kcal/mol) while that of outer-sphere transfer is positive, meaning that the C-C bond formation is favorable via an inner-sphere pathway (see Table S1 in the Supporting Information for energetics using other methods). Despite the

Table 2. Analysis of Distinct Alkyl Radical Reactivity in the Ni-Bipyridine System^a

| Radical | ΔG (kcal/mol; 298K) | | | BDE of Ni-C(sp ³) (ΔH ; kcal/mol) | $\Delta E_{\text{activation}}$ (kcal/mol) | $\Delta E_{\text{distortion}}$ (kcal/mol) | $\Delta E_{\text{interaction}}$ (kcal/mol) |
|---|-----------------------------|------------|---------------|---|--|--|---|
| | 1G | 2H' | 2I'-TS | | | | |
|  | | 5.6 | 15.0 | 11.0 | -3.9 | 41.0 | -44.9 |
|  | 0.0 | -2.3 | 4.2 | 18.3 | -13.9 | 37.4 | -51.2 |
|  | | -3.4 | 2.7 | 17.9 | -14.2 | 33.1 | -47.3 |
|  | | -3.3 | 7.3 | 18.3 | -8.0 | 32.4 | -40.4 |

^aGray: calculated energetics on the inner-sphere reductive elimination step with different alkyl radicals. Green: related analysis on bond dissociation energy of the Ni(III) intermediate. Yellow: activation strain-distortion/interaction analysis on the reductive elimination transition state [relative electronic energy values were calculated with respect to the separate corresponding Ni(II) species and *tert*-butyl radical]. Relative free energy values were computed concerning the Ni(II) species at the UB3LYP-D3/def2-TZVPP-CPCM(THF)//UB3LYP-D3/def2-SVP-CPCM(THF) level of theory; bond dissociation energy and relative electronic energy values were calculated at the UB3LYP-D3/def2-TZVPP//UB3LYP-D3/def2-SVP-CPCM(THF) level of theory.

larger distortion energy of the inner-sphere compared to the outer-sphere pathway, its interaction energy compensates for the larger distortion energy and makes the overall process favorable. On the other hand, for the Ni-TMHD system (blue background) both inner-sphere and outer-sphere transition states possess negative activation electronic energies, and both their distortion energy and interaction energy are close to each other. Although the inner-sphere and outer-sphere pathways of the Ni-TMHD system do not show as large a difference as those of the Ni-bipyridine system, the triplet spin state outer-sphere pathway is still found most favorable (-13.3 kcal/mol) because of its lower distortion energy (18.4 kcal/mol) and larger interaction energy (-31.7 kcal/mol).

Origin of Distinct Alkyl Reactivity in the Ni-Bipyridine System. Because of the observed experimental differences of structurally different alkyl radicals in Ni-bipyridine systems,⁹ we became interested in exploring the potential reactivity of different alkyl radicals in the above key pathways (Table 2). Specifically, in the dual photoredox-Ni catalytic system, C(sp²)-C(sp³) cross-coupling succeeded with aryl bromides as the electrophile and potassium 1-adamantyltrifluoroborate and potassium 1-phenylcyclopropyltrifluoroborate as the nucleophile (Scheme 1B).⁹ Therefore, we compare here the reactivity of the *tert*-butyl radical, isopropyl radical, 1-phenylcyclopropyl radical, and 1-adamantyl radical in the key inner-sphere reductive elimination step (see Figure S6 in the Supporting Information for the comparison of different radicals in other steps). As shown in Table 2 (gray), using distinct Ni(II) species **1G** and the purported alkyl radicals as a reference, we observed that the relative energy values of Ni(III) **2H'** intermediates, which are reactive toward inner-sphere reductive elimination, vary for different alkyl radicals. First, we observed that the Ni(III) intermediate with the *tert*-butyl radical (black) is endergonic by 5.6 kcal/mol, while all other Ni(III) intermediates with tertiary and secondary alkyl radicals (red, blue, and green) are exergonic (by 2–3 kcal/mol). These results suggest that the *tert*-butyl radical is more favorable to dissociate from the Ni(III) center to form Ni(II) and a *tert*-butyl radical, while for the other tertiary and secondary alkyl radicals the energetics favor the formation of a

Ni(III) complex. This trend is also observable in the barriers for reductive elimination. Specifically, the barriers for inner-sphere reductive elimination of cyclic and secondary alkyl radicals are significantly lower (by 7–12 kcal/mol) than with the *tert*-butyl radical. This observation is consistent with the results in experiments by Fu, where 1-iodoadamantane, with the assumption of the 1-adamantyl radical being generated *in situ*, can also be cross-coupled under nonphotocatalytic condition despite their slightly higher barrier of reductive elimination (7.3 kcal/mol) compared to a secondary isopropyl radical.⁶

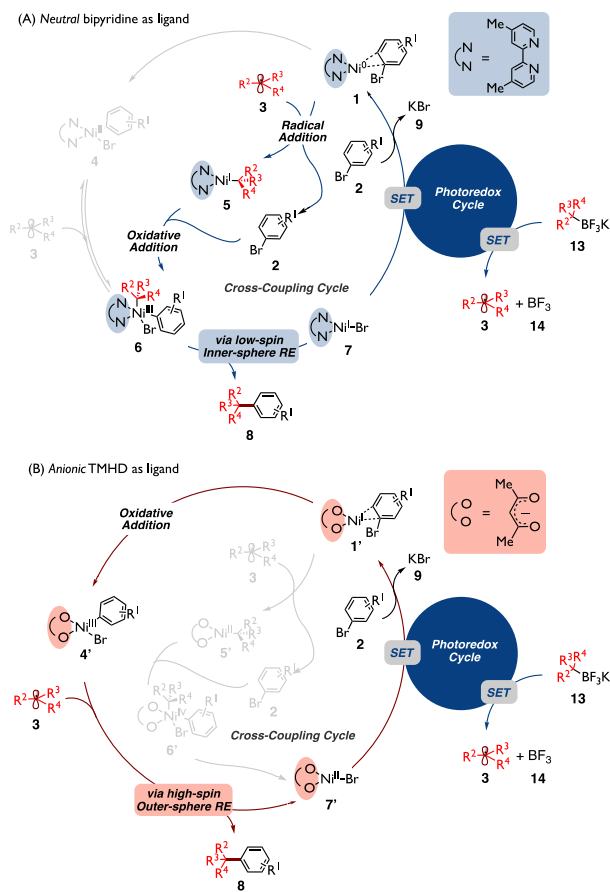
Further, to gain insight into the observed trends, we computed the BDE of the Ni-C(sp³) bond with different alkyl radicals. As shown in Table 2 (green), we found that the Ni-C(*tert*-butyl) bond has the lowest BDE (11.0 kcal/mol), which indicates that the dissociation of the *tert*-butyl radical from the Ni(III) center is easier than the dissociation of secondary and cyclic tertiary alkyl radicals (~18 kcal/mol). Also, from an activation strain-distortion/interaction analysis on the reductive elimination step (yellow), we found that the transition state with the *tert*-butyl radical shows a less negative activation energy and larger distortion energy compared to the rest of the systems. This suggests that reductive elimination with the *tert*-butyl radical is less favorable because it needs to pay a higher energy penalty for distortion to reach the geometry in the C(sp²)-C(sp³) bond-forming step. Although the exact mechanism of bipyridyl-nickel-involved radical cross-coupling reactions could be significantly different depending on the experimental condition and applied substrates/additives, our findings on the nature of C(sp²)-C(sp³) bond formation can be used to explain some of the observed selectivity in the selective dicarbofunctionalization of olefins with a broad variety of secondary and tertiary alkyl radical precursors.^{13c,16,17,22}

CONCLUDING REMARKS

In summary, quantum mechanical calculations and quasi-classical direct dynamics simulations have been used to investigate the mechanism of dual photoredox-Ni-catalyzed C(sp²)-C(sp³) cross-coupling reactions between tertiary

alkyltrifluoroborates and aryl halides with Ni bipyridine- and diketonate-based catalytic systems. Calculations showed the prominent effect of the charge on the ligand on key catalytic intermediates and the $C(sp^2)-C(sp^3)$ bond-forming step in such transformations. Specifically, as outlined in Scheme 3, in

Scheme 3. Catalytic Cycle for Photoredox/Ni Dual Catalytic System Using (A) Neutral (Blue) and (B) Anionic (Red) Ligands



the Ni-TMHD (anionic ligand) system, the tertiary alkyl radical can directly interact with the aryl-bromo-Ni species to obtain the desired product via a high-spin, outer-sphere reductive elimination pathway without engaging the Ni center first. In the Ni-bipyridine (neutral ligand) system, as shown by transition state calculations and supported by quasi-classical dynamics, the Ni(III) intermediate directly obtained from oxidative addition on alkyl Ni(I) species needs to undergo radical dissociation to form the singlet-spin square planar Ni(II) intermediate. Then, it needs to undergo a conformational change/intersystem crossing followed by radical addition to gain access to the productive tetrahedral triplet spin state Ni(III) intermediate, followed by subsequent low-spin, inner-sphere reductive elimination to generate the desired product and halide Ni(I). From a broader perspective, although the pathway for catalyst regeneration from the halide Ni(I) varies among different nickel-catalyzed cross-coupling methods [e.g., it could undergo SET by photocatalyst or external reductant to form a Ni(0) or, alternatively, could undergo transmetalation to form an aryl Ni(I)], calculations show that these systems share the same critical $C(sp^2)-C(sp^3)$ formation step!

The reactivity of different alkyl radicals was also compared in the Ni-bipyridine system. This information suggests that relatively subtle changes in the alkyl radical precursors and ligands have a dramatic effect on the mechanism of the reactions. Nonetheless, this investigation sheds light on mechanistic possibilities that were never considered previously and inspires the design of catalytic systems and modification of substrates for Ni-catalyzed $C(sp^2)-C(sp^3)$ cross-coupling reactions. Further exploration will be focused on the comparison of more neutral and anionic ligand systems and the behavior of different alkyl radicals based on the mechanistic models proposed here.

■ ASSOCIATED CONTENT

Supporting Information

The Supporting Information is available free of charge at <https://pubs.acs.org/doi/10.1021/jacs.0c02355>.

Experimental and computational details, coordinates, and spectral data (PDF)

■ AUTHOR INFORMATION

Corresponding Authors

Osvaldo Gutierrez – Department of Chemistry and Biochemistry, University of Maryland, College Park, Maryland 20742, United States; orcid.org/0000-0001-8151-7519; Email: ogs@umd.edu

Gary A. Molander – Roy and Diana Vagelos Laboratories, Department of Chemistry, University of Pennsylvania, Philadelphia, Pennsylvania 19104-6323, United States; orcid.org/0000-0002-9114-5584; Email: gmolandr@sas.upenn.edu

Authors

Mingbin Yuan – Department of Chemistry and Biochemistry, University of Maryland, College Park, Maryland 20742, United States

Zhihui Song – Department of Chemistry and Biochemistry, University of Maryland, College Park, Maryland 20742, United States

Shorouk O. Badir – Roy and Diana Vagelos Laboratories, Department of Chemistry, University of Pennsylvania, Philadelphia, Pennsylvania 19104-6323, United States

Complete contact information is available at: <https://pubs.acs.org/doi/10.1021/jacs.0c02355>

Author Contributions

‡M. Yuan and Z. Song contributed equally.

Notes

The authors declare no competing financial interest.

■ ACKNOWLEDGMENTS

We are grateful for the financial support by the NSF (CAREER 1751568). O.G. is grateful to the University of Maryland College Park for start-up funds and computational resources from UMD Deepthought2 and MARCC/BlueCrab HPC clusters and XSEDE (CHE160082 and CHE160053). G.M. thanks the National Institutes of General Medical Sciences for support (R35 GM 131680).

REFERENCES

- (1) de Meijere, A.; Brašė, S.; Oestreich, M., Eds. *Metal-Catalyzed Cross-Coupling Reactions and More*; Wiley-VCH Verlag GmbH: Weinheim, 2014.
- (2) (a) Cho, C. H.; Yun, H. S.; Park, K. Nickel(0)-Catalyzed Cross-Coupling of Alkyl Arenesulfonates with Aryl Grignard Reagents. *J. Org. Chem.* **2003**, *68*, 3017–3025. (b) Cheng, Y.; Wu, Y.; Tan, G.; You, J. Nickel Catalysis Enables Oxidative C(sp²)-H/C(sp²)-H Cross-Coupling Reactions between Two Heteroarenes. *Angew. Chem., Int. Ed.* **2016**, *55*, 12275–12279.
- (3) (a) Quasdorf, K. W.; Overman, L. E. Catalytic enantioselective synthesis of quaternary carbon stereocenters. *Nature* **2014**, *516*, 181–191. (b) Das, J. P.; Marek, I. Enantioselective synthesis of all-carbon quaternary stereogenic centers in acyclic systems. *Chem. Commun.* **2011**, *47*, 4593–4623. (c) Christoffers, J.; Baro, A. Stereoselective Construction of Quaternary Stereocenters. *Adv. Synth. Catal.* **2005**, *347*, 1473–1482.
- (4) Lohre, C.; Dröge, T.; Wang, C.; Glorius, F. Nickel-Catalyzed Cross-Coupling of Aryl Bromides with Tertiary Grignard Reagents Utilizing Donor-Functionalized N-Heterocyclic Carbenes (NHCs). *Chem. - Eur. J.* **2011**, *17*, 6052–6055.
- (5) Joshi-Pangu, A.; Wang, C.-Y.; Biscoe, M. R. Nickel-Catalyzed Kumada Cross-Coupling Reactions of Tertiary Alkylmagnesium Halides and Aryl Bromides/Triflates. *J. Am. Chem. Soc.* **2011**, *133*, 8478–8481.
- (6) Zultanski, S. L.; Fu, G. C. Nickel-Catalyzed Carbon–Carbon Bond-Forming Reactions of Unactivated Tertiary Alkyl Halides: Suzuki Arylations. *J. Am. Chem. Soc.* **2013**, *135*, 624–628.
- (7) (a) Wang, X.; Wang, S.; Xue, W.; Gong, H. Nickel-Catalyzed Reductive Coupling of Aryl Bromides with Tertiary Alkyl Halides. *J. Am. Chem. Soc.* **2015**, *137*, 11562–11565. (b) Wang, X.; Ma, G.; Peng, Y.; Pitsch, C. E.; Moll, B. J.; Ly, T. D.; Wang, X.; Gong, H. Ni-Catalyzed Reductive Coupling of Electron-Rich Aryl Iodides with Tertiary Alkyl Halides. *J. Am. Chem. Soc.* **2018**, *140*, 14490–14497.
- (8) Zhou, Q.; Cobb, K. M.; Tan, T.; Watson, M. P. Stereospecific Cross Couplings To Set Benzylic, All-Carbon Quaternary Stereocenters in High Enantiopurity. *J. Am. Chem. Soc.* **2016**, *138*, 12057–12060.
- (9) Primer, D. N.; Molander, G. A. Enabling the Cross-Coupling of Tertiary Organoboron Nucleophiles through Radical-Mediated Alkyl Transfer. *J. Am. Chem. Soc.* **2017**, *139*, 9847–9850.
- (10) (a) Chen, T.; Zhang, H.; Mykhailiuk, P. K.; Merchant, R. R.; Smith, C. A.; Qin, T.; Baran, P. S. Quaternary Centers by Nickel-Catalyzed Cross-Coupling of Tertiary Carboxylic Acids and (Hetero)-Aryl Zinc Reagents. *Angew. Chem., Int. Ed.* **2019**, *58*, 2454–2458. (b) Green, S. A.; Huffman, T. R.; McCourt, R. O.; Puyl, V.; Shenvi, R. A. Hydroalkylation of Olefins To Form Quaternary Carbons. *J. Am. Chem. Soc.* **2019**, *141*, 7709–7714.
- (11) (a) Tellis, J. C.; Primer, D. N.; Molander, G. A. Single-electron transmetalation in organoboron cross-coupling by photoredox/nickel dual catalysis. *Science* **2014**, *345*, 433–436. (b) Tellis, J. C.; Kelly, C. B.; Primer, D. N.; Joffroy, M.; Patel, N. R.; Molander, G. A. Single-Electron Transmetalation via Photoredox/Nickel Dual Catalysis: Unlocking a New Paradigm for sp³–sp² Cross-Coupling. *Acc. Chem. Res.* **2016**, *49*, 1429–1439. (c) Primer, D. N.; Karakaya, I.; Tellis, J. C.; Molander, G. A. Single-Electron Transmetalation: An Enabling Technology for Secondary Alkylboron Cross-Coupling. *J. Am. Chem. Soc.* **2015**, *137*, 2195–2198.
- (12) For recent reviews, see: (a) Sperger, T.; Sanhueza, I. A.; Kalvet, I.; Schoenebeck, F. Computational Studies of Synthetically Relevant Homogeneous Organometallic Catalysis Involving Ni, Pd, Ir, and Rh: An Overview of Commonly Employed DFT Methods and Mechanistic Insights. *Chem. Rev.* **2015**, *115*, 9532–9586. (b) Vogiatzis, K. D.; Polynski, M. V.; Kirkland, J. K.; Townsend, J.; Hashemi, A.; Liu, C.; Pidko, E. A. Computational Approach to Molecular Catalysis by 3d Transition Metals: Challenges and Opportunities. *Chem. Rev.* **2019**, *119*, 2453–2523.
- (13) For selected examples on computational analysis of nickel-catalyzed reactions, see: (a) Oshita, H.; Suzuki, T.; Kawashima, K.; Abe, H.; Tani, F.; Mori, S.; Yajima, T.; Shimazaki, Y. The effect of π – π stacking interaction of the indole ring with the coordinated phenoxyl radical in a nickel(II)-salen type complex. Comparison with the corresponding Cu(II) complex. *Dalton Trans.* **2019**, *48*, 12060–12069. (b) Slater, J. W.; Marguet, S. C.; Cirino, S. L.; Maugeri, P. T.; Shafaat, H. S. Experimental and DFT Investigations Reveal the Influence of the Outer Coordination Sphere on the Vibrational Spectra of Nickel-Substituted Rubredoxin, a Model Hydrogenase Enzyme. *Inorg. Chem.* **2017**, *56*, 3926–3938. (c) Matsui, J. K.; Gutierrez-Bonet, A.; Rotella, M.; Alam, R.; Gutierrez, O.; Molander, G. A. Photoredox/Nickel-Catalyzed Single-Electron Tsuji–Trost Reaction: Development and Mechanistic Insights. *Angew. Chem.* **2018**, *130*, 16073–16077. (d) Dohm, S.; Hansen, A.; Steinmetz, M.; Grimme, S.; Chęcinski, M. P. Comprehensive Thermochemical Benchmark Set of Realistic Closed-Shell Metal Organic Reactions. *J. Chem. Theory Comput.* **2018**, *14*, 2596–2608. (e) Yin, H.; Fu, G. C. Mechanistic Investigation of Enantioconvergent Kumada Reactions of Racemic α -Bromoketones Catalyzed by a Nickel/Bix(oxazoline) Complex. *J. Am. Chem. Soc.* **2019**, *141*, 15433–15440.
- (14) For an example of nickel-catalyzed transformations via an outer-sphere pathway, see: Jiang, J.; Fu, M.; Li, C.; Shang, R.; Fu, Y. Theoretical Investigation on Nickel-Catalyzed Hydrocarboxylation of Alkynes Employing Formic Acid. *Organometallics* **2017**, *36*, 2818–2825.
- (15) (a) Luo, Y.; Gutierrez-Bonet, A.; Matsui, J. K.; Rotella, M. E.; Dykstra, R.; Gutierrez, O.; Molander, G. A. Oxa- and Azabenzonorbornadienes as Electrophilic Partners under Photoredox/Nickel Dual Catalysis. *ACS Catal.* **2019**, *9*, 8835–8842. (b) Desrosiers, J. N.; Wei, X.; Gutierrez, O.; Savoie, J.; Qu, B.; Zeng, X.; Lee, H.; Grinberg, N.; Haddad, N.; Yee, N. K.; Roschangar, F.; Song, J. J.; Kozłowski, M. C.; Senanayake, C. H. Nickel-catalyzed C-3 direct arylation of pyridinium ions for the synthesis of 1-azafluorenes. *Chem. Sci.* **2016**, *7*, 5581–5586.
- (16) Shu, W.; Garcia-Dominguez, A.; Quiroś, M. T.; Mondal, R.; Cardenas, D. J.; Nevado, C. Ni-Catalyzed Reductive Dicarbofunctionalization of Nonactivated Alkenes: Scope and Mechanistic Insights. *J. Am. Chem. Soc.* **2019**, *141*, 13812–13821.
- (17) Gutierrez, O.; Tellis, J. C.; Primer, D. N.; Molander, G. A.; Kozłowski, M. C. Nickel-Catalyzed Cross-Coupling of Photoredox-Generated Radicals: Uncovering a General Manifold for Stereoconvergence in Nickel-Catalyzed Cross-Couplings. *J. Am. Chem. Soc.* **2015**, *137*, 4896–4899.
- (18) Green, S. A.; Vasquez-Céspedes, S.; Shenvi, R. Iron–Nickel Dual-Catalysis: A New Engine for Olefin Functionalization and the Formation of Quaternary Centers. *J. Am. Chem. Soc.* **2018**, *140*, 11317–11324.
- (19) Identification of geometry is based on the average angle of the corresponding Ni species; see Figure S10 in the [Supporting Information](#) for details.
- (20) (a) Liu, L.; Lee, W.; Zhou, J.; Bandyopadhyay, S.; Gutierrez, O. Radical-clock α -halo-esters as mechanistic probes for bisphosphine-iron-catalyzed cross-coupling reactions. *Tetrahedron* **2019**, *75*, 129–136. (b) Liu, L.; Lee, W.; Yuan, M.; Gutierrez, O. Mechanisms of Bisphosphine Iron-Catalyzed C(sp²)-C(sp³) Cross-Coupling Reactions: Inner-Sphere or Outer-Sphere Arylation? *Comments Inorg. Chem.* **2018**, *38*, 210–237. (c) Lee, W.; Zhou, J.; Gutierrez, O. Mechanism of Nakamura's Bisphosphine Iron-Catalyzed Asymmetric C(sp²)-C(sp³) Cross-Coupling Reaction: The Role of Spin in Controlling Arylation Pathway. *J. Am. Chem. Soc.* **2017**, *139*, 16126–16133.
- (21) Calculations using other substrates and different methods led to the same conclusions (see Figure S3 in the [Supporting Information](#)).
- (22) For selected examples, see: (a) Qin, T.; Cornella, J.; Li, C.; Malins, L. R.; Edwards, J. T.; Kawamura, S.; Maxwell, B. D.; Eastgate, M. D.; Baran, P. S. A General Alkyl-Alkyl Cross-Coupling Enabled by Redox-active Esters and Alkylzinc Reagents. *Science* **2016**, *352*, 801–805. (b) Gu, J.-W.; Min, Q.-Q.; Yu, L.-C.; Zhang, X. Tandem Difluoroalkylation-Arylation of Enamides Catalyzed by Nickel. *Angew. Chem., Int. Ed.* **2016**, *55*, 12270–12274. (c) Campbell, M. W.;

Compton, J. S.; Kelly, C. B.; Molander, G. A. Three-Component Olefin Dicarbofunctionalization Enabled by Nickel/Photoredox Dual Catalysis. *J. Am. Chem. Soc.* **2019**, *141*, 20069–20078.

(23) We investigated the possibility of ligand dissociation from a Ni(III) intermediate, which might invoke structural rearrangement of Ni(III) intermediates. However, based on our calculations the complete ligand dissociation is unlikely to occur on neither ^2H nor $^2\text{H}'$ since these processes are both uphill in energy (see Figure S19 for energetic details in the Supporting Information). In addition, although transient decoordination of one of the pyridine ligands was observed in quasi-classical dynamics simulations on $^2\text{K-TS}$ in the forward direction (see Figure S20 for an example trajectory), the Ni(III) intermediates did not undergo any structural rearrangement, but rather kept the same conformation until the end of the simulation (60% of trajectories) or underwent radical dissociation of the *t*-Bu radical from the axial position of the Ni center (40% of trajectories).

(24) For selected reviews, see: (a) Diccianni, J. B.; Diao, T. Mechanisms of Nickel-Catalyzed Cross-Coupling Reactions. *Trends in Chemistry*. **2019**, *1*, 830–844. (b) Shi, R.; Zhang, Z.; Hu, X. Nickamine and Analogous Nickel Pincer Catalysts for Cross-Coupling of Alkyl Halides and Hydrosilylation of Alkenes. *Acc. Chem. Res.* **2019**, *52*, 1471–1483. (c) Feng, Z.; Xiao, Y.; Zhang, X. Transition-Metal (Cu, Pd, Ni)-Catalyzed Difluoroalkylation via Cross-Coupling with Difluoroalkyl Halides. *Acc. Chem. Res.* **2018**, *51*, 2264–2278. (d) Gu, J.; Wang, X.; Xue, W.; Gong, H. Nickel-catalyzed reductive coupling of alkyl halides with other electrophiles: concept and mechanistic considerations. *Org. Chem. Front.* **2015**, *2*, 1411–1421. (e) Hu, X. Nickel-catalyzed cross coupling of non-activated alkyl halides: a mechanistic perspective. *Chem. Sci.* **2011**, *2*, 1867–1886.

(25) Further calculations suggest that these side reactions are feasible in the reaction system, which could explain the observation of THF-Ar adduct and Ar-H in the stoichiometric studies of aryl bromo Ni(II) with *t*-Bu-BF₃K in experiment (see Figures S11 and S12 in the Supporting Information for the calculation of possible side reaction pathways).

(26) For reviews, see: (a) Ess, D. H.; Houk, K. N. Distortion/Interaction Energy Control of 1,3-Dipolar Cycloaddition Reactivity. *J. Am. Chem. Soc.* **2007**, *129*, 10646–10647. (b) Ess, D. H.; Houk, K. N. Theory of 1,3-Dipolar Cycloadditions: Distortion/Interaction and Frontier Molecular Orbital Models. *J. Am. Chem. Soc.* **2008**, *130*, 10187–10198. (c) Fernandez, I.; Bickelhaupt, F. M. The activation strain model and molecular orbital theory: understanding and designing chemical reactions. *Chem. Soc. Rev.* **2014**, *43*, 4953–4967. (d) Wolters, L. P.; Bickelhaupt, F. M. The activation strain model and molecular orbital theory. *Wiley Interdisciplinary Reviews: Computational Molecular Science* **2015**, *5*, 324–343.

General and Practical Route to Diverse 1-(Difluoro)alkyl-3-aryl Bicyclo[1.1.1]pentanes Enabled by an Fe-Catalyzed Multicomponent Radical Cross-Coupling Reaction

Angel Rentería-Gómez,[§] Wes Lee,[§] Shuai Yin, Michael Davis, Achyut Ranjan Gogoi, and Osvaldo Gutierrez*



Cite This: *ACS Catal.* 2022, 12, 11547–11556



Read Online

ACCESS |

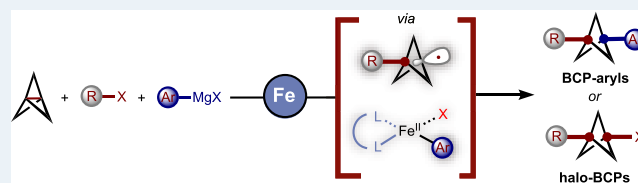
Metrics & More

Article Recommendations

Supporting Information

ABSTRACT: Bicyclo[1.1.1]pentanes (BCPs) are of great interest to the agrochemical, materials, and pharmaceutical industries. In particular, synthetic methods to access 1,3-dicarboxysubstituted BCP-aryls have recently been developed, but most protocols rely on the stepwise C–C bond formation via the initial manipulation of BCP core to make the BCP electrophile or nucleophile followed by a second step (e.g., transition-metal-mediated cross-coupling step) to form the second key BCP-aryl bond. Moreover, despite the prevalence of C–F bonds in bioactive compounds, one-pot, multicomponent cross-coupling methods to directly functionalize [1.1.1]propellane to the corresponding fluoroalkyl BCP-aryl scaffolds are lacking. In this work, we describe a conceptually different approach to access diverse (fluoro)alkyl BCP-aryls at low temperatures and fast reaction times enabled by an iron-catalyzed multicomponent radical cross-coupling reaction from readily available (fluoro)alkyl halides, [1.1.1]propellane, and Grignard reagents. Further, experimental and computational mechanistic studies provide insights into the mechanism and ligand effects on the nature of C–C bond formation. Finally, these studies are used to develop a method to rapidly access synthetic versatile (difluoro)alkyl BCP halides via bisphosphine-iron catalysis.

KEYWORDS: multicomponent, cross-couplings, dicarboxyfunctionalization, sustainable catalysis, iron



INTRODUCTION

Bicyclo[1.1.1]pentanes (BCPs) are of great interest to the agrochemical, materials, and pharmaceutical industries.¹ In particular, the BCP motif is important in drug design because of their well-known use as bioisosteres for *para*-substituted arenes, *tert*-butyl motifs, and alkynes to improve the pharmacokinetic profile of drug candidates by increasing metabolic stability, aqueous solubility, and membrane permeability.² In this vein, 1,3-dicarboxysubstituted BCP-aryls are found in numerous pharmaceutical-relevant molecules (Scheme 1A) and the development of new synthetic methods to access diverse BCP-aryls continues to be an active area of research. However, most methods rely on the stepwise C–C bond formation via the initial functionalization of [1.1.1]propellane to the corresponding electrophile or nucleophile followed by a second transition-metal cross-coupling step (Scheme 1B). For example, Szeimies,³ de Meijere,⁴ and Knochel⁵ have taken advantage of the addition of organometallic reagents to promote ring opening of [1.1.1]propellane to form BCP-Grignard or zinc nucleophiles, which can then be cross-coupled with aryl halides under palladium or nickel catalysis. Uchiyama,⁶ Walsh,⁷ and VanHeyst⁸ reported the use of organoboron BCPs as effective coupling partners in Pd- and dual Ni/photoredox-catalyzed BCP-aryl cross-couplings. The Baran⁹ and Molander¹⁰ groups have reported the use of

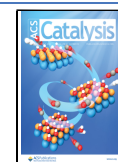
substituted redox-active esters in Fe- and Ni-catalyzed BCP-aryl cross-couplings with aryl zinc reagents and aryl halides, respectively. Finally, Anderson¹¹ has reported the use of BCP-iodides to cross-couple with (hetero)aryl Grignard reagents under iron catalysis.

However, in contrast to the aforementioned two-component cross-coupling approaches to diversify BCP-aryls, the development of one-step, multicomponent catalytic cross-coupling reactions (MC-CCR) could provide a more synthetically advantageous, versatile, and sustainable route to rapidly access diverse BCP-aryls.¹² In this context, despite the growing number of synthetic methods for accessing functionalized BCPs from **1** via multicomponent reactions,^{13–16} reports of MC-CCR to form the difunctionalized BCP-aryls are rare¹⁷ and the use of inexpensive and abundant iron complexes as catalysts in this type of process remains elusive. Finally, despite the omnipresence of C–F bonds in approved drugs,¹⁸ general, multicomponent, and catalytic methods for the synthesis of

Received: July 19, 2022

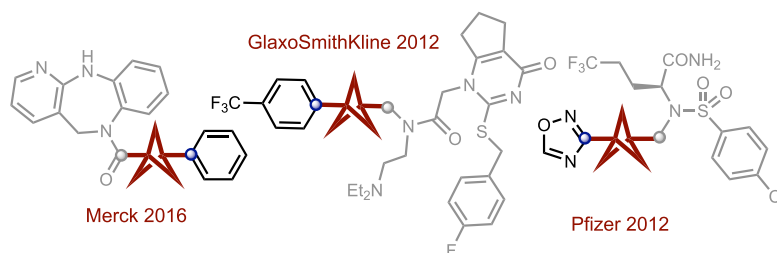
Revised: August 24, 2022

Published: September 8, 2022

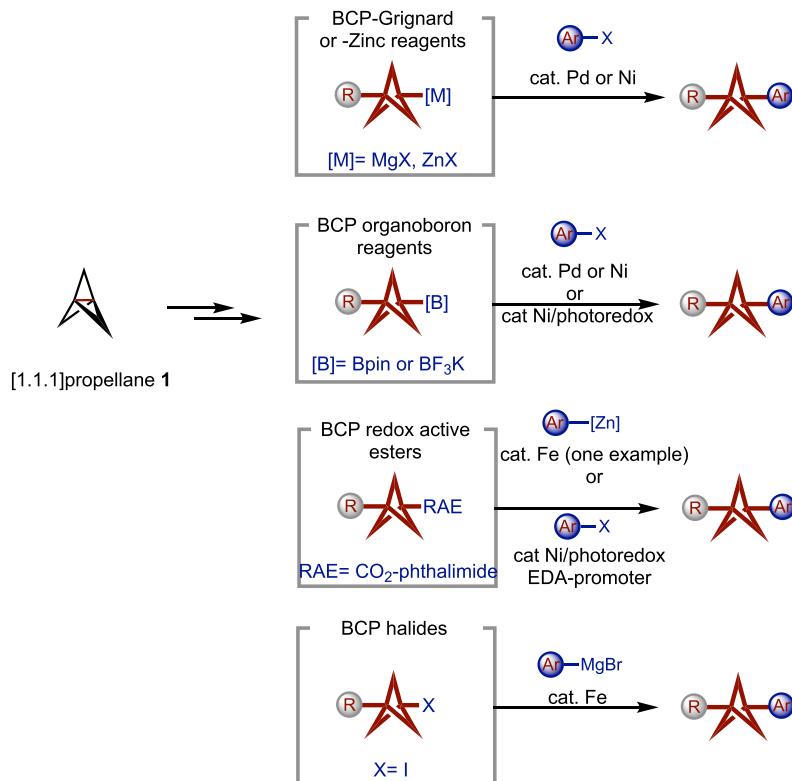


Scheme 1. Cross-Coupling Methods to Construct 1,3-Difunctionalized-Substituted BCP-Aryls

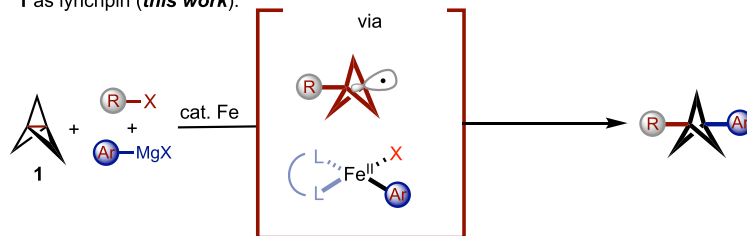
A. Disubstituted bicyclo[1.1.1]pentane aryl (BCP-aryl) cores in pharmaceuticals.



B. Stepwise (two-component) cross-coupling methods to access dicarbofunctionalized BCP-aryl motifs from [1.1.1]propellane.

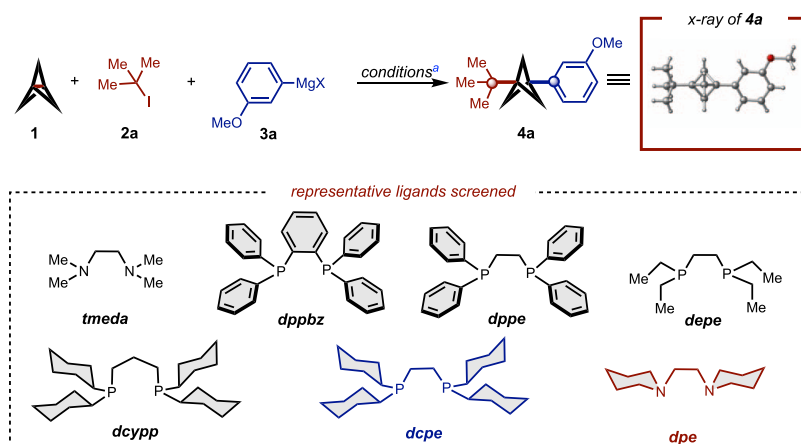


C. One-pot, three-component Fe-catalyzed radical cross-coupling using [1.1.1]propellane 1 as lynchpin (**this work**).



(difluoro)alkyl dicarbofunctionalized BCP-aryl motifs are lacking, likely due to challenges associated with (a) controlling the formation of alkyl radicals and, at the same time, (b) trapping the *in situ*-generated BCP radicals selectively with a transition-metal-aryl species prior to undergoing potential side reactions such as H-atom abstraction, elimination, polymerization, single electron transfer, etc. Based on our program in Fe-catalyzed MC-CCRs,¹⁹ we hypothesized that we could take advantage of the rapid kinetics associated with bisphosphine-iron catalysis to form and trap BCP alkyl radicals under the slow addition of Grignard reagents. If successful, in contrast to prior methods,

this protocol will allow the formation of disubstituted BCP-aryl directly from [1.1.1]propellane. Here, we present a general strategy for the synthesis of diverse 1,3-disubstituted difluoro-(alkyl) BCP-aryls that uses inexpensive iron salts and proceeds with low temperatures and exceeding fast reaction times (Scheme 1C). Finally, experimental and computational mechanistic studies shed light into the role of ligand in BCP-aryl bond formation and provide a catalytic platform to access synthetically useful (difluoro)alkyl BCP halides primed for further functionalization.

Table 1. Optimization of the One-Step, Multicomponent Fe-Catalyzed Cross-Coupling Method to Form 1,3-Difunctionalized Substituted BCP-Aryls

| entry | 1/2a/3a (equiv) | Fe/ligand | 4a yield (%) ^b |
|-----------------|---------------------------|------------------------------|---------------------------|
| 1 | 1.1/1.0/1.2 | Fe(acac) ₃ /dcpe | 29 |
| 2 | 2.0/1.0/3.0 | Fe(acac) ₃ /dcpe | 30 |
| 3 | 4.0/1.0/3.0 | Fe(acac) ₃ /dcpe | 7 |
| 4 | 1.0/2.0/4.2 | Fe(acac) ₃ /dcpe | 70 |
| 5 | 1.0 ^c /2.0/4.2 | Fe(acac) ₃ /dcpe | 69 (61) ^e |
| 6 | 1.0 ^d /2.0/4.2 | Fe(acac) ₃ /dcpe | 70 |
| 7 | 1.0/2.0/2.2 | Fe(acac) ₃ /dcpe | 29 |
| 8 | 1.0/4.0/4.2 | Fe(acac) ₃ /dcpe | 41 |
| 9 | 1.0/2.0/4.2 | none/dcpe | 0 |
| 10 | 1.0/2.0/4.2 | Fe(acac) ₃ /none | 13 |
| 11 | 1.0/2.0/4.2 | FeBr ₂ /dcpe | 34 |
| 12 | 1.0/2.0/4.2 | FeCl ₃ /dcpe | 9 |
| 13 | 1.0/2.0/4.2 | Fe(acac) ₃ /tmeda | 67 |
| 14 | 1.0/2.0/4.2 | Fe(acac) ₃ /dpe | 77 (67) ^e |
| 15 | 1.0/2.0/4.2 | Fe(acac) ₃ /dppbz | 0 |
| 16 | 1.0/2.0/4.2 | Fe(acac) ₃ /dppe | 0 |
| 17 | 1.0/2.0/4.2 | Fe(acac) ₃ /depe | 0 |
| 18 | 1.0/2.0/4.2 | Fe(acac) ₃ /dcyp | 53 |
| 19 ^f | 1.0/2.0/4.2 | Fe(acac) ₃ /dcpe | 41 |

^aReaction conditions: Fe catalyst (20 mol %), ligand (40 mol %), THF (1.0 M), 0 °C, slow addition of 3a in 1 h, argon atmosphere. ^bDetermined by ¹H NMR using 1,2-dibromomethane as an internal standard. ^cSolution of 0.45 M [1.1.1]propellane in Et₂O. ^dSolution of 1.0 M [1.1.1]propellane in Et₂O. ^eYield (%) of isolated product. ^fFe(acac)₃ (10 mol %), dcpe (20 mol %).

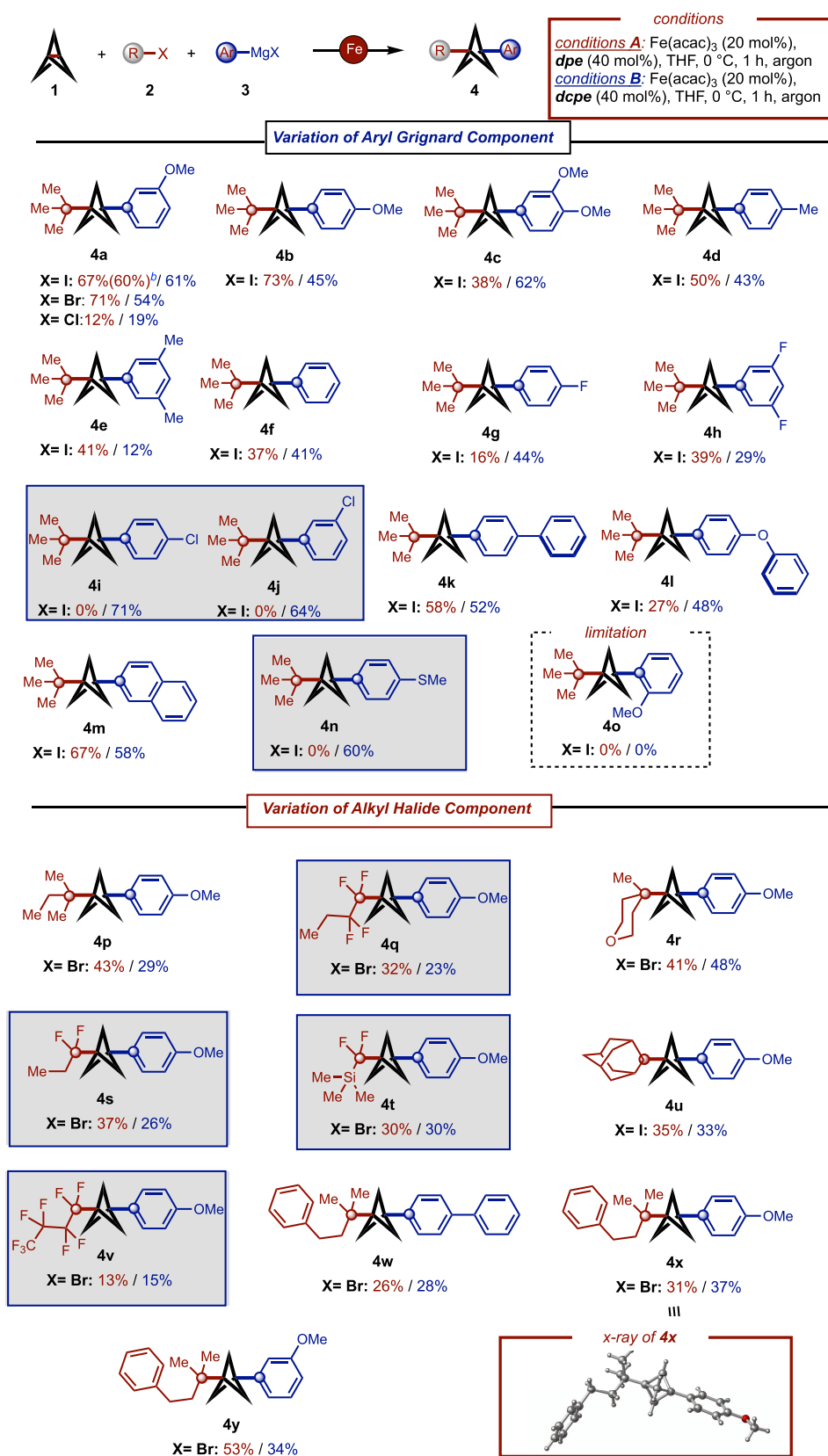
RESULTS AND DISCUSSION

To evaluate the feasibility of our designed multicomponent strategy, we selected [1.1.1]propellane (**1**, 1.1 equiv), *tert*-butyl iodide (**2a**, 1.0 equiv), and 3-methoxyphenylmagnesium bromide (**3a**, 1.2 equiv; X=Br) as the model substrates (Table 1). Notably, using our previously reported conditions for multicomponent dcpe-iron-catalyzed cross-couplings, we were able to observe the formation of the desired product **4a** albeit low (29%) yield (entry 1). Gratifyingly, additional optimization through variation of the alkyl halide, lynchpin **1**, and aryl Grignard reagent led to a significant increase in the overall yield (up to 70%) (entries 2–6). Not surprisingly, we observed that lowering the Grignard reagent (added via a syringe pump over the course of 1 h) had a drastic effect on the overall efficiency (29% yield) (entry 7), while increasing the alkyl halide had a slightly detrimental effect on the overall yield (entry 8). From these studies, it is clear that subtle changes to the relative concentrations among the three components can affect the overall efficiency. Control experiments show the

importance of the unique iron precatalyst and ligand combination to achieve good yields (entries 9–12).

Finally, to assess the ligand effect on this multicomponent transformation, we screened several commercially available diamines and bisphosphine ligands (entries 13–18). To our surprise, while all other bisphosphine ligands screened were found less efficient, diamine ligands, i.e., tmeda and, more specifically, hindered 1,2-dipiperidinoethane (dpe), lead to similar overall yields (~77%) as with the dcpe ligand (entries 13 and 14). Presumably, under these conditions, the crucial mono-ligated halo Fe-aryl and Fe-bisaryl species required for tandem effective radical formation and cross-coupling are formed.^{19a} Notably, at lower catalyst/ligand loadings, the reaction proceeded smoothly albeit with a slightly reduced overall yield (entry 19). Overall, the two sets of optimized conditions [i.e., conditions A: Fe(acac)₃ (20 mol %) and dpe (40 mol %) or conditions B: Fe(acac)₃ (20 mol %) and dcpe (40 mol %)] in THF at 0 °C led to the formation of the sterically encumbered BCP-aryl **4a** in 61% (dcpe) and 67% (dpe) isolated yields. Lastly, the product of the one-step Fe-

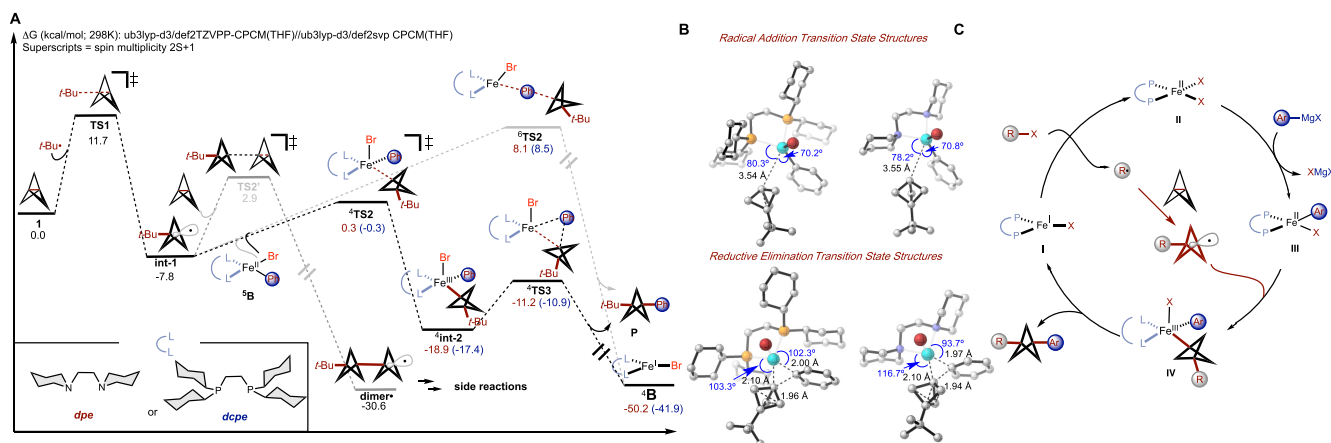
Scheme 2. Scope of Bisphosphine- and Diamine-Iron Catalytic Systems to Construct 1,3-Difunctionalized Substituted BCP-Aryls



catalyzed dicarbofunctionalization of the [1.1.1]propellane was confirmed by X-ray diffraction analysis of compound **4a**.

With catalytic diamine- and bisphosphine-iron optimized conditions in hand (i.e., conditions A and B, respectively), the

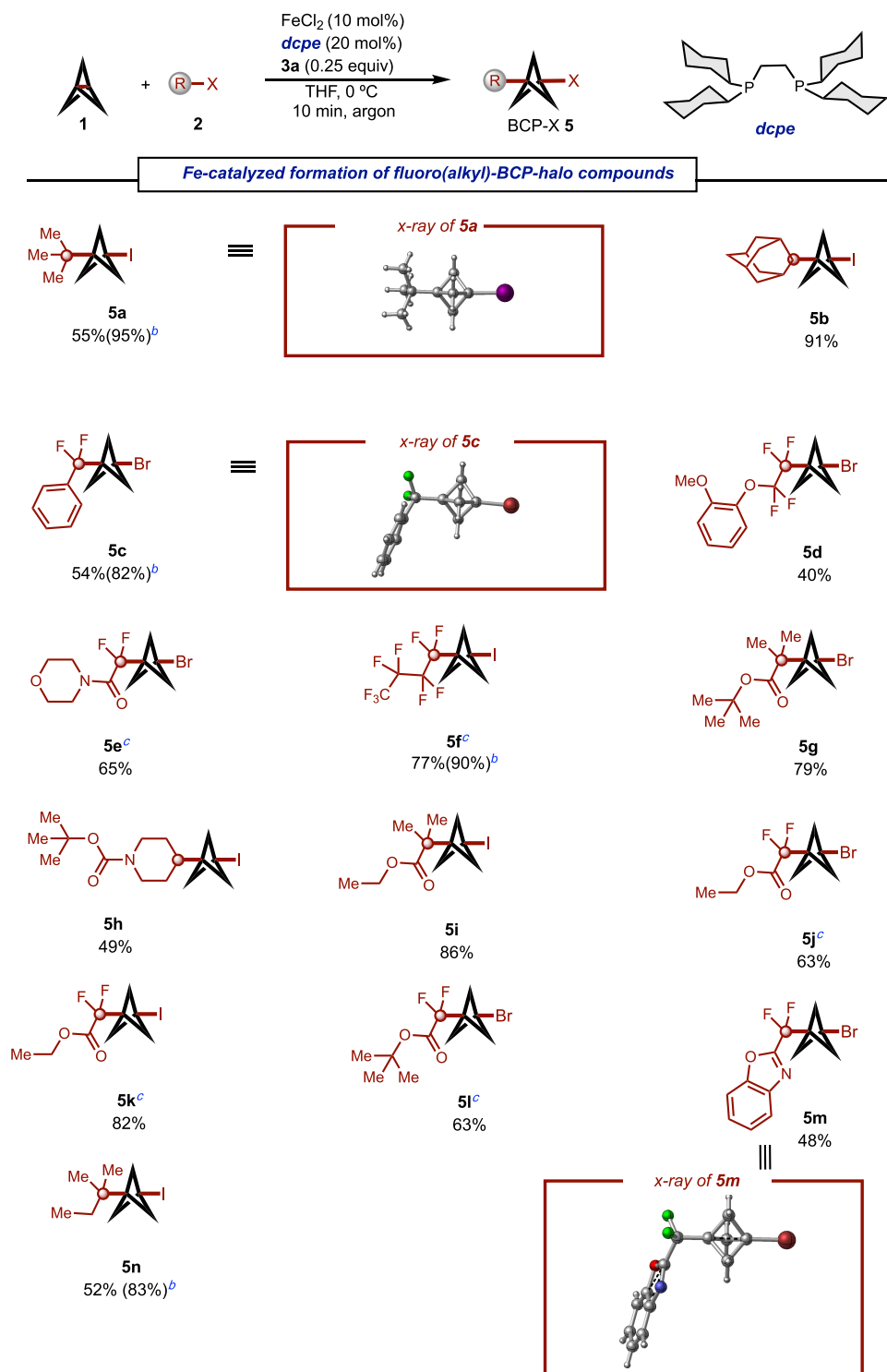
Scheme 3. (A) Computational Studies on the Ligand Effects (Red Using dpe and Blue Using dcpe) on the Mechanism of Three-Component Alkyl-Arylation of BCP (A); (B) Comparison of the Relevant Lowest Energy Radical Addition and Reductive Elimination Transition-State Structures Demonstrating Similar Energetic Profiles and Transition States for the C–C Bond Formation with Bisphosphine- and Diamine-Iron Catalytic Systems; and (C) Proposed Catalytic Cycle



scope of aryl Grignard reagent in this unique one-step, three-component reaction to form 1,3-dicarbofunctionalized BCP-aryls was first evaluated. As shown in **Scheme 2**, both conditions A and B allowed the Fe-catalyzed multicomponent cross-coupling of aryl Grignard **3a** with *tert*-butyl iodide, *tert*-butyl bromide, and even *tert*-butyl chloride, albeit at lower yields, to form the desired BCP-aryl **4a** with similar efficiency. Notably, at larger scale (2.0 mmol), the reaction proceeded smoothly forming the desired product **4a** in a 60% isolated yield. Overall, a wide range of aryl Grignard reagents were compatible in this one-pot procedure to form two carbon–carbon bonds with sterically hindered *tert*-butyl iodide and [1.1.1]propellane **1** leading to the corresponding 1,3-dicarbofunctionalized BCP-aryls **4a–n** in modest to good yields (up to 73%). In some cases, such as **4a** (67/61%), **4d** (50/43%), **4f** (37/41%), and **4k** (58/52%), both dcpe and dpe-iron catalytic systems led to similar overall efficiency. However, in other cases, there were significant differences in the overall outcome between these two catalytic systems. For example, for the formation of **4b** and **4e**, the dpe-iron catalytic system (condition A) was far superior. On the other hand, with aryl Grignard reagents bearing weak carbon–chlorine and –sulfur bonds (e.g., **4i**, **4j**, and **4n**), the dcpe-iron (condition B) was uniquely suited to form the desired three-component radical cross-coupling (60–71% overall yields), while the dpe-iron system failed to form any product. Finally, while *meta*- and *para*-substituted Grignard reagents afforded products, *ortho*-substituted Grignard reagents were not compatible (**4o**), presumably due to a higher energetic barrier to trap the BCP radical with sterically hindered Fe-aryl species, thus opening opportunities for side reactions (e.g., oligomerization) prior to BCP-aryl cross-coupling (*vide infra*). Having investigated the aryl Grignard scope, we then turn our attention to exploring the scope of alkyl halides as radical precursors in this radical multicomponent cross-coupling reaction. As shown in **Scheme 2** (bottom), this method tolerated a range of sterically hindered alkyl halides (**4p**, **4r**, **4u**, **4w**, **4x**, and **4y**) although slightly lower yields were observed with tertiary alkyl radicals bearing β -hydrogens, independent of conditions A or B, presumably due to competitive β -elimination prior to the desired radical addition to **1**, thus lowering overall the efficiency of the three-component reaction. Notably, we

found that this method is uniquely suited toward the rapid and modular synthesis of difluoro-BCP-aryls (**4q**, **4s**, **4t**, **4v**), which to date remain unprecedented in one-pot, multicomponent cross-coupling reactions, using readily available difluoroalkyl bromides as radical precursors. Although lower yields were observed in this transformation, we envision that in the initial stages of pharmaceutical drug discovery, where rapid access to diverse analogs is needed for screening, this method could be broadly applicable. Finally, the dicarbofunctionalization of the [1.1.1]propellane was unequivocally confirmed by X-ray diffraction analysis of compound **4x**.

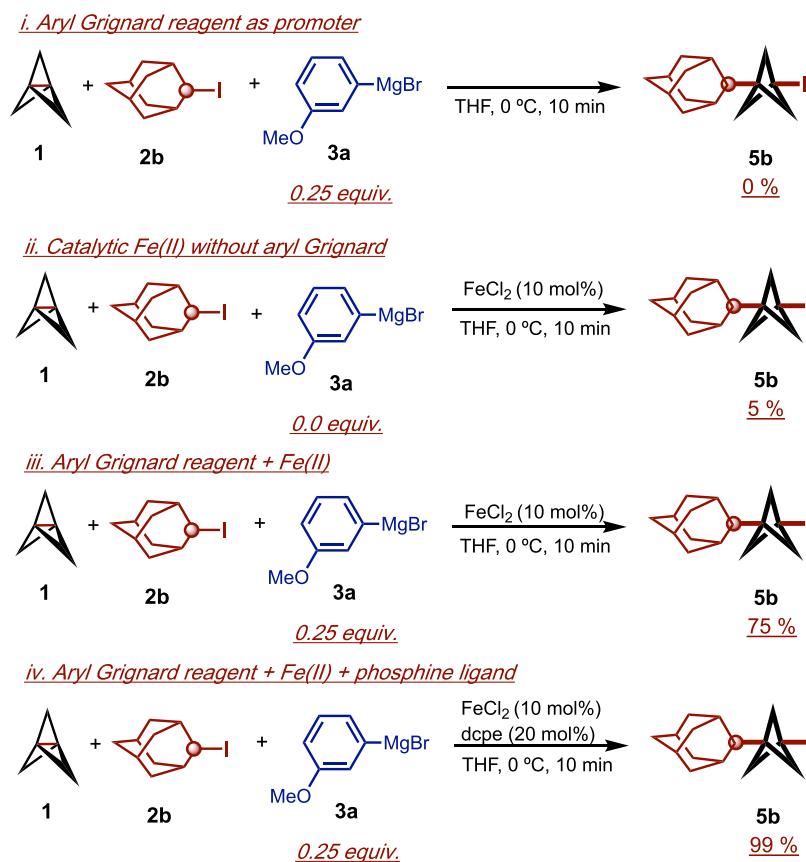
To gain insight into the nature of the ligand in the C–C bond formation, we turned to dispersion-corrected density functional theory (DFT) calculations (see the **Supporting Information** for additional details). Based on prior mechanistic studies from our group and others,^{19a,23} we envisioned alkyl radical undergoing halogen abstraction by an iron species (not shown) to form *t*-Bu \cdot radical. In turn, as shown in **Scheme 3A**, radical addition to [1.1.1]propellane **1** (via **TS1**) proceeds via a low energy barrier (11.7 kcal/mol) leading to *tert*-butyl BCP radical **int-1**. Notably, in contrast to prior work with acyclic tertiary alkyl radicals,^{19a} in both diamine- and bisphosphine-iron model systems, this strained, cyclic alkyl radical can rapidly and irreversibly add to ligated mono-aryl Fe(II) species **5B** via spin-selective **4TS2** (barrier, \sim 8.0 kcal/mol) to form the corresponding distorted square pyramidal Fe(III)-alkyl intermediate **4int-2**. Finally, irreversible reductive elimination via **4TS3** (barrier only \sim 6.5 kcal/mol) will lead to the desired product BCP-aryl product **P** and Fe(I) species **4B**, which can then restart the catalytic cycle (*vide infra*). In addition, we also considered an alternative pathway in which the C–C bond is formed through outer-sphere **6TS4** but, consistent with prior studies,^{19,22,23} this pathway is ruled out based on a much higher energy barrier (\sim 16.0 kcal/mol) compared with the inner-sphere stepwise C–C bond formation in *both* diamine- and bisphosphine systems. To highlight the crucial effect of relative concentrations in these transformations, we also computed the radical addition of **int-1** to another [1.1.1]-propellane molecule (gray). These calculations show that the barrier for radical addition is only 2–3 kcal/mol higher in energy than addition to the mono-aryl Fe(II) species. Thus, for effective three-component radical cross-coupling, it is crucial to

Scheme 4. Substrate Scope of Bisphosphine-Fe-Catalyzed Atom-Transfer Radical Addition (ATRA) to [1.1.1]Propellane^a

^aReactions were carried out using **1** (0.2 mmol), **2** (0.4 mmol), **3a** (0.1 mmol), FeCl₂ (10 mol %), dcpe (20 mol %), THF (0.2 mL) at 0 °C under an argon atmosphere, and isolated yields were reported. ^b¹H NMR yield (in parentheses) determined using 1,2-dibromomethane as an internal standard. ^cSimilar yields were obtained in the absence of FeCl₂, dcpe, and **3a**.

couple the addition of Grignard reagent to generate the corresponding mono-aryl Fe(II) *in situ* (so it can rapidly trap the BCP radical) without over transmetallating this species to the unproductive diaryl Fe(II). Otherwise, other side reactions (e.g., oligomerization)²¹ can quickly take place. Finally, we note that both ligands (dcpe and dpe) gave extremely similar

energy profiles for the C–C bond formation, which we attribute to comparable sterics imposed by both of these ligands in the key radical addition and reductive elimination transition states (Scheme 3B). As such, on the basis of the aforementioned controls and prior mechanistic studies,^{19–23} a possible catalytic cycle is depicted in Scheme 3C. Upon the

Scheme 5. Control Reactions to Shed Light into the Role of Iron and Ligand in the Atom-Transfer Radical Addition Reaction Using [1.1.1]-Propellane as a Radical Acceptor^a


^a¹H NMR yield determined using 1,2-dibromomethane as an internal standard.

formation of putative Fe(I) I, this can, in turn, undergo halogen-atom abstraction to form the alkyl radical and Fe(II) II species. Alkyl radical R[•] can escape the solvent cage to undergo radical addition to [1.1.1]propellane and form BCP radical with the concomitant formation of organoiron III from transmetalation of II with aryl Grignard reagent. Finally, under the slow addition of Grignard reagent to prevent over transmetalation of III, the stepwise C–C formation will occur, thus restarting the catalytic cycle. However, at this stage, further mechanistic studies are needed to convincingly identify the iron species responsible for radical formation and C–C bond formation.

En route to optimizing the three-component dicarbofunctionalization of [1.1.1]propellane 1, we noticed the formation of the 1,3-*tert*-butyl BCP iodide 5a, presumably from the competing Fe-catalyzed atom-transfer radical addition (ATRA) to [1.1.1]propellane. Although 5a could be an intermediate in the multicomponent dicarbofunctionalization of [1.1.1]-propellane, we hypothesize that under conditions A or B the alkyl halo BCP is an off-cycle species in the current Fe-catalyzed three-component radical cross-coupling (*vide infra*). Nonetheless, given the current interest in generating (fluoro)-alkyl halo BCP species as key intermediates for subsequent modifications in pharmaceutical research and the limitations in the methodologies reported,^{2k,24} we proceeded to optimize reaction conditions for bisphosphine-Fe-catalyzed ATRA to [1.1.1]propellane. Notably, although Fe(acac)₃ gives the best yield for the three-component reaction (Table 1, entry 14), we found that the use of FeCl₃ is more efficient to obtain the

halogen transfer product 5 (Table S1). Gratifyingly, after several rounds of optimization, we found suitable reaction conditions that afforded the corresponding alkyl BCP iodide 5a in excellent yields (up to 95% yield). With the optimized conditions in hand, the scope varying the nature of alkyl halides was thoroughly examined. As shown in Scheme 4, acyclic and cyclic tertiary alkyl iodides and α -tertiary alkyl bromides provided the desired 1-halo-3-alkyl BCPs (5a, 5b, 5g, and 5n) including those bearing versatile ester functionalities for further modifications (e.g., via radical cross-couplings).²⁴ In addition, given that ~20% of drugs in the market contain at least one fluorine atom,¹⁸ we found that a wide range of difluoroalkyl bromides and iodides were also compatible in this transformation, yielding the desired 1,3-fluoroalkyl-halo BCPs (5c–f and 5j–m). Notably, additional control experiments revealed that when FeCl₃, dcpe, and aryl Grignard 3a are omitted, in some cases significant background reaction is operative leading to the corresponding (5e, 5f, 5j, 5k, and 5l) in similar yields, presumably from radical-induced atom-transfer radical addition (see the Supporting Information). Finally, the structure for the BCP halides 5a, 5c, and 5m was confirmed by X-ray diffraction analysis. We anticipate that this catalytic method will provide an attractive complementary approach to the current use of photoredox catalysts, triethylborane initiators, heating with organometallic reagents, or high-pressure mercury lamp irradiation to provide access to carbon-substituted halo BCP intermediates.

To gain insight into the mechanism of this transformation to form alkyl halo BCPs, control experiments were carried out

(Scheme 5). Stirring a solution of compounds **1** and **2b** in THF with only 0.25 equiv of Grignard (**3a**) did not afford the desired product. Further, traces of compound were observed when the reaction is carried out using catalytic amounts of FeCl₂ in the absence of Grignard reagent. However, the combination of catalytic FeCl₂ with 0.25 equiv of aryl Grignard reagent afforded the desired product in good yield. Nonetheless, the use of catalytic bisphosphine ligand significantly increases the yield. Overall, we attribute the reactivity to form the alkyl BCP halides to a unique bisphosphine-iron catalytic system that, under aryl Grignard as a promoter, is able to generate the active bisphosphine-iron species that enables halogen-atom abstraction from the alkyl halide to form alkyl radical, which, in turn, adds to the [1.1.1]propellane and, finally, undergoes halogen rebound to restart the catalytic cycle. On the other hand, under three-component catalytic conditions and with Fe(acac)₃ (using either bisphosphine or diamine ligand), the aryl-iron catalytic species traps BCP radical (prior halogen transfer to BCP from alkyl halide or Fe-halo species) to form the final BCP-aryl (Scheme 3C). In this case, the ATRA is a background reaction leading to the unproductive formation of off-cycle 1-halo-3-alkyl BCP. Detailed mechanistic studies are underway to determine the origin of Fe catalyzes ATRA vs multicomponent cross-coupling and will be reported in due course.

CONCLUSIONS

In summary, we have developed a multicomponent, one-pot three-component reaction that utilizes [1.1.1]propellane as a lynchpin to form a range of synthetically valuable 1,3-difunctionalized BCP-aryls under diamine- and bisphosphine-iron catalysis. In addition, using a mechanistic-driven approach, we have developed an efficient iron-promoted method to synthesize (fluoro)alkyl halo-substituted bicyclo[1.1.1]pentanes from readily available (fluoro)alkyl-iodide and -bromide starting materials. Further mechanistic studies are underway to elucidate the factors controlling halogen rebound vs C–C bond formation in these transformations.

ASSOCIATED CONTENT

Supporting Information

The Supporting Information is available free of charge at <https://pubs.acs.org/doi/10.1021/acscatal.2c03498>.

General considerations, reaction optimization details, synthetic procedures, computational studies, and full characterization of all compounds synthesized (PDF)

Accession Codes

CCDC 2118415, 2113560, 2189723, 2189728, and 2189730 contain the supplementary crystallographic data for this paper. These data can be obtained free of charge via www.ccdc.cam.ac.uk/data_request/cif, or by emailing data_request@ccdc.cam.ac.uk, or by contacting The Cambridge Crystallographic Data Centre, 12 Union Road, Cambridge CB2 1EZ, UK; fax: +44 1223 336033.

AUTHOR INFORMATION

Corresponding Author

Oswaldo Gutierrez – Department of Chemistry, Texas A&M University, College Station, Texas 77843, United States; Department of Chemistry and Biochemistry, University of Maryland, College Park, Maryland 20742, United States;

orcid.org/0000-0001-8151-7519; Email: og.labs@tamu.edu

Authors

Angel Rentería-Gómez – Department of Chemistry, Texas A&M University, College Station, Texas 77843, United States

Wes Lee – Department of Chemistry and Biochemistry, University of Maryland, College Park, Maryland 20742, United States

Shuai Yin – Department of Chemistry, Texas A&M University, College Station, Texas 77843, United States

Michael Davis – Department of Chemistry and Biochemistry, University of Maryland, College Park, Maryland 20742, United States

Achyut Ranjan Gogoi – Department of Chemistry, Texas A&M University, College Station, Texas 77843, United States; orcid.org/0000-0002-7609-3720

Complete contact information is available at: <https://pubs.acs.org/10.1021/acscatal.2c03498>

Author Contributions

[§]A.R.-G. and W.L. contributed equally.

Funding

The authors are grateful for the financial support provided by the National Institutes of Health (R35GM137797), National Science Foundation CAREER Award (1751568), Camille and Henry Dreyfus Foundation, and the Welch Foundation (A-2102-20220331). A.R.-G. acknowledges the Fulbright-Garcia Robles scholarship program for partial funding. Texas A&M University HPRC resources (<https://hprc.tamu.edu>) and XSEDE (CHE160082 and CHE160053) used computational resources.

Notes

The authors declare no competing financial interest.

ACKNOWLEDGMENTS

The authors are thankful to Dr. Joseph H. Reibenspies and Dr. Nattamai Bhuvanesh at Texas A&M University for obtaining X-ray data.

REFERENCES

- (1) (a) Mykhailiuk, P. K. Saturated bioisosteres of benzene: where to go next? *Org. Biomol. Chem.* **2019**, *17*, 2839–2849. (b) Locke, G. M.; Bernhard, S. S. R.; Senge, M. O. Nonconjugated Hydrocarbons as Rigid-Linear Motifs: Isosteres for Material Sciences and Bioorganic and Medicinal Chemistry. *Chem. – Eur. J.* **2019**, *25*, 4590–4647.
- (2) (a) Pellicciari, R.; Raimondo, M.; Marinozzi, M.; Natalini, B.; Costantino, G.; Thomsen, C. (S)-(+)-2-(3'-Carboxybicyclo[1.1.1]pentyl)-glycine, a Structurally New Group I Metabotropic Glutamate Receptor Antagonist. *J. Med. Chem.* **1996**, *39*, 2874–2876. (b) Stepan, A. F.; Subramanyam, C.; Efremov, I. V.; Dutra, J. K.; O'Sullivan, T. J.; DiRico, K. J.; McDonald, W. S.; Won, A.; Dorff, P. H.; Nolan, C. E.; Becker, S. L.; Pustilnik, L. R.; Riddell, D. R.; Kauffman, G. W.; Kormos, B. L.; Zhang, L.; Lu, Y.; Capetta, S. H.; Green, M. E.; Karki, K.; Sibley, E.; Atchison, K. P.; Hallgren, A. J.; Oborski, C. E.; Robshaw, A. E.; Sneed, B.; O'Donnell, C. J. Application of the Bicyclo[1.1.1]pentane Motif as a Nonclassical Phenyl Ring Bioisostere in the Design of a Potent and Orally Active γ -Secretase Inhibitor. *J. Med. Chem.* **2012**, *55*, 3414–3424. (c) Westphal, M. V.; Wolfstaedter, B. T.; Plancher, J.; Gatfield, J.; Carreira, E. M. Evaluation of tert-Butyl isosteres: case studies of physicochemical and pharmacokinetic properties, efficacies, and activities. *ChemMedChem* **2015**, *10*, 461–469. (d) Costantino, G.; Maltoni, K.; Marinozzi,

- M.; Camaioni, E.; Prezeau, L.; Pin, J.-P.; Pellicciari, R. Synthesis and biological evaluation of 2-(3'-(1H-tetrazol-5-yl)bicyclo[1.1.1]pent-1-yl)glycine (S-TBPG), a novel mGlu1 receptor antagonist. *Bioorg. Med. Chem.* **2001**, *9*, 221–227. (e) Filosa, R.; Carmela Fulco, M.; Marinozzi, M.; Giacche, N.; Macchiarulo, A.; Peduto, A.; Massa, A.; de Caprariis, P.; Thomsen, C.; Christoffersen, C. T.; Pellicciari, R. Design, synthesis and biological evaluation of novel bicyclo[1.1.1]pentane-based ω -acidic amino acids as glutamate receptors ligands. *Bioorg. Med. Chem.* **2009**, *17*, 242–250. (f) Nicolaou, K. C.; Vourloumis, D.; Totokotsopoulos, S.; Papakyriakou, A.; Karsunky, H.; Fernando, H.; Gavrilyuk, J.; Webb, D.; Stepan, A. F. Synthesis and Biopharmaceutical Evaluation of Imatinib Analogues Featuring Unusual Structural Motifs. *ChemMedChem* **2016**, *11*, 31–37. (g) Nicolaou, K. C.; Yin, J.; Mandal, D.; Erande, R. D.; Klahn, P.; Jin, M.; Aujay, M.; Sandoval, J.; Gavrilyuk, J.; Vourloumis, D. Total Synthesis and Biological Evaluation of Natural and Designed Tubulysins. *J. Am. Chem. Soc.* **2016**, *138*, 1698–1708. (h) Measom, N. D.; Down, K. D.; Hirst, D. J.; Jamieson, C.; Manas, E. S.; Patel, V. K.; Somers, D. O. Investigation of a Bicyclo[1.1.1]pentane as a Phenyl Replacement within an LpPLA2 Inhibitor. *ACS Med. Chem. Lett.* **2017**, *8*, 43–48. (i) Goh, Y. L.; Cui, Y. T.; Pendharkar, V.; Adsool, V. A. Toward Resolving the Resveratrol Conundrum: Synthesis and in Vivo Pharmacokinetic Evaluation of BCP-Resveratrol. *ACS Med. Chem. Lett.* **2017**, *8*, 516–520. (j) Auberson, Y. P.; Brocklehurst, C.; Furegati, M.; Fessard, T. C.; Koch, G.; Decker, A.; La Vecchia, L.; Briard, E. Improving Nonspecific Binding and Solubility: Bicycloalkyl Groups and Cubanes as para-Phenyl Bioisosteres. *ChemMedChem* **2017**, *12*, 590–598. (k) Wiberg, K. B.; Waddell, S. T. Reactions of [1.1.1]propellane. *J. Am. Chem. Soc.* **1990**, *112*, 2194–2216. (l) Ma, X.; Nhat Pham, L. Selective topics in the syntheses of bicyclo[1.1.1]pentane (BCP) analogues. *Asian J. Org. Chem.* **2020**, *9*, 8–22. (m) Kanazawa, J.; Uchiyama, M. Recent Advances in the Synthetic Chemistry of Bicyclo[1.1.1]pentane. *Synlett* **2019**, *30*, 1–11. (n) Wiberg, K. B. Small ring propellanes. *Chem. Rev.* **1989**, *89*, 975–983. (o) Dilmaç, A. M.; Spuling, E.; de Meijere, A.; Brase, S. Propellanes- From a Chemical Curiosity to “Explosive” Materials and Natural Products. *Angew. Chem., Int. Ed.* **2017**, *56*, 5684–5718. (p) Levin, M. D.; Kaszynski, P.; Michl, J. Bicyclo[1.1.1]pentanes, [n]Staffanes, [1.1.1]Propellanes, and Tricyclo[2.1.0.0(2,5)]pentanes. *Chem. Rev.* **2000**, *100*, 169–234. (q) Delia, E. W.; Lochert, I. J. Synthesis of bridgehead-substituted bicyclo[1.1.1]pentanes. A review. *Org. Prep. Proc. Int.* **1996**, *28*, 411–441.
- (3) Rehm, J. D. D.; Ziemer, B.; Szeimies, G. A Facile Route to Bridgehead Disubstituted Bicyclo[1.1.1]pentanes Involving Palladium-Catalyzed Cross-Coupling Reactions. *Eur. J. Org. Chem.* **1999**, 1999, 2079–2085.
- (4) Messner, M.; Kozhushkov, S. I.; de Meijere, A. Nickel- and Palladium-Catalyzed Cross-Coupling Reactions at the Bridgehead of Bicyclo[1.1.1]pentane Derivatives- A Convenient Access to Liquid Crystalline Compounds Containing Bicyclo[1.1.1]pentane Moieties. *Eur. J. Org. Chem.* **2000**, *2000*, 1137–1155.
- (5) (a) Makarov, I. S.; Brocklehurst, C. E.; Karaghiosoff, K.; Koch, G.; Knochel, P. Synthesis of Bicyclo[1.1.1]pentane Bioisosteres of Internal Alkynes and para-Disubstituted Benzenes from [1.1.1]-Propellane. *Angew. Chem., Int. Ed.* **2017**, *56*, 12774–12777. (b) Schwärzer, K.; Zipse, H.; Karaghiosoff, K.; Knochel, P. Highly Regioselective Addition of Allylic Zinc Halides and Various Zinc Enolates to [1.1.1]Propellane. *Angew. Chem., Int. Ed.* **2020**, *59*, 20235–20241.
- (6) Kondo, M.; Kanazawa, J.; Ichikawa, T.; Shimokawa, T.; Nagashima, Y.; Miyamoto, K.; Uchiyama, M. Silaboration of [1.1.1]Propellane: A Storable Feedstock for Bicyclo[1.1.1]pentane Derivatives. *Angew. Chem., Int. Ed.* **2020**, *59*, 1970–1974.
- (7) Shelp, R. A.; Ciro, A.; Pu, Y.; Merchant, R. R.; Hughes, J. M. E.; Walsh, P. J. Strain Release 2-Azaallyl Anion Addition/Borylation of [1.1.1]Propellane: Synthesis and Functionalization of Benzylamine Bicyclo[1.1.1]pentyl Boronates. *Chem. Sci.* **2021**, *12*, 7066–7072.
- (8) VanHeyst, M. D.; Qi, J.; Roecker, A. J.; Hughes, J. M. E.; Cheng, L.; Zhao, Z.; Yin, J. Continuous Flow-Enabled Synthesis of Bench-Stable Bicyclo[1.1.1]pentane Trifluoroborate Salts and Their Utilization in Metallaphotoredox Cross-Couplings. *Org. Lett.* **2020**, *22*, 1648–1654.
- (9) Toriyama, F.; Cornella, J.; Wimmer, L.; Chen, T.-G.; Dixon, D. D.; Creech, G.; Baran, P. S. Redox-Active Esters in Fe-Catalyzed C–C Coupling. *J. Am. Chem. Soc.* **2016**, *138*, 11132–11135.
- (10) Polites, V. C.; Badir, S. O.; Keess, S.; Jolit, A.; Molander, G. A. Nickel-Catalyzed Decarboxylative Cross-Coupling of Bicyclo[1.1.1]pentyl Radicals Enabled by Electron Donor Acceptor Complex Photoactivation. *Org. Lett.* **2021**, *23*, 4828–4833.
- (11) Nugent, J.; Shire, B. R.; Caputo, D. F. J.; Pickford, H. D.; Nightingale, F.; Houlsby, I. T. T.; Mousseau, J. J.; Anderson, E. A. Synthesis of All-Carbon Disubstituted Bicyclo[1.1.1]pentanes by Iron-Catalyzed Kumada Cross-Coupling. *Angew. Chem., Int. Ed.* **2020**, *59*, 11866–11870.
- (12) Dömling, A.; Wang, W.; Wang, K. Chemistry and biology of multicomponent reactions. *Chem. Rev.* **2012**, *112*, 3083–3135.
- (13) Zhang, X.; Smith, R. T.; Le, C.; McCarver, S. J.; Shireman, B. T.; Carruthers, N. I.; MacMillan, D. W. C. Copper-mediated synthesis of drug-like bicyclopentanes. *Nature* **2020**, *580*, 220–226.
- (14) Kim, J. H.; Ruffoni, A.; AlFaizy, Y. S. S.; Sheikh, N. S.; Leonori, D. Divergent Strain-Release Amino-Functionalization of [1.1.1]-Propellane with Electrophilic Nitrogen-Radicals. *Angew. Chem., Int. Ed.* **2020**, *59*, 8225–8231.
- (15) Yu, S.; Jing, C.; Noble, A.; Aggarwal, V. K. 1,3-Difunctionalizations of [1.1.1]Propellane via 1,2-Metalate Rearrangements of Boronate Complexes. *Angew. Chem., Int. Ed.* **2020**, *59*, 3917–3921.
- (16) Kanazawa, J.; Maeda, K.; Uchiyama, M. Radical Multi-component Carboamination of [1.1.1]Propellane. *J. Am. Chem. Soc.* **2017**, *139*, 17791–17794.
- (17) While this paper was under preparation, Molander and co-workers disclosed an elegant study on three-component dicarbofunctionalization of BCPs to form the corresponding 1,3-alkylaryl BCPs under dual nickel/photoredox catalysis. Huang, W.; Kees, S.; Molander, G. A. Dicarbofunctionalization of [1.1.1]Propellane Enabled by Nickel/Photoredox Dual Catalysis: One-Step Multi-component Strategy for the Synthesis of BCP-Aryl Derivatives. *J. Am. Chem. Soc.* **2022**, *144*, 12961–12969.
- (18) (a) Wang, J.; Sánchez-Roselló, M.; Aceña, J. L.; del Pozo, C.; Sorochinsky, A. E.; Fustero, S.; Soloshonok, V. A.; Liu, H. Fluorine in Pharmaceutical Industry: Fluorine-Containing Drugs Introduced to the Market in the Last Decade (2001–2011). *Chem. Rev.* **2014**, *114*, 2432–2506. (b) Böhm, H.-J.; Banner, D.; Bendels, S.; Kansy, M.; Kuhn, B.; Müller, K.; Obst-Sander, U.; Stahl, M. Fluorine in medicinal chemistry. *ChemBioChem* **2004**, *5*, 637–643. (c) Gillis, E. P.; Eastman, K. J.; Hill, M. D.; Donnelly, D. J.; Meanwell, N. A. Applications of Fluorine in Medicinal Chemistry. *J. Med. Chem.* **2015**, *58*, 8315–8359. (d) Meanwell, N. A. Fluorine and Fluorinated Motifs in the Design and Application of Bioisosteres for Drug Design. *J. Med. Chem.* **2018**, *61*, 5822–5880. (e) Müller, K.; Faeh, C.; Diederich, F. Fluorine in pharmaceuticals: Looking beyond intuition. *Science* **2007**, *317*, 1881–1886. (f) Zhou, Y.; Wang, J.; Gu, Z.; Wang, S.; Zhu, W.; Aceña, J. L.; Soloshonok, V. A.; Izawa, K.; Liu, H. Next Generation of Fluorine Containing Pharmaceuticals, Compounds Currently in Phase II–III Clinical Trials of Major Pharmaceutical Companies: New Structural Trends and Therapeutic Areas. *Chem. Rev.* **2016**, *116*, 422–518. (g) Inoue, M.; Sumii, Y.; Shibata, N. Contribution of Organofluorine Compounds to Pharmaceuticals. *ACS Omega* **2020**, *5*, 10633–10640.
- (19) (a) Liu, L.; Aguilera, M. C.; Lee, W.; Youshaw, C. R.; Neidig, M. L.; Gutierrez, O. General method for iron-catalyzed multicomponent radical cascades-cross-couplings. *Science* **2021**, *374*, 432–439. (b) Rotella, M. E.; Sar, D.; Liu, L.; Gutierrez, O. Fe-Catalyzed dicarbofunctionalization of electron-rich alkenes with Grignard reagents and (fluoro)alkyl halides. *Chem. Commun.* **2021**, *57*, 12508–12511. (c) Liu, L.; Lee, W.; Youshaw, C. R.; Yuan, M.; Geherty, M. B.; Zavalij, P. Y.; Gutierrez, O. Fe-Catalyzed Three-Component Dicarbofunctionalization of Unactivated Alkenes with

Grignard Reagents. *Chem. Sci.* **2020**, *11*, 8301–8305. (d) Liu, L.; Lee, W.; Yuan, M.; Acha, C.; Geherty, M. B.; Williams, B.; Gutierrez, O. Intra- and intermolecular Fe-catalyzed dicarbofunctionalization of vinyl cyclopropanes. *Chem. Sci.* **2020**, *11*, 3146–3151.

(20) (a) Neidig, M. L.; Carpenter, S. H.; Curran, D. J.; DeMuth, J. C.; Fleischauer, V. E.; Iannuzzi, T. E.; Neate, P. G. N.; Sears, J. D.; Wolford, N. J. Development and Evolution of Mechanistic Understanding in Iron-Catalyzed Cross-Couplings. *Acc. Chem. Res.* **2019**, *52*, 140–150. (b) Sears, J. D.; Neate, P. G. N.; Neidig, M. K. Intermediates and Mechanism in Iron-Catalyzed Cross-Coupling. *J. Am. Chem. Soc.* **2018**, *140*, 11872–11883.

(21) Bakas, N. J.; Sears, J. D.; Brennessel, W. W.; Neidig, M. L. A TMEDA-Iron Adduct Reaction Manifold in Iron-Catalyzed C(sp²)-C(sp³) Cross-Coupling Reactions. *Angew. Chem., Int. Ed.* **2022**, *61*, No. e202114986.

(22) Lee, W.; Zhou, J.; Gutierrez, O. Mechanism of Nakamura's Iron-Catalyzed Asymmetric Cross-coupling Reaction: The Role of Spin in Controlling Selectivity. *J. Am. Chem. Soc.* **2017**, *139*, 16126–16133.

(23) Sharma, A. K.; Sameera, W. M. C.; Jin, M.; Adak, L.; Okuzono, C.; Iwamoto, T.; Kato, M.; Nakamura, M.; Morokuma, K. DFT and AFIR Study on the Mechanism and the Origin of Enantioselectivity in Iron-Catalyzed Cross-Coupling Reactions. *J. Am. Chem. Soc.* **2017**, *139*, 16117–16125.

(24) Chiba, S.; Kaga, A. Engaging Radicals in Transition Metal-Catalyzed Cross-Coupling with Alkyl Electrophiles: Recent Advances. *ACS Catal.* **2017**, *7*, 4697–4706.

Recommended by ACS

Ni/Photoredox-Catalyzed C(sp³)-C(sp³) Coupling between Aziridines and Acetals as Alcohol-Derived Alkyl Radical Precursors

Sun Dongbang and Abigail G. Doyle

OCTOBER 18, 2022

JOURNAL OF THE AMERICAN CHEMICAL SOCIETY

READ 

Photoexcited Direct Amination/Amidation of Inert Csp³-H Bonds via Tungsten-Nickel Catalytic Relay

Qing Wang, Yi Wang, *et al.*

AUGUST 26, 2022

ACS CATALYSIS

READ 

Nickel Catalyzed Regiodivergent Cross-Coupling Alkylation of Aryl Halides with Redox-Active Imines

Long Huang, Magnus Rueping, *et al.*

SEPTEMBER 08, 2022

ACS CATALYSIS

READ 

Reductive Elimination from Sterically Encumbered Ni-Polypyridine Complexes

Craig S. Day, Ruben Martin, *et al.*

SEPTEMBER 21, 2022

ORGANOMETALLICS

READ 

Get More Suggestions >


 Cite this: *Chem. Commun.*, 2021, 57, 12508

 Received 19th August 2021,
 Accepted 26th October 2021

DOI: 10.1039/d1cc04619e

rsc.li/chemcomm

Fe-Catalyzed dicarbofunctionalization of electron-rich alkenes with Grignard reagents and (fluoro)alkyl halides†

 Madeline E. Rotella,^{‡a} Dinabandhu Sar,^{‡ab} Lei Liu,^{‡ab} and Osvaldo Gutierrez^{‡*ab}

An iron-catalyzed regioselective dicarbofunctionalization of electron-rich alkenes is described. In particular, aryl- and alkyl vinyl ethers are used as effective linchpins to couple alkyl or (fluoro)alkyl halides and sp^2 -hybridized Grignard nucleophiles. Preliminary results demonstrate the ability to engage thioethers as linchpins and control enantioselectivity in these transformations, an area which is largely unexplored in iron-catalyzed three-component cross-coupling reactions.

Alkenes are prevalent motifs in natural products and pharmaceuticals, and are valuable building blocks in organic synthesis.¹ Recently, the difunctionalization of alkenes has attracted interest from the pharmaceutical community due to the potential for cost-effective, rapid, and modular synthesis of complex scaffolds.² In this vein, transition metal-catalyzed three-component cross-coupling reactions have been used to selectively install functional groups across the alkene moiety, thereby building molecular complexity in one step.^{3–11} However, much of the efforts in the development of these reactions has been spent on electron-deficient alkenes and alkenes bearing directing groups to control the reactivity and selectivity.¹² As such, catalytic methods for the selective 1,2-dicarbofunctionalization of electron-rich alkenes, which could deliver straightforward access to complex compounds (Scheme 1A), are scarce¹³ and most of them are limited to the use of nickel or dual nickel/photoredox as catalysts (Scheme 1B).^{14–17}

Seeking to continue to expand the utility of Fe-catalyzed multicomponent cross-couplings,¹⁸ we hypothesized that bisphosphine-iron complexes could serve as cost-effective, practical, and sustainable catalysts to promote regioselective 1,2-dicarbofunctionalization of electron-rich vinyl ethers and, if successful, could complement existing nickel and dual

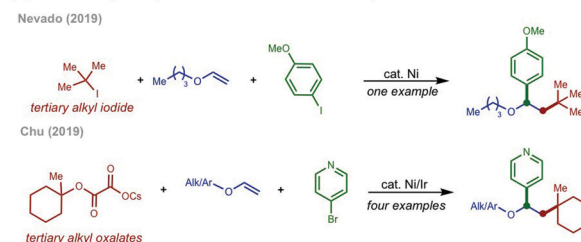
nickel/photoredox methods. Herein, we report a three-component iron-catalyzed regioselective dicarbofunctionalization of aryl- and alkyl vinyl ethers that engage both alkyl halides and (fluoro)alkyl bromides with sp^2 -hybridized Grignard reagents (Scheme 1C). We expect that this method will find applications in the cost-effective synthesis of analogues of antidepressive drugs and, in particular, in the introduction of fluorine atoms into larger scaffolds with applications in pharmaceutical chemistry (Scheme 1A).¹⁹

Recently we developed an iron-catalyzed three-component radical cross-coupling reaction using strain-release vinyl cyclopropanes as the conjunctive reagent under exceptionally rapid reaction times (< 1 h).^{18a,b} Furthermore, the reaction scope was

(A) Selected pharmaceutical compounds with 1,2-aryllalkyl ethers motifs



(B) Nickel-catalyzed 1,2-dicarbofunctionalization of vinyl ethers



(C) Fe-catalyzed 1,2-dicarbofunctionalization of vinyl ethers (This work)



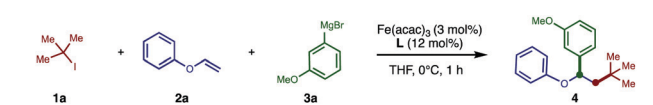
Scheme 1 Transition-metal catalyzed 1,2-dicarbofunctionalization of electron-rich alkenes and its pharmaceutical relevance.

^a Department of Chemistry and Biochemistry, University of Maryland, College Park, Maryland 20742, USA

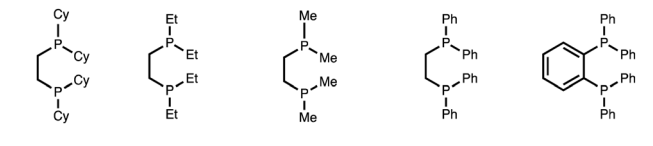
^b Department of Chemistry, Texas A&M University, College Station, Texas 77843, USA. E-mail: og.labs@tamu.edu

† Electronic supplementary information (ESI) available. See DOI: 10.1039/d1cc04619e
 ‡ M. E. R. and D. S. contributed equally.

Table 1 Evaluation of reaction conditions



| Entry | Deviations from standard conditions | NMR yield [%] |
|-------|---|---------------|
| 1 | L1 (12 mol%) | 75 |
| 2 | L2 (12 mol%) | 0 |
| 3 | L3 (12 mol%) | 0 |
| 4 | L4 (12 mol%) | 45 |
| 5 | L5 (12 mol%) | 0 |
| 6 | Using FeBr ₂ (3 mol%) | 63 |
| 7 | Using FeCl ₃ (3 mol%) | 60 |
| 8 | Using Fe(OTf) ₂ (3 mol%) | 63 |
| 9 | Neat | 67 |
| 10 | No L1 | 0 |
| 11 | No Fe(acac) ₃ and no L1 | 0 |



The reaction was performed with *tert*-butyl iodide **1a** (0.1 mmol, 1.0 equiv.), phenyl vinyl ether **2a** (0.4 mmol, 4 equiv.) and 3-methoxyphenyl Grignard **3a** (0.15 mmol, 1.5 equiv.). Aryl Grignard **3a** was added dropwise *via* a syringe pump for 1 h. The yield was determined by ¹H NMR using dibromomethane as an internal standard.

extended to the use of unactivated alkenes without the use of directing groups.^{18c} However, the main drawback of this method is the need for a high concentration of alkene (*i.e.*, as solvent) to drive the equilibrium towards the Giese adduct (*i.e.*, alkyl radicals) for effective and subsequent cross-coupling with the presumed iron-aryl species. We hypothesized that the Giese addition of alkyl radicals to vinyl ethers will lead to more stable α -oxy radicals and provide the driving force to ensure subsequent cross-coupling.

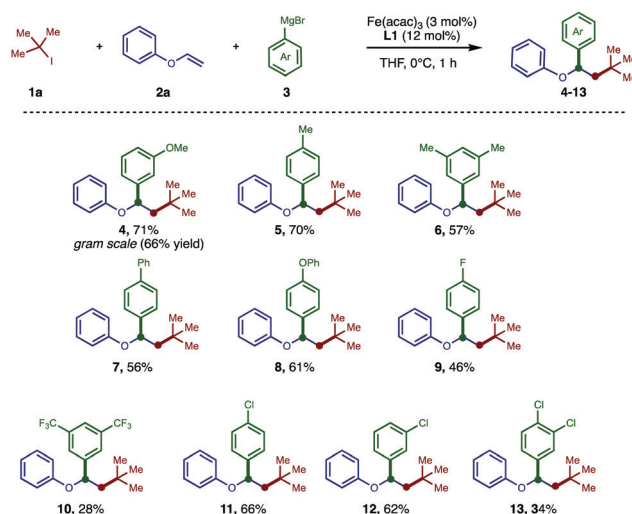
To test this hypothesis, we began our study of iron-catalyzed dicarbofunctionalization of vinyl ethers with the commercially available phenyl vinyl ether as the alkene linchpin (Table 1). To our delight, with excess alkene (14 equiv.), the desired three-component cross-coupling product **4** was formed with the 1,2-addition of the aryl Grignard and the alkyl group in high yields (89%; Table S1, entry 1, ESI[†]). However, we sought to lower our alkene loading from 14 equivalents to increase the practical application of this method. Notably, we found that 4 equiv. of phenyl vinyl ether also gave a reasonably high yield (75%; Table 1, entry 1) and we were able to recover 2.4 equiv. of the alkene after workup. Overall, under these conditions, effectively only 1.6 equiv. of phenyl vinyl ether is consumed in the reaction. Furthermore, screening of various iron salts and ligands did not improve the yields (Table 1). Finally, control experiments verified that the solvent, ligand, and iron catalyst were essential to the reactivity (see Tables S1–S3 in the ESI[†] for full details of the reaction optimization).

With the optimized conditions identified (Table 1, entry 1), we proceeded to study the generality of this iron-catalyzed dicarbofunctionalization reaction. Initially, we focused on

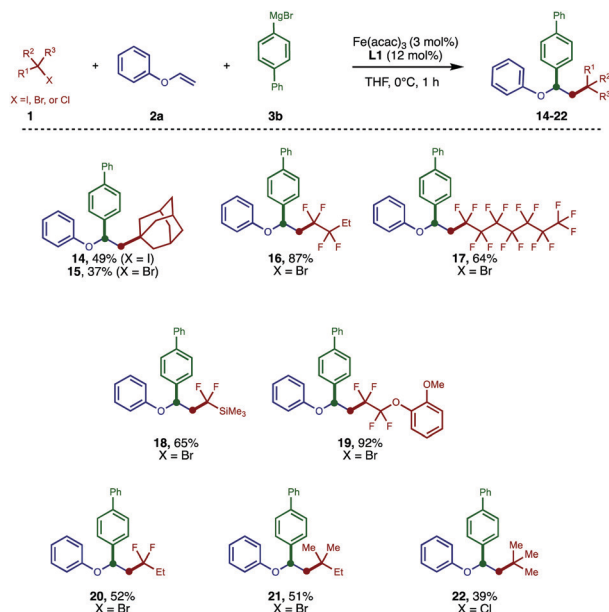
examining the diversity of Grignard nucleophiles for this reaction (Scheme 2). Electron-rich Grignard reagents afforded products (**4–8**) in good yields while mildly electron-deficient Grignard reagents were tolerated as well, giving products (**11, 12**) in moderate yields. Notably, electron-poor Grignard reagents gave products (**9, 10, 13**) albeit in lower yields. Although *meta*- and *para*-substituted Grignard reagents alike afforded products, the *ortho*-methoxy Grignard reagent was not compatible, presumably due to the increased steric hindrance between the *ortho*-substituent and the incipient alkyl component. Finally, to demonstrate the scalability of the method, we prepared 1.02 g of compound **4** (66% yield; 3.59 mmol).

With the scope of the Grignard reagent explored, the alkyl halide scope was then investigated (Scheme 3). In addition to the *tert*-butyl iodide used during reaction screening, we found that 1-iodo- and 1-bromoadamantane (**14, 15**) and fluoroalkyl halides (**16–20**) were compatible in this transformation. Given that ~20% of drugs in the market contain at least one fluorine atom, this method shows promise for applications in pharmaceutical settings.²⁰ In addition, 2-bromo-2-methylbutane successfully gave products in moderate yields (**21, 51%**). Finally, to highlight the potential applications of an alkyl chloride as a viable radical precursor in multicomponent cross-coupling reactions, we used *tert*-butyl chloride as the alkyl halide and, gratifyingly, obtained product **22** in moderate yield (39%), albeit lower than when *tert*-butyl iodide was used as the alkyl halide (7, 56%, Scheme 2).

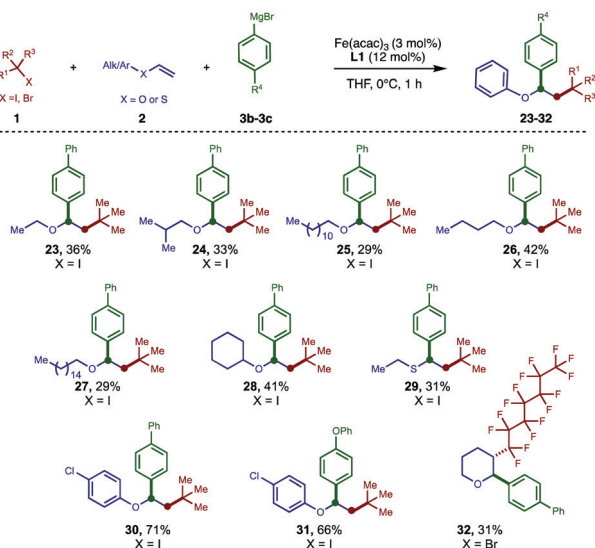
Finally, the alkene substrate scope was investigated (Scheme 4). Overall, attempts to extend the reaction to linear and branched alkyl vinyl ethers were modestly successful, giving products (**23–28**) in 29–42% yields. These results show that alkyl vinyl ethers, in addition to aryl vinyl ethers (**30, 31**), can function as effective linchpins in this three-component reaction. To highlight the potential expansion to thioethers, we



Scheme 2 Scope of Grignard nucleophile in the 3-component cross-coupling reaction with *tert*-butyl iodide and phenyl vinyl ether. All the reactions were carried out under optimized conditions (Table 1, entry 1) using 0.2 mmol *tert*-butyl iodide. Isolated yields are reported.

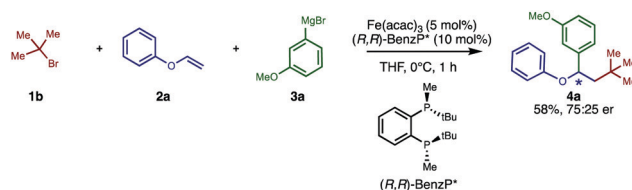


Scheme 3 Scope of alkyl halides in the 3-component cross-coupling reaction with phenyl vinyl ether and 4-biphenylmagnesium bromide **3b**. All the reactions were carried out under optimized conditions (Table 1, entry 1) using 0.2 mmol alkyl halide. Isolated yields are reported.



Scheme 4 Scope of vinyl ethers in the 3-component conjunctive cross-coupling reaction with alkyl halides and 4-biphenylmagnesium bromide **3b** or 4-phenoxyphenylmagnesium bromide **3c**. All the reactions were carried out under optimized conditions (Table 1, entry 1) using 0.2 mmol of alkyl halide. Isolated yields are reported.

used vinyl ethyl thioether as an alternative π -acceptor and were pleased to observe the desired product in a modest yield (**29**). Interestingly, even the internal alkene 3,4-dihydro-2H-pyran reacted in this method to give a moderate yield of product **32** as the *trans* isomer, as determined by NOESY (see Fig. S4, ESI[†]). The ability of this reaction to functionalize internal vinyl ethers



Scheme 5 Preliminary results on the asymmetric version of the 3-component conjunctive cross-coupling reaction. The given yield is an isolated yield and the enantiomeric ratio was determined by chiral HPLC, both determined as an average of the results from four trials.

opens the possibility for this method to be used in the formation of *C*-aryl glycosides from carbohydrate derivatives, thereby expanding the utility of this reaction. In an aim to improve the practicality of this method, we tested other vinyl ethers with more easily removed protecting groups but unfortunately these were not compatible in the reaction (see Fig. S1-S3 in the ESI[†] for full details).

Finally, under optimized reaction conditions, preliminary results show the potential for an enantioselective variant of this transformation (Scheme 5 and Table S4 in the ESI[†]). The development of enantioselective three-component radical cross-coupling reactions remains a considerable challenge in the field and currently is being pursued in our laboratories.²¹

In summary, we have developed an iron-catalyzed regioselective 1,2-dicarbofunctionalization of electron-rich alkenes with (fluoro) alkyl halides and aryl Grignard reagents. This reaction successfully gives products with both electron-donating aryl Grignard reagents and mildly electron-withdrawing aryl Grignard reagents. Furthermore, we have shown that this method functionalizes both aryl and alkyl vinyl ethers. Notably, this method can introduce fluoroalkyl groups to a vinyl ether in a one-step synthesis, whereby molecular complexity for pharmaceutical applications can be rapidly increased. Ongoing work on the asymmetric variant of this reaction is currently underway in our laboratory and will be reported in due course.

This research was supported by the NSF (CAREER 1751568) and by the NIGMS of the NIH (R35GM137797).

Conflicts of interest

There are no conflicts to declare.

References

- X. Qi and T. Diao, *ACS Catal.*, 2020, **10**, 8542–8556.
- H. Cao, H. Liu and A. Domling, *Chem. – Eur. J.*, 2010, **16**, 12296–12298.
- (a) J. Derosa, V. T. Tran, V. A. van der Puyl and K. M. Engle, *Aldrichimica Acta*, 2018, **51**, 21–32; (b) R. Giri and S. KC, *J. Org. Chem.*, 2018, **83**, 3013–3022; (c) L. Liao, R. Jana, K. B. Urkalan and M. S. Sigman, *J. Am. Chem. Soc.*, 2011, **133**, 5784–5787; (d) A. García-Domínguez, Z. Li and C. Nevado, *J. Am. Chem. Soc.*, 2017, **139**, 6835–6838.
- H.-Y. Tu, F. Wang, L. Huo, Y. Li, S. Zhu, X. Zhao, H. Li, F. Qing and L. Chu, *J. Am. Chem. Soc.*, 2020, **142**, 9604–9611.
- M. Yan, J. C. Lo, J. T. Edwards and P. S. Baran, *J. Am. Chem. Soc.*, 2016, **138**, 12692–12714.

- 6 M. W. Campbell, J. S. Compton, C. B. Kelly and G. A. Molander, *J. Am. Chem. Soc.*, 2019, **141**, 20069–20078.
- 7 T. Qin, J. Cornella, C. Li, L. R. Malins, J. T. Edwards, S. Kawamura, B. D. Maxwell, M. D. Eastgate and P. S. Baran, *Science*, 2016, **352**, 801–805.
- 8 P. Basnet, S. KC, R. K. Dhungana, B. Shrestha, T. J. Boyle and R. Giri, *J. Am. Chem. Soc.*, 2018, **140**, 15586–15590.
- 9 For representative examples of Cu, Pd and Ni-catalyzed conjunctive cross-couplings, refer to the following: (a) G. J. Lovinger and J. P. Morken, *J. Am. Chem. Soc.*, 2017, **139**, 17293–17296; (b) J. Derosa, R. Kleinmans, V. T. Tran, M. K. Karunananda, S. R. Wisniewski, M. D. Eastgate and K. M. Engle, *J. Am. Chem. Soc.*, 2018, **140**, 17878–17883; (c) G. J. Lovinger, M. D. Aparece and J. P. Morken, *J. Am. Chem. Soc.*, 2017, **139**, 3153–3160; (d) E. K. Edelstein, S. Namirembe and J. P. Morken, *J. Am. Chem. Soc.*, 2017, **139**, 5027–5030; (e) L. Wu, F. Wang, X. Wan, D. Wang, P. Chen and G. Liu, *J. Am. Chem. Soc.*, 2017, **139**, 2904–2907; (f) J.-S. Lin, T.-T. Li, J.-R. Liu, G.-Y. Jiao, Q.-S. Gu, J.-T. Cheng, Y.-L. Guo, X. Hong and X.-Y. Liu, *J. Am. Chem. Soc.*, 2019, **141**, 1074–1083; (g) A. A. Kadam, T. L. Metz, Y. Qian and L. M. Stanley, *ACS Catal.*, 2019, **9**, 5651–5656; (h) X.-X. Wang, X. Lu, S.-J. He and Y. Fu, *Chem. Sci.*, 2020, **11**, 7950–7956; (i) Y. Zhang, G. Chen and D. Zhao, *Chem. Sci.*, 2019, **10**, 7952–7957.
- 10 D. Ni and M. K. Brown, *ACS Catal.*, 2021, **11**, 1858–1862.
- 11 S. Xu, H. Chen, Z. Zhou and W. Kong, *Angew. Chem., Int. Ed.*, 2021, **60**, 7405–7411.
- 12 W. Shu, A. García-Domínguez, M. T. Quiros, R. Mondal, D. J. Cardenas and C. Nevado, *J. Am. Chem. Soc.*, 2019, **141**, 13812–13821.
- 13 L. Wickham and R. Giri, *Acc. Chem. Res.*, 2021, **54**(17), 3415–3437.
- 14 S. O. Badir and G. A. Molander, *Chem*, 2020, **6**, 1327–1339.
- 15 L. Guo, H. Tu, S. Zhu and L. Chu, *Org. Lett.*, 2019, **21**, 4771–4776.
- 16 (a) A. García-Domínguez, R. Mondal and C. Nevado, *Angew. Chem., Int. Ed.*, 2019, **58**, 12286–12290; (b) W. Shu, A. García-Domínguez, M. T. Quiros, R. Mondal, D. J. Cardenas and C. Nevado, *J. Am. Chem. Soc.*, 2019, **141**, 13812–13821.
- 17 J. Derosa, O. Apolinar, T. Kang, V. T. Tran and K. M. Engle, *Chem. Sci.*, 2020, **11**, 4287–4296.
- 18 (a) L. Liu, W. Lee, M. Yuan, C. Acha, M. B. Geherty, B. Williams and O. Gutierrez, *Chem. Sci.*, 2020, **11**, 3146–3151; (b) L. Liu, W. Lee, J. Zhou, S. Bandyopadhyay and O. Gutierrez, *Tetrahedron*, 2019, **75**, 129–136; (c) L. Liu, W. Lee, C. R. Youshaw, M. Yuan, M. B. Geherty, P. Y. Zavalij and O. Gutierrez, *Chem. Sci.*, 2020, **11**, 8301–8305.
- 19 I. Bauer and H.-J. Knölker, *Chem. Rev.*, 2015, **115**, 3170–3387.
- 20 (a) J. Wang, M. Sánchez-Roselló, J. L. Aceña, C. del Pozo, A. E. Sorochinsky, S. Fustero, V. A. Soloshonok and H. Liu, *Chem. Rev.*, 2014, **114**, 2432–2506; (b) C. M. Hong, A. M. Whittaker and D. M. Schultz, *J. Org. Chem.*, 2021, **86**, 3999–4006.
- 21 H.-Y. Tu, F. Wang, L. Huo, Y. Li, S. Zhu, X. Zhao, H. Li, F.-L. Qing and L. Chu, *J. Am. Chem. Soc.*, 2020, **142**, 9604–9611.

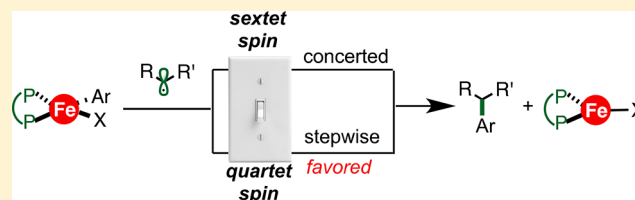
Mechanism of Nakamura's Bisphosphine-Iron-Catalyzed Asymmetric C(sp²)–C(sp³) Cross-Coupling Reaction: The Role of Spin in Controlling Arylation Pathways

Wes Lee, Jun Zhou, and Osvaldo Gutierrez*^{1b}

Department of Chemistry and Biochemistry, University of Maryland, College Park, Maryland 20742, United States

S Supporting Information

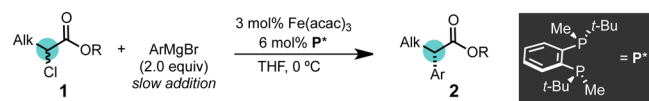
ABSTRACT: Quantum mechanical calculations are employed to investigate the mechanism and origin of stereoinduction in asymmetric iron-catalyzed C(sp²)–C(sp³) cross-coupling reaction between Grignard reagents and α -chloroesters. A coherent mechanistic picture of this transformation is revealed. These results have broad implications for understanding the mechanisms of iron-catalyzed cross-coupling reactions and rational design of novel iron-based catalysts for asymmetric transformations.



INTRODUCTION

Pd- and Ni-catalyzed cross-coupling reactions (CCRs) are a powerful methods for the construction of C–C bonds.¹ Pioneering works by Kharasch,² Vavon,³ and Kochi⁴ disclosed the potential of simple iron salts as catalysts for CCR. Recently, iron has been recognized as an inexpensive, sustainable, and environmentally benign transition metal catalysts in Kumada, Negishi, Sonagashira, Heck, and Suzuki–Miyaura CCRs.⁵ In particular, Nakamura,⁶ Chai,⁷ Bedford⁸ and Fürstner⁹ have reported iron catalytic systems employing bisphosphine ligands (i.e., SciOPP, Xantphos, dppbz, dppe, and depe) to promote CCRs using a range of electrophiles including alkyl halides and, more recently by Baran and co-workers,¹⁰ redox-active esters. Seminal work by Nakamura in 2015 disclosed the first example of enantioselective iron-catalyzed CCR of α -chloroesters **1** and aryl Grignard reagents using chiral bisphosphine ligand **P*** (Scheme 1).¹¹ Unfortunately, in spite of the growth in the

Scheme 1. Nakamura's Asymmetric Iron-Catalyzed Cross-Coupling Reactions of α -Chloroesters and Aryl Grignard Reagents



development of bisphosphine-iron-catalyzed CCRs, mechanistic information on these processes is limited.^{5,12} Noteworthy are mechanistic studies of iron-catalyzed CCRs from the groups of Bedford,^{8b–d,13} Norrby,¹⁴ and, more recently, from elegant *in situ* spectroscopic studies by Neidig.¹⁵

Yet, molecular-level analysis from reaction coordinate calculations in these systems is lacking, especially in the critical C–C forming events and the role of spin in controlling selectivity and reaction pathways.¹⁶ Herein, we use transition-

state calculations (DFT) to elucidate at the mechanism and origin of enantioselectivity of (*R,R*)-BenzP*-iron-catalyzed asymmetric CCR. Implications for the mechanisms of bisphosphine-iron catalysis and rational catalyst design are discussed.

Figure 1 shows the commonly proposed Fe(I)/Fe(II) and Fe(II)/Fe(III) mechanisms for bisphosphine-iron-catalyzed cross-coupling reactions between aryl Grignard reagents and alkyl halides.⁵ However, the exact mechanism is likely dependent on the ligand, additives, and nature of nucleophile and electrophile.^{6–15} Nonetheless, there is strong evidence for the participation of carbon centered radicals in this transformation (*vide infra*) and related iron-catalyzed CCRs in support for halogen abstraction via one electron process.¹⁷ Neidig's sophisticated *in situ* spectroscopic studies provide support for the Fe(II)/Fe(III) mechanisms shown in Figure 1A,B. Specifically, Neidig invoked a bisarylated iron(II) [(SciOPP)FeMes₂] as the active species in Kumada CCR using bulky mesityl Grignard reagent (MesMgBr) and primary alkyl halides.^{15a} However, mechanistic studies, from the same group, using phenyl nucleophiles and secondary alkyl halides in Kumada and Suzuki–Miyaura iron-catalyzed CCRs support a monophenyl iron(II) species [(SciOPP)FePhCl] as the predominant reactive species, suggestive of the mechanism shown in Figure 1B.^{15c} Studies by Bedford and co-workers found a five-coordinate iron(I) species [e.g., (dppbz)₂FeBr and (dppbz)₂FeAr] catalytically competent in iron-catalyzed CCRs.^{8b} However, studies using related dppe ligand found a five-coordinate (dppe)₂FeCl in equilibrium with a three-coordinate iron(I) [(dppe)FeCl] species.^{8d} Thus it is likely that a three-coordinated iron(I) can also participate in halogen abstraction (e.g., Figure 1C,D).¹³ In the title reaction,

Received: June 19, 2017

Published: October 11, 2017

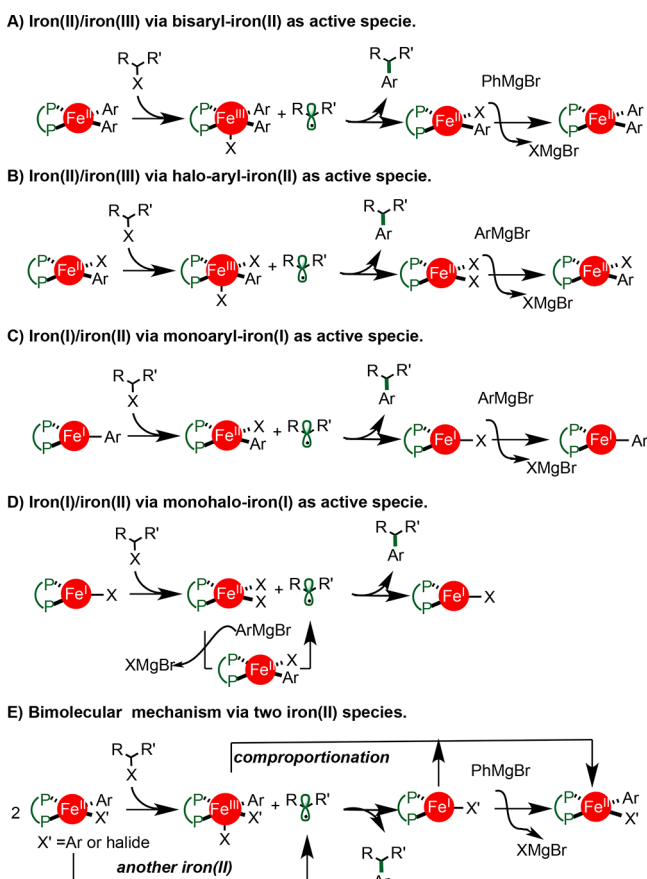
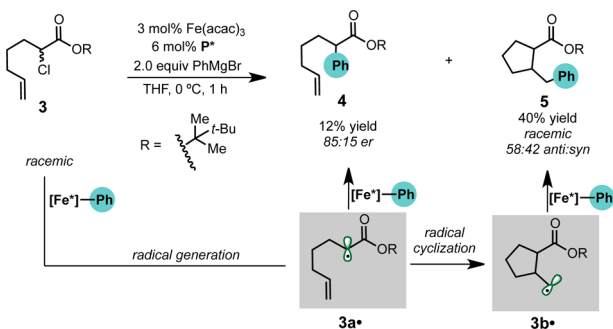


Figure 1. Proposed mechanisms for bisphosphine-iron-catalyzed cross-coupling reactions.

Nakamura observed formation of products **4** and **5** from the reaction using racemic radical probe **3** (Scheme 2).¹¹ This

Scheme 2. Radical Probe Experiments by Nakamura and Co-workers



observation supports the intermediacy of alkyl radicals (e.g., **3a**[•] and **3b**[•]). Furthermore, a first-order linear relationship between 4:5 ratio and catalyst concentration led the authors proposed a bimolecular mechanism (Figure 1E) involving alkyl radical formation and consumption by two distinct metal centers.¹⁸ This experiment ruled out a concerted and/or rapid rebound mechanism akin to H-abstraction/OH-rebound mechanism in C–H iron-catalyzed hydroxylations. However, other mechanisms are possible including radical escape from the solvent cage and recombination with the iron species prior to arylation. Herein, we use spin-unrestricted DFT to elucidate the

mechanism, the role of spin in competing reaction pathways, and origin of enantioselectivity.

METHODS

Due to the robustness of B3LYP¹⁹ to locate the open-shell stationary points, we used spin unrestricted UB3LYP/6-31G(d) gas-phase optimizations without symmetry constraints to examine competing pathways. The expectation values of $\langle S^2 \rangle$ were evaluated as a diagnostic value of the spin state of the systems. Frequency analysis was used to verify nature of stationary points and acquire thermal corrections. However, due to the well-known errors²⁰ associated with B3LYP including systematic bias for high-spin structures in iron complexes^{20b,c} and failure to account well for dispersion interactions^{20d} (crucial aspects to assess competing pathways in iron catalysis and in accounting for stereoselectivity) we deemed necessary to describe the energetics of competing pathways using a range of DFT functionals (UM06L,²¹ UPBEPBE,²² and UM06²³) and large basis sets (6-311+G(d,p)-SDD (for Fe) and/or 6-311+G(d,p)) in implicit THF solvent using the SMD²⁴ continuum solvation model. These methods are routinely used to study organometallic systems²⁵ and iron-catalyzed transformations including CCRs.^{14a,c,18,26} As such we refined all energies and assessed the relative barriers for all competing pathways by performing single-point energy calculations at the UM06L/6-311+G(d,p)-SDD (for Fe)-THF(SMD), UPBEPBE/6-311+G(d,p)-SDD (for Fe)-THF(SMD), UM06/6-311+G(d,p)-SDD (for Fe)-THF(SMD), and UM06/6-311+G(d,p)-THF(SMD) levels of theory. In our calculations, we considered all commonly proposed pathways (shown in Figure 1), including stepwise and concerted C–C bond-forming events, and computed all low, medium, and high spin states (noted by superscripts) in determining the lowest free energy pathway. Only the lowest energy spin states and conformers are shown and discussed in the text. Unsurprisingly, we found that the absolute barriers varied significantly with the DFT functional but relative energies and overall conclusions remain the same (*vide infra*). For simplicity, only UM06L/6-311+G(d,p)-SDD (for Fe)-THF(SMD)//UB3LYP/6-31G(d) and UPBEPBE/6-311+G(d,p)-SDD (for Fe)-THF(SMD)//UB3LYP/6-31G(d) energies are discussed in the text. (See Supporting Information for all values.) All calculations were performed using Gaussian09,²⁷ and structural figures were generated using CYLview.²⁸

RESULTS AND DISCUSSION

Fe(II)/Fe(III) Pathway with Biphenyl Iron(II). We initiated our studies by computing the energetic feasibility from biphenyl iron(II) ³Fe(II)^{Ph-Ph} as active species (Figure 2, red). Halogen abstraction by ³Fe(II)^{Ph-Ph} from methyl 2-chloropropanoate is found energetically feasible (overall barrier is ca. 20 kcal/mol via A0-TS) leading to alkyl radical and trivalent iron(III) ⁴Fe(III)^{Ph-Ph-Cl} downhill in energy (4–13 kcal/mol). Subsequent inner-sphere arylation will proceed in a stepwise manner via radical rebound (via C0-TS) to form iron(IV) intermediate D0. In turn, iron(IV) will undergo reductive elimination (via D0-TS) to form the desired product and ⁵Fe(II)^{Ph-Cl}. Overall, the reaction is 47–58 kcal/mol downhill in energy. Finally, transmetalation with PhMgBr (not calculated) will restart the catalytic cycle.

However, we located a lower energy pathway from B0 via quartet spin state (Figure 2, blue) akin to the bimolecular mechanism depicted in Figure 1E. That is, DFT calculations favor radical addition to another molecule of ³Fe(II)^{Ph-Ph} (by ca. 8–12 kcal/mol; via C0-TS') leading to iron(III) D0' intermediate. Importantly, the barrier for biphenyl reductive elimination (via D0-TS'') is significantly lower in energy than the desired C(sp²)-C(sp³) reductive elimination (D0-TS'). Thus, the overall pathway from ³Fe(II)^{Ph-Ph} as active species will lead to unproductive biphenyl formation.

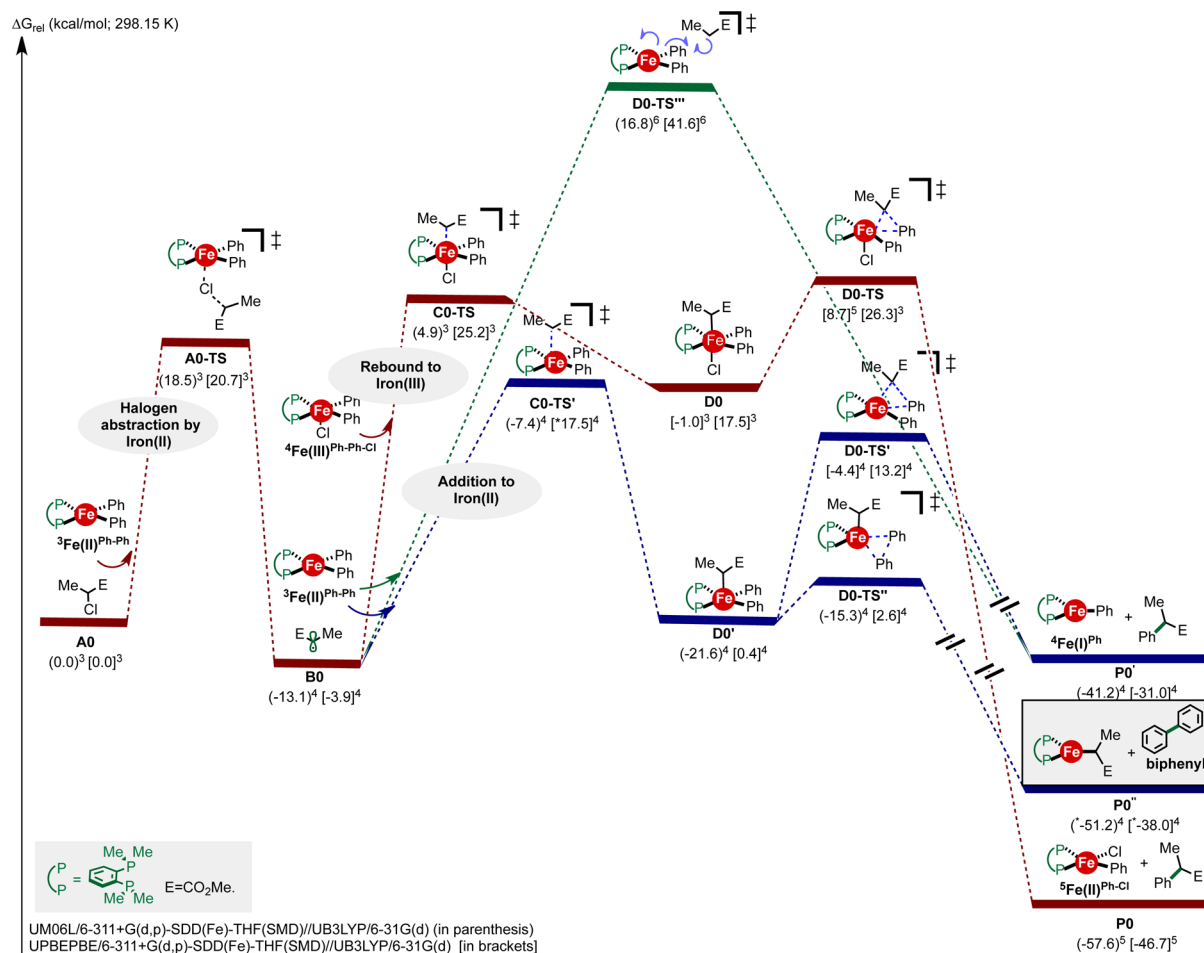


Figure 2. Competing pathways using biphenyl iron(II) as active species in iron-catalyzed cross-coupling.

Moreover, we also found the transition-state structure (**D0-TS''**) corresponding to the commonly proposed “concerted out-of-sphere” arylation mechanism but only via the sextet spin state (Figure 2, green). However, this arylation pathway is much higher (ca. 24 kcal/mol) in energy than alternative stepwise quartet spin-state mechanism (Figure 2, blue). Overall, we conclude that all pathways leading to formation of biphenyl-alkyl iron(III) **D0'** intermediates (i.e., from radical addition to $^3\text{Fe(II)}^{\text{Ph-Ph}}$) are unproductive. Such pathways favor the undesired formation of biphenyl (Figure 2, inset) via quartet spin PES. Calculations using full chiral ligand and (*vide infra*) different methods (see Supporting Information) led to the same conclusions.

Fe(II)/Fe(III) Pathway with Phenyl-chloro Iron(II). Alternatively, monophenyl iron(II) $^5\text{Fe(II)}^{\text{Ph-Cl}}$ can participate in arylation with alkyl radical (e.g., Figure 1B).^{5,15c} As shown in Figure 3 (red), the barrier for halogen abstraction by $^5\text{Fe(II)}^{\text{Ph-Cl}}$ (via **A-TS**) is also feasible (ca. 20 kcal/mol) leading to corresponding iron(III) $^4\text{Fe(III)}^{\text{Ph-Cl-Cl}}$ and alkyl radical. In turn, radical addition to iron(III) $^4\text{Fe(III)}^{\text{Ph-Cl-Cl}}$ (via **C-TS**) will lead to very shallow iron(IV) **D** intermediate, which will quickly undergo facile reductive elimination (via **D-TS**) to form the desired product and iron(II) $^5\text{Fe(II)}^{\text{Cl-Cl}}$. Finally, transmetalation with PhMgBr (not calculated) will restart the catalytic cycle (akin to Figure 1B).

However, similar to biphenyl-iron(II) $^3\text{Fe(II)}^{\text{Ph-Ph}}$ pathways (Figure 2), DFT calculations using a series of functionals (see Supporting Information) predict much lower energy barriers

(ca. 7–9 kcal/mol) for the stepwise radical addition (via **C-TS'**) to another iron(II) $^5\text{Fe(II)}^{\text{Ph-Cl}}$ species (Figure 3, green). In turn, iron(III) intermediate **D'** will undergo reductive elimination (via **D-TS'**) to form $^4\text{Fe(I)}^{\text{Cl}}$ with concomitant formation of the desired product. Presumably, comproportionation between $^4\text{Fe(I)}^{\text{Cl}}$ and $^4\text{Fe(III)}^{\text{Ph-Cl-Cl}}$ followed by transmetalation (not calculated) will restart the catalytic cycle (Figure 1E). Notice that, in contrast to biphenyl alkyl Fe(III), **D'** will not lead to formation of biphenyl. Further, we were also able to successfully locate the alternative “out-of-sphere” concerted arylation transition state (**D-TS''**) via sextet spin state albeit much higher (10–15 kcal/mol) energy. This “bimetallic” mechanism (Figure 3, green), invoked by Nakamura,¹¹ is consistent with experimental observations (e.g., formation of alkyl radical and first-order linear relationship between uncyclized/cyclized products and catalyst concentration; Scheme 2). However, it is unlikely that the concentration of $^5\text{Fe(II)}^{\text{Ph-Cl}}$ accumulates at the experimental conditions given that aryl Grignard reagents can promote transmetalation to biphenyl iron(II). As such, we considered alternative pathways leading to $^5\text{Fe(II)}^{\text{Ph-Cl}}$ (*vide infra*).

Fe(I)/Fe(II) Pathway with Monophenyl Iron(I). Iron(I) has also been invoked in bisphosphine-iron-catalyzed cross-coupling between alkyl halides and aryl Grignard reagents (Figure 1C).⁵ As such, we also considered the pathway from monophenyl $^4\text{Fe(I)}^{\text{Ph}}$ (Figure 3, blue). The barrier for halogen abstraction by $^4\text{Fe(I)}^{\text{Ph}}$ is much lower in energy (only 5–9 kcal/mol barrier) than halogen abstraction by iron(II) or

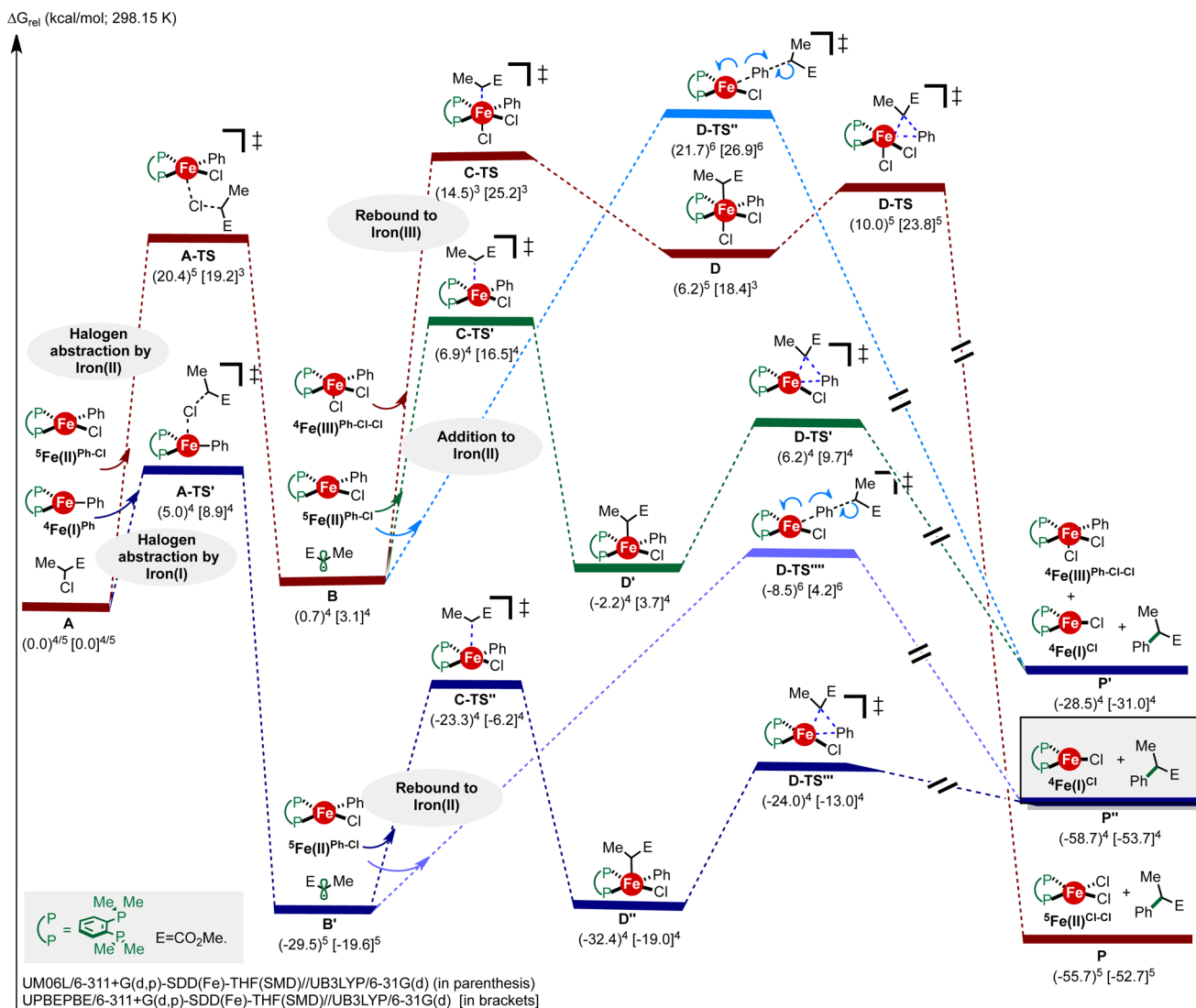


Figure 3. Competing pathways using monophenyl iron(II) as active species in iron-catalyzed cross-coupling.

iron(III) (not shown; See Supporting Information) leading to $^5\text{Fe}(\text{II})^{\text{Ph-Cl}}$ and alkyl radical. In turn, arylation will then occur in a stepwise (Figure 3, blue) rather than a concerted manner (Figure 3, purple) through radical rebound (via C-TS'') to form iron(III) intermediate D''. Subsequent and facile reductive elimination will lead to the formation of the desired $C(sp^2)-C(sp^3)$ bond and $^4\text{Fe}(\text{I})^{\text{Cl}}$. Finally, transmetalation of $^4\text{Fe}(\text{I})^{\text{Cl}}$ with aryl Grignard reagent (i.e., PhMgBr) will close the catalytic cycle (Figure 1C). Calculations using full chiral ligand led to the same conclusions (*vide infra*).

Summary of Arylation Pathways. The initial halogen abstraction step by iron(I) or iron(II) is energetically feasible and therefore likely dependent on the relative concentration of phenyl-iron(I) $^4\text{Fe}(\text{I})^{\text{Ph}}$ and monophenyl iron(II) $^5\text{Fe}(\text{II})^{\text{Ph-Cl}}$,²⁹ predicting the relative concentrations of species remains a computational challenge.³⁰ However, independent of which pathway is operative, both pathways will proceed to same stepwise arylation process via quartet spin state stemming from alkyl radical addition to $^5\text{Fe}(\text{II})^{\text{Ph-Cl}}$. Furthermore, this mechanistic picture is consistent with the need for slow addition of aryl Grignard reagents to avoid deleterious formation of biphenyl, presumably from transmetalation of monophenyl iron(II) $^5\text{Fe}(\text{II})^{\text{Ph-Cl}}$ to form unproductive bi-

phenyl iron(II) $^3\text{Fe}(\text{II})^{\text{Ph-Ph}}$ (Figure 2). Specifically, in the bimetallic iron(II) pathway (Figure 3, green), $^5\text{Fe}(\text{II})^{\text{Ph-Cl}}$ is involved in both the halogen abstraction and radical addition. In the presence of excess PhMgBr , transmetalation of $^5\text{Fe}(\text{II})^{\text{Ph-Cl}}$ to $^3\text{Fe}(\text{II})^{\text{Ph-Ph}}$ is expected to compete with both of these two steps resulting in an increase of biphenyl and concomitant decrease of the desired cross-coupled product. Likewise, in the iron(I)/iron(III) pathway (Figure 3, blue) excess PhMgBr will lead to increase transmetalation of $^5\text{Fe}(\text{II})^{\text{Ph-Cl}}$ to unproductive $^3\text{Fe}(\text{II})^{\text{Ph-Ph}}$ and/or compete with radical addition to $^5\text{Fe}(\text{II})^{\text{Ph-Cl}}$ thus diminishing overall yields.

Overall, the lowest energy pathway proceeds via halogen abstraction by $^4\text{Fe}(\text{I})^{\text{Ph}}$ to form alkyl radical and $^5\text{Fe}(\text{II})^{\text{Ph-Cl}}$ followed by stepwise $C(sp^2)-C(sp^3)$ bond formation via the quartet spin state (Figure 3, blue). These results are also in accord to first-order linear relationship observed by Nakamura (Scheme 2). That is, higher catalyst concentrations are expected to increase the overall concentration of catalytic active species $^5\text{Fe}(\text{II})^{\text{Ph-Cl}}$ via Fe(I)/Fe(II) or bimetallic pathways, leading to rapid trapping of uncyclized radical (prior to solvent escape and cyclization; Scheme 2) thus increasing the formation of uncyclized arylated product. It is expected that substrates with much faster rates of radical

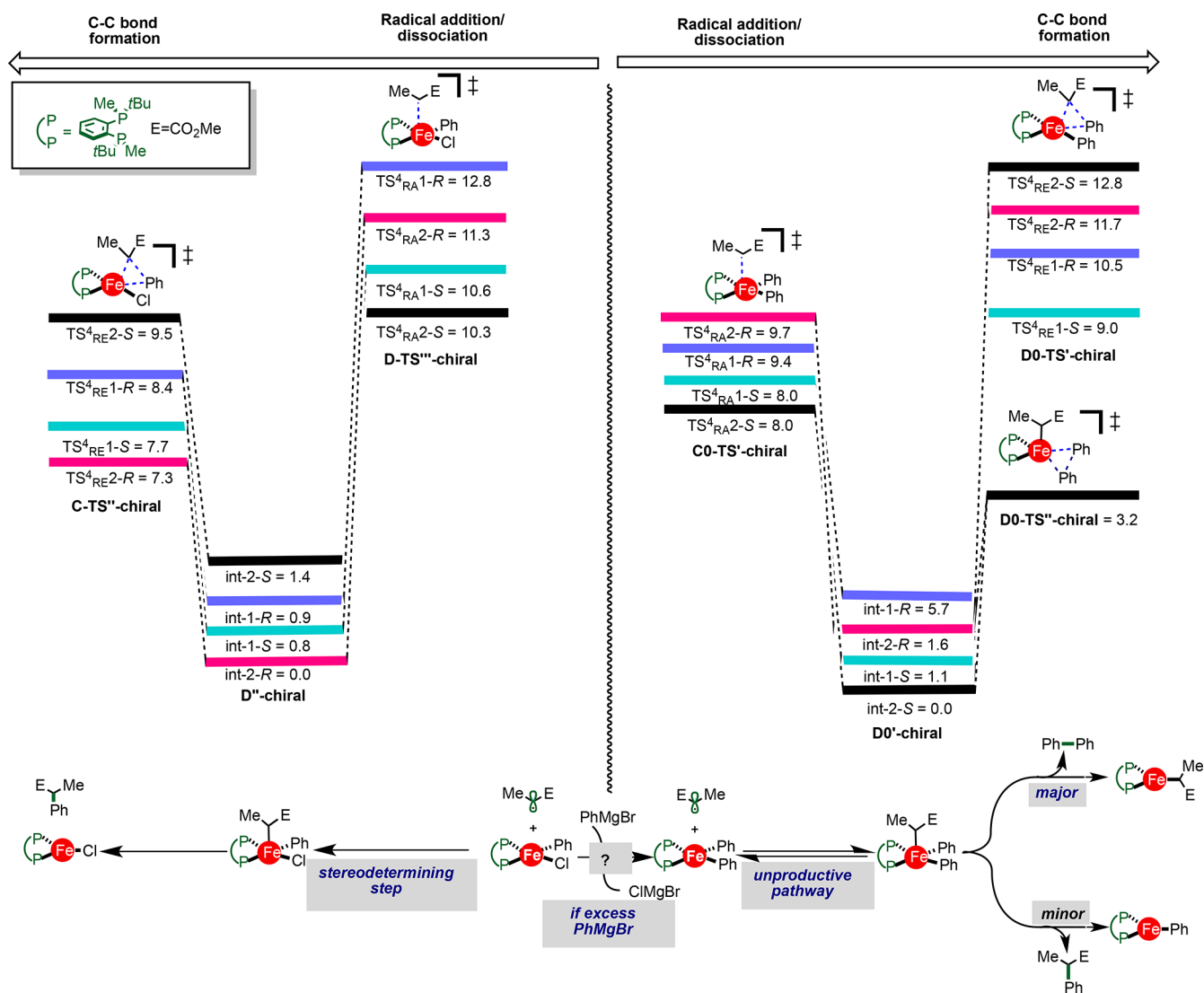


Figure 4. Relative free energies (kcal/mol) for the quartet spin state diastereomeric radical addition and reductive elimination transition states calculated using UPBEPBE/6-311+G(d,p)-SDD-(Fe)-THF(SMD)// UB3LYP/6-31G(d).

cyclization to form exclusive cyclized arylated products independent of catalyst concentration. We are currently testing this hypothesis and will report in due time.

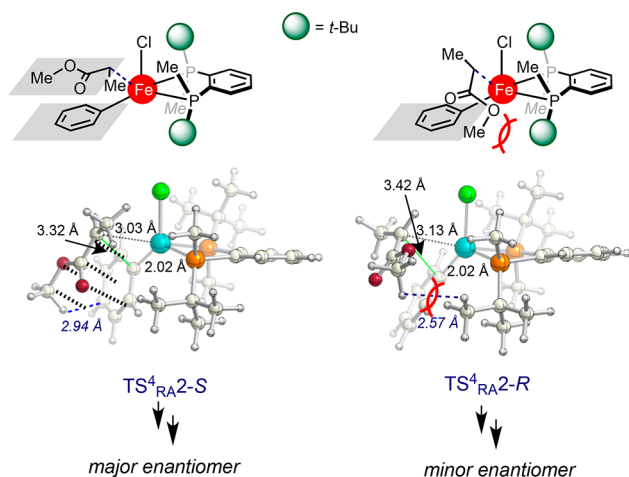
Enantioselectivity. The title reaction represents the first general iron-catalyzed enantioselective cross-coupling method using organometallic compounds.^{11,31} To gain insight into the origin of enantioselectivity and effect of chiral ligand in the reaction pathways, we examined the arylation event using both $\text{Ph}_2\text{Fe}^{\text{II}}$ and $\text{PhClFe}^{\text{II}}$ with the chiral ligand (Figure 4). Noncovalent interactions and the spin state are likely to influence the relative energies between the diastereomeric transition states and, hence, the enantioselectivity.³² As such, we refined the energies using DFT methods known to properly account for noncovalent interactions and are used extensively to rationalize stereoselectivity in organometallic systems (see Supporting Information for all methods and energies).²⁵ Similar to model ligand results, calculations using $\text{Ph}_2\text{Fe}^{\text{II}}$ and chiral bisphosphine ligand predict formation of undesired biphenyl as the lowest energy pathway (Figure 4, right). Specifically, the energy for reductive elimination of biphenyl (via **D0-TS''-chiral**) is 6–9 kcal/mol lower in energy than corresponding $\text{C}(\text{sp}^2)\text{-C}(\text{sp}^3)$ reductive elimination transition states. There-

fore, we conclude that pathways from radical addition to $\text{Ph}_2\text{Fe}^{\text{II}}$ will result in greater side reactions (i.e., biphenyl formation) but are not expected to affect the enantioselectivity (*vide infra*). On the other hand, calculations using monophenyl iron(II) $\text{PhClFe}^{\text{II}}$ with chiral ligand, like model ligand system, also predicted a stepwise $\text{Fe}(\text{II})/\text{Fe}(\text{III})$ process via quartet spin state for formation of desired $\text{C}(\text{sp}^2)\text{-C}(\text{sp}^3)$ bond formation (Figure 4, left). Notably, we also located the diastereomeric transition state (only via sextet spin state) corresponding to concerted “out-of-sphere” arylation but much higher (11–14 kcal/mol) in energy (not shown; see Supporting Information). Finally, iron(I) can then undergo transmetalation with PhMgBr thus restarting the catalytic cycle. Calculations indicate the stereodetermining step is the radical addition (**D-TS''-chiral**).

The agreement between experimental and theoretical enantioselectivity values using a Boltzmann calculation (at 0 °C) with the four lowest energy radical addition transition-state structures is excellent (e.g., (S) as major product and er ratio ($er_{\text{calc}} = 91:9$)). Calculations based on UM06L/6-311+G(d,p)-SDD-(Fe)-THF(SMD)//UB3LYP/6-31G(d) energies predict similar but slightly higher ratio ($er_{\text{calc}} = 98:2$). Further, all calculated ratios based on relative enthalpies and/or electronic

energies using both methods predict similar results (see Supporting Information).³³ On the other hand, a Boltzmann calculation of the four lowest energy reductive elimination transition-state structures predict the wrong stereoisomer (see Supporting Information). Closer inspection of the two lowest energy diastereomeric transition states (Scheme 3) reveals

Scheme 3. Model for Stereoinduction^a



^aDistances are in angstroms.

crucial noncovalent interactions playing a role in the enantioselectivity. In the radical addition transition state leading to the major (*S*) product, the ester group is directly sitting on top of the phenyl ring, which stabilizes TS^4_{RA2-S} through π -donor/acceptor and C–H $\cdots\pi$ interactions. On the other hand, the lowest energy transition state leading to the minor (*R*) enantiomer TS^4_{RA2-R} has the alkyl group of the ester in close proximity to the bulky *tert*-butyl of the ligand that may contribute to destabilizing this transition state as the size of the alkyl group increases.

CONCLUSION

In summary, we have employed quantum mechanical calculations to investigate the mechanism and origin of enantioselectivity of bisphosphine-iron-catalyzed cross-coupling reaction of α -chloro esters with aryl Grignard nucleophiles. Halogen abstraction by iron(I) and iron(II) is found energetic feasible and both can be operative at generating the alkyl radical. However, independent of which iron species abstracts the halogen, these calculations provide strong support for *stepwise Fe(II)/Fe(III) arylation via quartet spin state*. The commonly proposed concerted out-of-sphere arylation was found only via sextet spin state and much higher in energy. Further, it is found that all pathways from bisphenyl iron(II) $^3Fe(II)^{Ph-Ph}$ species lead to the unproductive formation of biphenyl. Overall, the lowest energy pathway proceeds via halogen abstraction by $^4Fe(I)^{Ph}$ to form alkyl radical³⁴ and $^5Fe(II)^{Ph-Cl}$ followed by *enantio-determining radical addition to generate iron(III) which, in turn, undergoes facile reductive elimination to form the C(sp²)-C(sp³) bond via the quartet spin state*. Further, from these calculations, a model for stereoinduction is constructed to explain the observed stereoselectivity, which involves key π -donor/acceptor and C–H $\cdots\pi$ interactions noncovalent interactions as enantiocontrol elements. The mechanism investigated herein has broad implications to

increase fundamental understanding of the mechanisms of iron-catalyzed CCRs and rational design of novel chiral catalyst for asymmetric C–C bond formation. We are currently investigating the mechanisms computationally and experimentally of related iron-catalyzed cross-coupling reactions.

ASSOCIATED CONTENT

Supporting Information

The Supporting Information is available free of charge on the ACS Publications website at DOI: 10.1021/jacs.7b06377.

Full computational details, energies, and coordinates (PDF)

AUTHOR INFORMATION

Corresponding Author

*ogs@umd.edu

ORCID

Osvaldo Gutierrez: 0000-0001-8151-7519

Notes

The authors declare no competing financial interest.

ACKNOWLEDGMENTS

We are grateful to the University of Maryland College Park for startup funds. Calculations were performed using DeepThought2 at the University of Maryland College Park and Engineering Discovery Environment (XSEDE; CHE160082 and CHE160053) supported by the NSF. We thank Prof. Dionicio Martinez Solorio, (Drexel University) and Dr. Jason G. Harrison and Prof. Andrei Vedernikov (University of Maryland) for helpful suggestions. Finally, we are indebted to the reviewers for all suggestions and insights.

REFERENCES

- (1) *Metal-Catalyzed Cross-Coupling Reactions and More*; de Meijere, A., Bräse, S., Oestreich, M., Eds.; Wiley-VCH Verlag GmbH: Weinheim, 2014.
- (2) Kharasch, M. S.; Fields, E. K. *J. Am. Chem. Soc.* **1941**, *63*, 2316–2320.
- (3) Vavon, G.; Mottez, P. C. *R. Hebd. Séances Acad. Sci.* **1944**, *218*, 557–559.
- (4) (a) Tamura, M.; Kochi, J. K. *J. Am. Chem. Soc.* **1971**, *93*, 1487–1489. (b) Tamura, M.; Kochi, J. K. *J. Organomet. Chem.* **1971**, *31*, 289–309. (c) Neumann, S. M.; Kochi, J. K. *J. Org. Chem.* **1975**, *40*, 599–606. (d) Smith, R. S.; Kochi, J. K. *J. Org. Chem.* **1976**, *41*, 502–509. (e) Tamura, M.; Kochi, J. K. *Bull. Chem. Soc. Jpn.* **1971**, *44*, 3063–3073.
- (5) For recent reviews, see: (a) Czaplak, W. M.; Mayer, M.; Cvengroš, J.; von Wangelin, A. *J. ChemSusChem* **2009**, *2*, 396–417. (b) Cassani, C.; Bergonzini, G.; Wallentin, C.-J. *ACS Catal.* **2016**, *6*, 1640–1648. (c) Mako, T. L.; Byers, J. A. *Inorg. Chem. Front.* **2016**, *3*, 766–790.
- (6) (a) Hatakeyama, T.; Kondo, Y.; Fujiwara, Y.; Takaya, H.; Ito, S.; Nakamura, E.; Nakamura, M. *Chem. Commun.* **2009**, 1216–1218. (b) Hatakeyama, T.; Fujiwara, Y.; Okada, Y.; Itoh, T.; Hashimoto, T.; Kawamura, S.; Ogata, K.; Takaya, H.; Nakamura, M. *Chem. Lett.* **2011**, *40*, 1030–1032. (c) Hatakeyama, T.; Hashimoto, T.; Kathiriarachchi, K. K. A. D. S.; Zenmyo, T.; Seike, H.; Nakamura, M. *Angew. Chem., Int. Ed.* **2012**, *51*, 8834–8837. (d) Hatakeyama, T.; Hashimoto, T.; Kondo, Y.; Fujiwara, Y.; Seike, H.; Takaya, H.; Tamada, Y.; Ono, T.; Nakamura, M. *J. Am. Chem. Soc.* **2010**, *132*, 10674–10676. (e) Hatakeyama, T.; Okada, Y.; Yoshimoto, Y.; Nakamura, M. *Angew. Chem., Int. Ed.* **2011**, *50*, 10973–10976. (f) Kawamura, S.; Nakamura, M. *Chem. Lett.* **2013**, *42*, 183–185. (g) Nakagawa, N.; Hatakeyama, T.; Nakamura, M. *Chem. Lett.* **2015**, *44*, 486–488.

- (h) Hashimoto, T.; Hatakeyama, T.; Nakamura, M. *J. Org. Chem.* **2012**, *77*, 1168–1173.
- (7) Dongol, K. G.; Koh, H.; Sau, M.; Chai, C. L. *Adv. Synth. Catal.* **2007**, *349*, 1015–1018.
- (8) (a) Bedford, R. B.; Huwe, M.; Wilkinson, M. C. *Chem. Commun.* **2009**, 600–602. (b) Adams, C. J.; Bedford, R. B.; Carter, E.; Gower, N. J.; Haddow, M. F.; Harvey, J. N.; Huwe, M.; Cartes, M. A.; Mansell, S. M.; Mendoza, C.; Murphy, D. M.; Neeve, E. C.; Nunn, J. *J. Am. Chem. Soc.* **2012**, *134*, 10333–10336. (c) Bedford, R. B.; Carter, E.; Cogswell, P. M.; Gower, N. J.; Haddow, M. F.; Harvey, J. N.; Murphy, D. M.; Neeve, E. C.; Nunn, J. *Angew. Chem., Int. Ed.* **2013**, *52*, 1285–1288. (d) Bedford, R. B.; Brenner, P. B.; Carter, E.; Carvell, T. W.; Cogswell, P. M.; Gallagher, T.; Harvey, J. N.; Murphy, D. M.; Neeve, E. C.; Nunn, J.; Pye, D. R. *Chem. - Eur. J.* **2014**, *20*, 7935–7938.
- (9) Sun, C.-L.; Krause, H.; Fürstner, A. *Adv. Synth. Catal.* **2014**, *356*, 1281–1291.
- (10) (a) Toriyama, F.; Cornella, J.; Wimmer, L.; Chen, T.-G.; Dixon, D. D.; Creech, G.; Baran, P. S. *J. Am. Chem. Soc.* **2016**, *138*, 11132–11135. (b) Edwards, J. T.; Merchant, R. R.; McClymont, K. S.; Knouse, K. W.; Qin, T.; Malins, L. R.; Vokits, B.; Shaw, S. A.; Bao, D.-H.; Wei, F.-L.; Zhou, T.; Eastgate, M. D.; Baran, P. S. *Nature* **2017**, *545*, 213–218.
- (11) Jin, M.; Adak, L.; Nakamura, M. *J. Am. Chem. Soc.* **2015**, *137*, 7128–7134.
- (12) For selected example, see: Takaya, H.; Nakajima, S.; Nakagawa, N.; Isozaki, K.; Iwamoto, T.; Imayoshi, R.; Gower, N. J.; Adak, L.; Hatakeyama, T.; Honma, T.; Takagaki, M.; Sunada, T.; Nagashima, H.; Hashizume, D.; Takahashi, O.; Nakamura, M. *Bull. Chem. Soc. Jpn.* **2015**, *88*, 410–418.
- (13) (a) Bedford, R. B.; Brenner, P. B.; Carter, E.; Clifton, J.; Cogswell, P. M.; Gower, N. J.; Haddow, M. F.; Harvey, J. N.; Kehl, J. A.; Murphy, D. M.; Neeve, E. C.; Neidig, M. L.; Nunn, J.; Snyder, B. E.; Taylor, J. *Organometallics* **2014**, *33*, 5767–5780. (b) Bedford, R. B.; Brenner, P. B.; Carter, E.; Cogswell, P. M.; Haddow, M. F.; Harvey, J. N.; Murphy, D. M.; Nunn, J.; Woodall, C. H. *Angew. Chem., Int. Ed.* **2014**, *53*, 1804–1808.
- (14) (a) Kleimark, J.; Hedström, A.; Larsson, P.-F.; Johansson, C.; Norrby, P.-O. *ChemCatChem* **2009**, *1*, 152–161. (b) Hedström, A.; Bollmann, U.; Bravidor, J.; Norrby, P.-O. *Chem. - Eur. J.* **2011**, *17*, 11991–11993. (c) Hedström, A.; Izakian, Z.; Vreto, I.; Wallentin, C.-J.; Norrby, P.-O. *Chem. - Eur. J.* **2015**, *21*, 5946–5953.
- (15) (a) Daifuku, S. L.; Al-Afyouni, M. H.; Snyder, B. E. R.; Kneebone, J. L.; Neidig, M. L. *J. Am. Chem. Soc.* **2014**, *136*, 9132–9143. (b) Al-Afyouni, M. H.; Fillman, K. L.; Brennessel, W. W.; Neidig, M. L. *J. Am. Chem. Soc.* **2014**, *136*, 15457–15460. (c) Daifuku, S. L.; Kneebone, J. L.; Snyder, B. E. R.; Neidig, M. L. *J. Am. Chem. Soc.* **2015**, *137*, 11432–11444. (d) Muñoz, S. B., III; Daifuku, S. L.; Brennessel, W. W.; Neidig, M. L. *J. Am. Chem. Soc.* **2016**, *138*, 7492–7495. (e) Kneebone, J. L.; Brennessel, W. B.; Neidig, M. L. *J. Am. Chem. Soc.* **2017**, *139*, 6988–7003.
- (16) During the review of this manuscript, Nakamura, Morokuma, and co-workers submitted a computational study using the DFT/AFIR method: Sharma, A. K.; Sameera, W. M. C.; Jin, M.; Adak, L.; Okuzono, C.; Iwamoto, T.; Kato, M.; Nakamura, M.; Morokuma, K. *J. Am. Chem. Soc.* **2017**, DOI: 10.1021/jacs.7b05917.
- (17) (a) Asahara, T.; Seno, M.; Ohtani, N. *Bull. Chem. Soc. Jpn.* **1973**, *46*, 3193–3197. (b) Davis, R.; Durrant, J. L. A.; Khazai, N. M. S.; Bitterwolf, T. E. *J. Organomet. Chem.* **1990**, *386*, 229–239. (c) Forti, L.; Ghelfi, F.; Pagnoni, U. M. *Tetrahedron* **1997**, *53*, 4419–4426. (d) Noda, D.; Sunada, Y.; Hatakeyama, T.; Nakamura, M.; Nagashima, H. *J. Am. Chem. Soc.* **2009**, *131*, 6078–6079. (e) Vallée, F.; Mousseau, J. J.; Charette, A. B. *J. Am. Chem. Soc.* **2010**, *132*, 1514–1516. (f) Denmark, S. E.; Cresswell, A. K. *J. Org. Chem.* **2013**, *78*, 12593–12628.
- (18) Bauer, G.; Wodrich, M. D.; Scopelliti, R.; Hu, X. *Organometallics* **2015**, *34*, 289–298.
- (19) Becke, A. D. *J. Chem. Phys.* **1993**, *98*, 5648–5652.
- (20) See (a) Cohen, A. J.; Mori-Sanchez, P.; Yang, W. *Chem. Rev.* **2012**, *112*, 289–320. (b) Reiher, M.; Salomon, O.; Artur Hess, B. *Theor. Chem. Acc.* **2001**, *107*, 48–55. (c) Bowman, D. N.; Jakubikova, E. *Inorg. Chem.* **2012**, *51*, 6011–6019. (d) Grimme, S. *WIREs Comput. Mol. Sci.* **2011**, *1*, 211–228. and references therein.
- (21) Zhao, Y.; Truhlar, D. G. *J. Chem. Phys.* **2006**, *125*, 194101–194118.
- (22) (a) Perdew, J. P.; Burke, K.; Ernzerhof, M. *Phys. Rev. Lett.* **1996**, *77*, 3865–3868. (b) Perdew, J. P.; Burke, K.; Ernzerhof, M. *Phys. Rev. Lett.* **1997**, *78*, 1396–1396.
- (23) Zhao, Y.; Truhlar, D. G. *Theor. Chem. Acc.* **2008**, *120*, 215–241.
- (24) Marenich, A. V.; Cramer, C. J.; Truhlar, D. G. *J. Phys. Chem. B* **2009**, *113*, 6378–6396.
- (25) (a) Sperger, T.; Sanhueza, I. A.; Kalvet, I.; Schoenebeck, F. *Chem. Rev.* **2015**, *115*, 9532–9586. (b) Sperger, T.; Sanhueza, I. A.; Schoenebeck, F. *Acc. Chem. Res.* **2016**, *49*, 1311–1319.
- (26) For selected examples on computational analysis of iron-catalyzed reactions, see: (a) Wang, Y.; Janardanan, D.; Usharani, D.; Han, K.; Que, L., Jr.; Shaik, S. *ACS Catal.* **2013**, *3*, 1334–1341. (b) Sameera, W. M. C.; Hatanaka, M.; Kitanosono, T.; Kobayashi, S.; Morokuma, K. *J. Am. Chem. Soc.* **2015**, *137*, 11085–11094. (c) Heggen, B.; Thiel, W. *J. Organomet. Chem.* **2016**, *804*, 42–47. (d) Sun, Y.; Tang, H.; Chen, K.; Hu, L.; Yao, J.; Shaik, S.; Chen, H. *J. Am. Chem. Soc.* **2016**, *138*, 3715–3730. (e) Ren, Q.; Guan, S.; Shen, X.; Fang, J. *Organometallics* **2014**, *33*, 1423–1430. (f) Ren, Q.; Wu, N.; Cai, Y.; Fang, J. *Organometallics* **2016**, *35*, 3932–3938. (g) Kneebone, J. L.; Fleischauer, V. E.; Daifuku, S. L.; Shaps, A. A.; Bailey, J. M.; Iannuzzi, T. E.; Neidig, M. L. *Inorg. Chem.* **2016**, *55*, 272–282.
- (27) Frisch, M. J., et al. *Gaussian 09*. Revision D.01; Gaussian, Inc.: Wallingford, CT, 2009.
- (28) *CYLVview, 1.0b*; Legault, C. Y., Université de Sherbrooke, 2009 (<http://www.cylvview.org>).
- (29) Guisán-Ceinos, M.; Tato, F.; Buñuel, E.; Calle, P.; Cárdenas, D. *J. Chem. Sci.* **2013**, *4*, 1098–1104 An alternative possibility is that the 3-coordinate iron(I) species, akin to the observed species by Bedford (reference 8c), is generated from ligand dissociation. However, as a reviewer correctly points out, at present time there is no experimental evidence for formation of either species with this chiral ligand. We are currently pursuing validation of this computational prediction and will report in due course.
- (30) *Essentials of Computational Chemistry: Theories and Models*. Cramer, C. J., Ed.; Wiley: Chichester, England, 2002.
- (31) (a) Egami, H.; Matsumoto, K.; Oguma, T.; Kunisu, T.; Katsuki, T. *J. Am. Chem. Soc.* **2010**, *132*, 13633–13635. (b) Nakamura, M.; Hirai, A.; Nakamura, E. *J. Am. Chem. Soc.* **2000**, *122*, 978–979. (c) Gopalaiah, K. *Chem. Rev.* **2013**, *113*, 3248–3296.
- (32) Houk, K. N.; Cheong, P. H.-Y. *Nature* **2008**, *455*, 309–313.
- (33) As noted by a reviewer, given that the energy differences between the radical addition/dissociation and reductive elimination steps are small, we assessed different functionals including UM06, UM06L, and UPBEPBE. However, only UPBEPBE was able to reproduce the experimental enantioselectivity using a Boltzmann calculation of the 4 lowest energy diastereomeric transition-state structures from the predicted stereodetermining step. Specifically, Boltzmann distribution analysis predicts 91:9 to 98:2 ratio in favor of the experimentally observed S product using the four lowest energy radical addition steps at the UM06L/6-311+G(d,p)-SDD(Fe)-THF(SMD)//UB3LYP/6-31G(d), UM06/6-311+G(d,p)-SDD(Fe)-THF(SMD)//UB3LYP/6-31G(d), and UM06/6-311+G(d,p)-THF(SMD)//UB3LYP/6-31G(d) level. On the other hand, all four methods predict a ca. 30:70 in favor of the opposite R enantiomer using the four lowest diastereomeric reductive elimination transition-state structures (see Supporting Information).
- (34) As a reviewer correctly points out, an alternative pathway involves C-Cl activation by Fe(I)–Cl and is explored by Nakamura and Morokuma (ref 16). However, such scenario will lead to formation of Fe(II)–Cl₂ and alkyl radical. Under slow nucleophile addition, the concentration of PhMgBr is likely to be low and thereby slowing down the rate of transmetalation leading to side reactions of short-lived and highly reactive alkyl radical species. In either case, both pathways will converge at the Fe(II)-Ph-Cl as the active species for the crucial C-C

bond formation event and therefore will not change the overall conclusions of this manuscript.

Cite this: *Chem. Sci.*, 2020, 11, 8301

All publication charges for this article have been paid for by the Royal Society of Chemistry

Fe-catalyzed three-component dicarbofunctionalization of unactivated alkenes with alkyl halides and Grignard reagents†

Lei Liu, , Wes Lee, , Cassandra R. Youshaw, , Mingbin Yuan, , Michael B. Geherty, , Peter Y. Zavalij and Osvaldo Gutierrez *

A highly chemoselective iron-catalyzed three-component dicarbofunctionalization of unactivated olefins with alkyl halides (iodides and bromides) and sp^2 -hybridized Grignard reagents is reported. The reaction operates under fast turnover frequency and tolerates a diverse range of sp^2 -hybridized nucleophiles (electron-rich and electron-deficient (hetero)aryl and alkenyl Grignard reagents), alkyl halides (tertiary alkyl iodides/bromides and perfluorinated bromides), and unactivated olefins bearing diverse functional groups including tethered alkenes, ethers, protected alcohols, aldehydes, and amines to yield the desired 1,2-alkylarylated products with high regiocontrol. Further, we demonstrate that this protocol is amenable for the synthesis of new (hetero)cyclopropanes including tetrahydrofurans and pyrrolidines *via* a three-component radical cascade cyclization/arylation that forges three new C–C bonds.

Received 14th April 2020
Accepted 21st July 2020

DOI: 10.1039/d0sc02127j

rsc.li/chemical-science

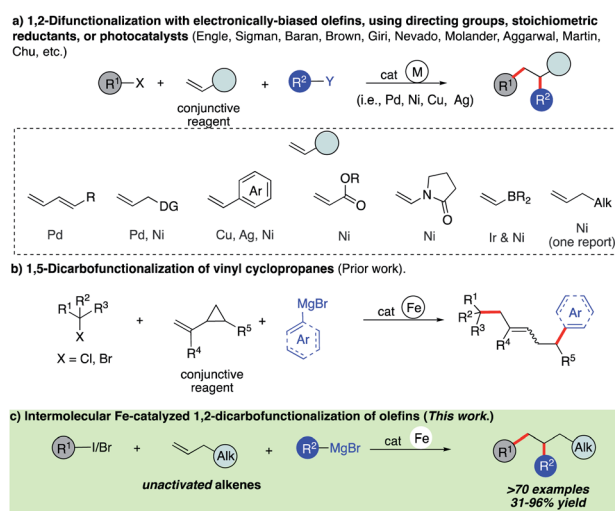
Introduction

Olefins are ubiquitous in natural products and bioactive compounds and serve as versatile commodity feedstocks. 1,2-Difunctionalization of olefins represents one of the most widely used strategies to build synthetic complexity in organic synthesis and serves as a platform to introduce concepts of chemo-, regio-, and stereoselectivity.¹ Recently, there has been a surge in the development of three-component transition metal-catalyzed difunctionalization that employs olefins because of its potential to rapidly increase diversity in a single step (Scheme 1a).^{2–4} However, selective transition metal-catalyzed three-component alkylarylation of *unactivated* alkenes without electronically biased substrates or directing groups is rare.⁵ Moreover, despite the inherent attractive features of iron as a catalyst (Earth abundant, less toxic, inexpensive, and environmentally benign in comparison to Pd or Ni) in pharmaceutical settings, *there are no general methods for iron-catalyzed three-component 1,2-dicarbofunctionalization of olefins.*^{6–13} Recently, our group reported the use of a strained *vinyl cyclopropanes* to promote a three-component Fe-catalyzed reaction leading to *1,5-alkylarylation products* (Scheme 1b).^{14,15} Unfortunately, despite numerous attempts, the 1,2-difunctionalization products were not observed, presumably due to much more

rapid ring-opening of the incipient alkyl radical followed by C–C bond formation. Herein, we report the first iron-catalyzed 3-component dicarbofunctionalization of *unactivated* alkenes with *both alkyl iodides and bromides* with sp^2 -hybridized Grignard nucleophiles leading to 1,2-alkylarylation or 1,2-alkylvinylation of alkenes with broad scope and excellent regio- and chemoselectivity (Scheme 1c). Further, we applied this concept to develop a three-component radical alkylation/cyclization/arylation cascade leading to diverse (hetero)cyclic compounds. We anticipate that this report will lead to greater

Department of Chemistry and Biochemistry, University of Maryland, College Park, Maryland, 20742, USA. E-mail: ogs@umd.edu

† Electronic supplementary information (ESI) available: Synthetic procedures and full characterization of all starting materials and products, spectroscopic data, and computational details. CCDC 1996911. For ESI and crystallographic data in CIF or other electronic format see DOI: 10.1039/d0sc02127j



Scheme 1 Transition metal-catalyzed three-component difunctionalization of olefins.

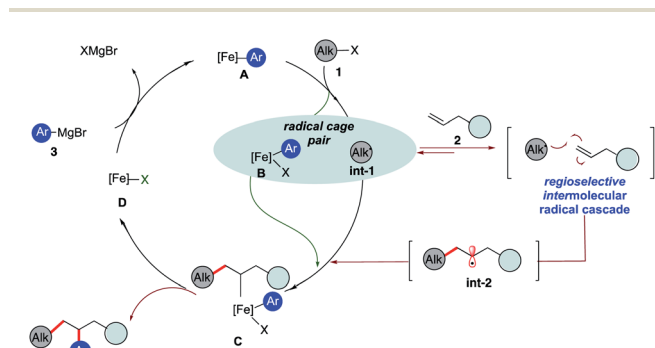
application of Fe as a catalyst in three-component difunctionalization of olefins.

As shown in Scheme 2, we hypothesize that alkyl halide **1** would react with Fe species **A** to form the alkyl radical **int-1** and **B**.^{12,13} Due to the high barrier associated with sterically hindered alkyl radicals and aryl iron **B** to undergo direct cross-coupling, we anticipate that the tertiary radical **int-1** (or a fast reacting alkyl radical) would favor regioselective Giese addition to olefin **2** to form, in the absence of cyclopropyl groups, a transient secondary alkyl radical **int-2**.¹⁶ Then the longer lived (persistent) aryl iron species **B** can trap the less sterically hindered 2° alkyl radical **int-2**, and undergo reductive elimination from **C** to form the desired 1,2-dicarbofunctionalization product and **D**. Finally, facile transmetalation with aryl Grignard **3** restarts the catalytic cycle.¹⁷ Recognizing that the success of the 3-component dicarbofunctionalization hinges on driving the equilibrium towards formation of **int-2**, presumably by favoring Giese addition over addition to aryl iron **B**, we initiated our studies under solvent-free conditions and at high concentrations of alkenes.

The challenge remains whether (a) we can drive the kinetics towards the Giese addition to **2**, (b) **int-2** is sufficiently long-lived to be intercepted by the persistent iron species **B**, and (c) **C** will undergo reductive elimination to form the desired 1,2-dicarbofunctionalization product.

Results and discussion

Initially, we elected to use *tert*-butyl iodide **1**, 4-phenyl-1-butene **2**, and *meta*-methoxy phenyl Grignard **3** as model substrates (Table 1). Gratifyingly, under our modified conditions for radical cross-coupling with vinyl cyclopropanes (*i.e.*, using Fe(acac)₃ as a precatalyst and 1,2-bis(dicyclohexylphosphino)ethane as a ligand),^{14a} we observed the formation of the desired 1,2-alkylaryl product **4** in 86% yield and complete regioselectivity with unactivated olefin **2** (Table 1, entry 1). Notably, other bisphosphine ligands commonly employed in direct Fe-catalyzed cross-coupling reactions with alkyl halides¹⁰ significantly decrease the yield (entries 2–5). Further, the use of the iron precatalyst bearing strongly coordinating ligands inhibits the reaction (entry 6) while other precatalysts were less efficient (entries 7 and 8). Moreover, the use of THF as solvent had



Scheme 2 Proposed pathway to realize the 1,2-dicarbofunctionalization of alkenes using iron catalysis.

Table 1 Evaluation of reaction conditions^a

| Entry | Deviations from above | Yield ^b [%] |
|-------------------|--|------------------------|
| 1 | None | 86 |
| 2 | L2 (20 mol%) | 0 |
| 3 | L3 (20 mol%) | 0 |
| 4 | L4 (20 mol%) | 2 |
| 5 | L5 (20 mol%) | 14 |
| 6 | Using Fe(OAc) ₂ (5 mol%) | <5 |
| 7 | Using FeBr ₂ (5 mol%) | 80 |
| 8 | Using Fe(OTf) ₂ (5 mol%) | 41 |
| 9 ^c | In THF (0.2 mL) | 83 |
| 10 ^{c,d} | Using Fe(acac) ₃ (3 mol%) and L1 (12 mol%) | 90 (85) |
| 11 ^c | No L1 | <5 |
| 12 ^c | No Fe(acac) ₃ and no L1 | 0 |

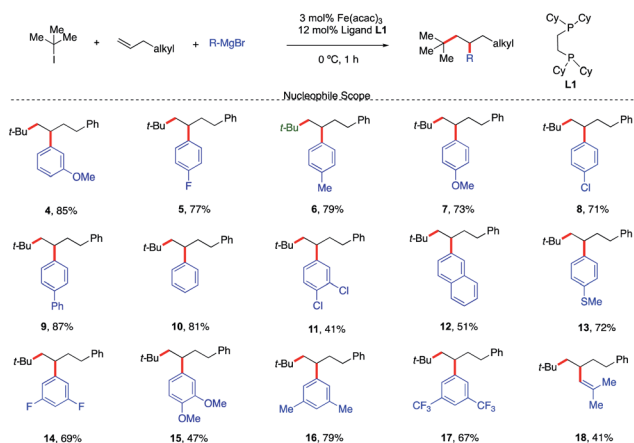
^a The reaction was performed with *tert*-butyl iodide **1** (0.1 mmol, 1.0 equiv.), 4-phenyl-1-butene **2** (14 equiv.; 1–1.3 equiv. based on the recovered starting material; see the ESI) and *meta*-methoxy phenyl Grignard **3** (1.4 equiv.) without any additional solvent. Aryl Grignard **3** was added dropwise *via* a syringe pump over 1 h. ^b The yield was determined by ¹H NMR using dibromomethane as the internal standard. In parentheses is given the isolated yield after column chromatography. ^c 1.5 equiv. of **3**. ^d 0.20 mmol scale.

a minor effect on the overall efficiency of the 3-component 1,2-dicarbofunctionalization (entry 9). Finally, we could also perform the reaction in high yield under lower catalytic loading (entry 10). Control experiments show that the Fe and ligand are both critical for the reaction (entries 11 and 12). For full details of reaction optimization and screening conditions, see the ESI.†

With a set of optimized reaction conditions in hand, an exploration of the reaction scope and limitations of this bisphosphine iron-catalyzed 3-component dicarbofunctionalization was undertaken. As shown in Scheme 3, the reaction tolerated a wide range of electron-rich (*e.g.*, **4**, **6**, **7**, **9**, **12**, **13**, **15**, and **16**) and electron-deficient aryl Grignard nucleophiles (*e.g.*, **5**, **8**, **11**, **14**, and **17**) forming the desired 1,2-alkylaryl products. Further, various substituent positions on the aryl nucleophiles were tolerated including *meta* and *para* mono- and disubstituted aryl Grignard nucleophiles. Importantly, *vinyl* Grignard reagents are also competent nucleophilic partners forming the regioselective 1,2-alkylvinyl product **18** in 41% yield. This represents the first example of transition-metal catalyzed 1,2-alkylvinyl functionalization of unactivated olefins. Unfortunately, sterically hindered Grignard reagents are not compatible reagents in this transformation, presumably due to the high energy required to undergo inner-sphere reductive elimination.^{11,12}

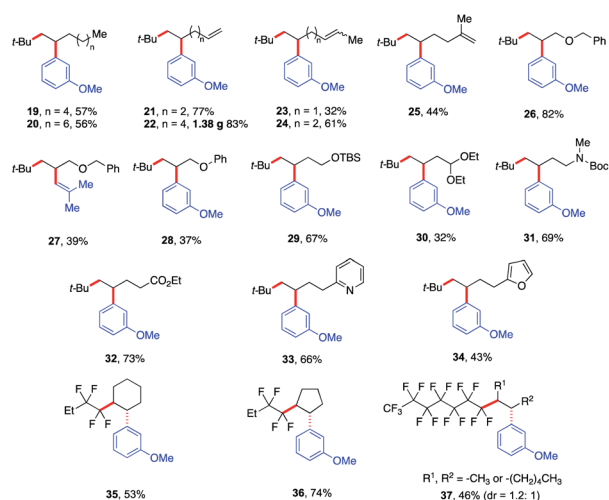
Next, we explored the olefin scope using *tert*-butyl iodide **1** and *meta*-methoxy phenyl Grignard **3** as dicarbofunctionalization partners (Scheme 4). In general, a wide range of





Scheme 3 Scope of the Grignard nucleophile in the 3-component dicarbofunctionalization with unactivated alkenes. Unless otherwise stated, all reactions were performed under the optimized conditions (Table 1, entry 10). Isolated yields.

unactivated olefinic partners were tolerated. Compatible partners include olefins with tethered aliphatic chains, alkenes, alkoxy, protected alcohols, aldehydes and amines, esters, and even pyridine and furan moieties producing the desired products in 32–83% yield (19–34). However, alkenes bearing O- and S-heteroatoms were not compatible with this transformation (see the ESI†). Importantly, this Fe-catalyzed three-component method provides unique reactivity with dienes. In particular, we found that the method is highly chemo- and regioselective for monofunctionalization of less substituted alkenes (23–25) even at lower concentrations of alkenes (see the ESI†). To showcase the practical application of this method, we also scaled up the reaction that formed the monofunctionalized product **22** in 83% yield (1.38 g). Furthermore, we also found that the perfluorinated *n*-alkyl bromides were competent partners with unactivated *cyclic* alkenes (35 and 36) yielding the desired

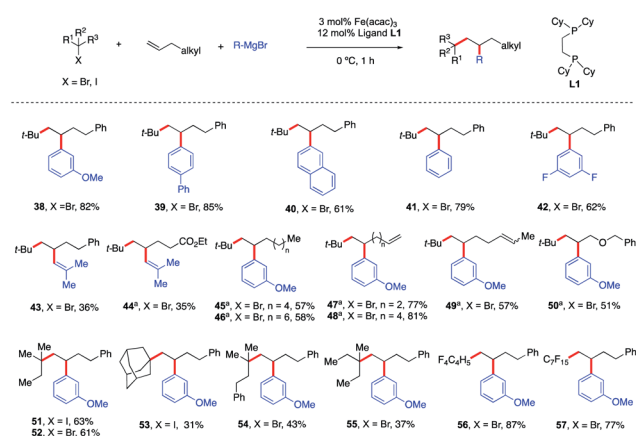


Scheme 4 Scope of alkenes in the reaction. Unless otherwise stated, all reactions were performed under the optimized conditions (Table 1, entry 10) in THF (0.2 mL). Isolated yields.

products as single diastereoisomers in 53–74% yield. For aliphatic chain internal alkene (37) using the perfluorated *n*-alkyl radical, we obtained the desired products as a mixture of diastereomers (dr = 1.2 : 1; see the ESI†) in 46% yield.

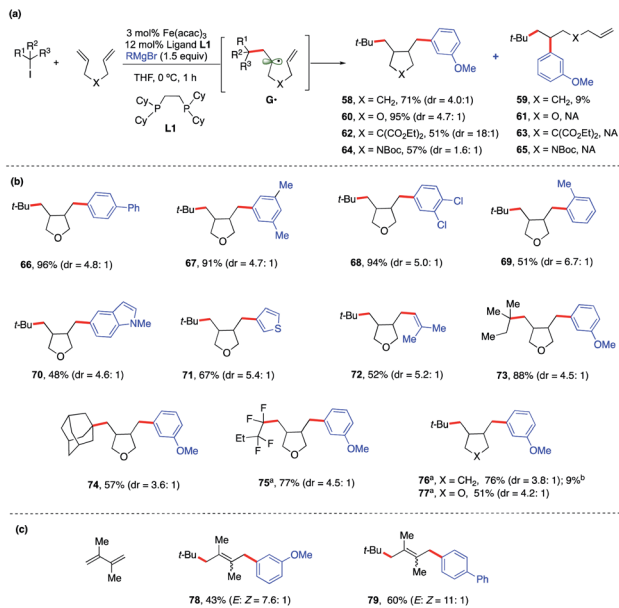
As shown in Scheme 5, contrary to current state-of-the-art TM-catalyzed three-component dicarbofunctionalization, this method tolerates a range of diverse radical precursors and operates under short reaction times and at low temperatures. Specifically, tertiary alkyl bromides also form the desired 1,2-alkylaryl products **38–50** with similar efficiency to alkyl iodides. These results represent the first examples of using alkyl bromides in a transition metal-catalyzed 3-component intermolecular 1,2-alkylarylation of unactivated olefins and can complement existing methods using reductive cross-couplings as reported by Nevado.⁵ Furthermore, other tertiary alkyl iodides/bromides are compatible in this transformation yielding the desired products **51–55** in 31–63% yield. Finally, consistent with our hypothesis (Scheme 2), we also found that perfluorinated *n*-alkyl radicals (much more reactive towards Giese addition to alkenes)¹⁸ were competent in this Fe-catalyzed three-component dicarbofunctionalization reaction yielding the desired products **56–57** in 77–87% yield. Unfortunately, other primary and secondary alkyl halides are not compatible in this transformation due to the competing direct cross-coupling formation (see the ESI†).

To expand the synthetic utility of this Fe-catalyzed three-component dicarbofunctionalization, we next explored the possibility of performing a radical cascade cyclization/arylation with a series of 1,6-dienes leading to the formation of *three carbon-carbon bonds in one synthetic step* (Scheme 6a). We hypothesize that regioselective Giese addition to the olefin will form the secondary alkyl radical intermediate **G•**. If the rates of Fe-arylation are slower than the rate of ring-closure, then we should only observe the ring-closed arylated product (*i.e.*, **58**). However, if the rate for Fe-arylation of **G•** is faster than the rate for Fe-arylation of radical 5-*exo*-trig, then we should observe only the uncyclized product (*i.e.*, **59**). As shown in Scheme 6a, we found that this method delivered the desired carbocycle **58** in



Scheme 5 Scope of alkenes in the reaction. Unless otherwise stated, all reactions were performed under the optimized conditions (Table 1, entry 10). Isolated yields. (a) THF (0.2 mL).





Scheme 6 Scope and energetics for radical cascade cyclization/arylation. Unless otherwise stated, all reactions were performed under the optimized conditions (Table 1, entry 10) in THF (0.2 mL). Isolated yield. (a) Alkyl bromides. (b) Yield of the acyclic/arylation product.

good yield (71%). We also observed the uncyclized product **59**, presumably from direct arylation of G^\bullet , albeit in low yield (9%).

Notably, incorporation of heteroatoms (O or N) or addition of diester linkage results in exclusive formation of the cyclic product. Specifically, we found the desired formation of alkylaryl tetrahydrofuran **60**, di-ester substituted carbocycle **62**, and pyrrolidine **64** in good to excellent yield (51–95%) and without the formation of the uncyclized product. DFT calculations [UPBEPBE-D3/6-311+G(d,p)-CPCM(THF)//UB3LYP/6-31G(d)] using the *t*Bu radical and 1,6-heptadiene predict a barrier of 13.2 kcal mol⁻¹ for irreversible Giese addition leading to G^\bullet , 5.2 kcal mol⁻¹ downhill in energy. In agreement with the experiment, G^\bullet preferentially favors radical cyclization leading to a *cis* isomer, while (irreversible) radical cyclization leading to a *trans* isomer is only 1.2 kcal mol⁻¹ higher in energy. However, consistent with the experiment, the rates for radical cyclization for X=O substituted diene are faster and the energy difference between *cis* and *trans* radical cyclization is much higher (1.7 kcal mol; see the ESI[†]). However, at this stage, we cannot rule out alternative mechanistic pathways such as olefin coordination to the metal center preceding alkyl radical addition or 1,2-migratory insertion of the iron-aryl into the alkene. Future work on elucidating the mechanism of this transformation is ongoing and will be reported in due course. Given the prevalence of saturated heterocyclic compounds (tetrahydrofurans and pyrrolidines) in pharmaceuticals, we used an oxygen-substituted diene as a model compound to explore the reaction scope of this Fe-catalyzed three-component radical cascade cyclization/arylation (Scheme 6b). As shown in Scheme 6b, this reaction is very robust with aryl Grignard nucleophiles forming the desired products in excellent yields, and the *cis*-isomer is the major product (as determined by ¹H NMR and *via* crystal

structure determination of **66**; see the ESI[†]). The use of sterically hindered, heteroaryl or *vinyl* nucleophiles was also tolerated (**69**–**72**). Moreover, other tertiary alkyl iodides and perfluorinated alkyl and tertiary bromides also work in this transformation forming the radical cascade cyclization/arylation products **73**–**77** in 51–88% yield. Finally, the method is regioselective for addition to conjugated 1,3-diene to form 1,4-alkylarylation products **78**–**79** in good yield (up to 11 : 1 *E* : *Z*, Scheme 6c).

Conclusions

In summary, we have developed a three-component 1,2-alkylarylation of unactivated olefins using bisphosphine iron as the catalyst. Further, we demonstrated that this protocol can forge three carbon–carbon bonds in one synthetic step leading to a diverse set of carbo- and heterocyclic compounds. We expect that this method will be adapted by the pharmaceutical community for the synthesis of bioactive products, fine chemicals, and late-stage diversification of promising leads. Although this method is currently limited to the use of a large excess of olefins, preliminary experiments show that the use of activated alkenes could circumvent the need for excess alkenes, and this will be reported in due course. Future work is ongoing to elucidate the mechanism of this transformation using computational, experimental, and spectroscopic tools. We are actively pursuing other three-component Fe-catalyzed reactions with other π -acceptors, nucleophiles, and electrophiles including asymmetric variants and will report in due course.

Conflicts of interest

There are no conflicts to declare.

Acknowledgements

This research was supported by the NSF (CAREER 1751568) and by the NIGMS of the NIH (R35GM137797). The content is solely the responsibility of the authors and does not necessarily represent the official views of the NIH. A provisional patent application has been submitted by the University of Maryland for this reaction, with L.L., W.L., and O.G. as inventors. We are grateful to the University of Maryland College Park for start-up funds and computational resources from UMD Deepthought2 and MARCC/BlueCrab HPC clusters and XSEDE (CHE160082 and CHE160053).

References

- For representative reviews on alkene functionalization, see: (a) V. Saini, B. J. Stokes and M. S. Sigman, *Angew. Chem., Int. Ed.*, 2013, **52**, 11206; (b) J. R. Coombs and J. P. Morken, *Angew. Chem., Int. Ed.*, 2016, **55**, 2636.
- For representative reviews on dicarbofunctionalization of alkenes, see: (a) J. Derosa, V. T. Tran, V. A. van der Puy and K. M. Engle, *Aldrichimica Acta*, 2018, **51**, 21; (b) R. Giri and S. KC, *J. Org. Chem.*, 2018, **83**, 3013.



- 3 For some examples leading to dicarbofunctionalization of alkenes, see: (a) L. Liao, R. Jana, K. B. Urkalan and M. S. Sigman, *J. Am. Chem. Soc.*, 2011, **133**, 5784; (b) T. Qin, J. Cornella, C. Li, L. R. Malins, J. T. Edwards, S. Kawamura, B. D. Maxwell, M. D. Eastgate and P. S. Baran, *Science*, 2016, **352**, 801; (c) A. García-Domínguez, Z. Li and C. Nevado, *J. Am. Chem. Soc.*, 2017, **139**, 6835; (d) S. Kc, R. K. Dhungana, B. Shrestha, S. Thapa, N. Khanal, P. Basnet, R. W. Lebrun and R. Giri, *J. Am. Chem. Soc.*, 2018, **140**, 9801; (e) P. Gao, L.-A. Chen and M. K. Brown, *J. Am. Chem. Soc.*, 2018, **140**, 10653; (f) M. Chierchia, P. Xu, G. J. Lovinger and J. P. Morken, *Angew. Chem., Int. Ed.*, 2019, **58**, 14245; (g) M. W. Campbell, J. S. Compton, C. B. Kelly and G. A. Molander, *J. Am. Chem. Soc.*, 2019, **141**, 20069; (h) R. S. Mega, V. K. Duong, A. Noble and V. K. Aggarwal, *Angew. Chem., Int. Ed.*, 2020, **59**, 4375; (i) S.-Z. Sun, Y. Duan, R. S. Mega, R. J. Somerville and R. Martin, *Angew. Chem., Int. Ed.*, 2020, **59**, 4370; (j) S. KC, R. K. Dhungana, N. Khanal and R. Giri, *Angew. Chem., Int. Ed.*, 2020, **59**, 8047.
- 4 For recent examples using directing groups, see: (a) J. Derosa, T. Kang, V. T. Tran, S. R. Wisniewski, M. K. Karunananda, T. C. Jenkins, K. L. Xu and K. M. Engle, *Angew. Chem., Int. Ed.*, 2020, **59**, 1201; (b) Y. Tao, X. Chen, W. Rao and M. J. Koh, *Chem*, 2020, **6**, 738.
- 5 W. Shu, A. García-Domínguez, M. T. Quirós, R. Mondal, D. J. Cárdenas and C. Nevado, *J. Am. Chem. Soc.*, 2019, **141**, 13812.
- 6 For a recent review, see: A. Piontek, E. Bisz and M. Szostak, *Angew. Chem., Int. Ed.*, 2018, **57**, 11116.
- 7 (a) C.-L. Sun, H. Krause and A. Fürstner, *Adv. Synth. Catal.*, 2014, **356**, 1281; (b) T. Hatakeyama, Y. Okada, Y. Yoshimoto and M. Nakamura, *Angew. Chem., Int. Ed.*, 2011, **50**, 10973; (c) K. G. Dongol, H. Koh, M. Sau and C. L. L. Chai, *Adv. Synth. Catal.*, 2007, **349**, 1015.
- 8 (a) F. Toriyama, J. Cornella, L. Wimmer, T.-G. Chen, D. D. Dixon, G. Creech and P. S. Baran, *J. Am. Chem. Soc.*, 2016, **138**, 11132; (b) J. C. Lo, D. Kim, C.-M. Pan, J. T. Edwards, Y. Yabe, J. Gui, T. Qin, S. Gutiérrez, J. Giacoboni, M. W. Smith, P. L. Holland and P. S. Baran, *J. Am. Chem. Soc.*, 2017, **139**, 2484; (c) R. B. Bedford, E. Carter, P. M. Cogswell, N. J. Gower, M. F. Haddow, J. N. Harvey, D. M. Murphy, E. C. Neeve and J. Nunn, *Angew. Chem., Int. Ed.*, 2013, **52**, 1285; (d) C. J. Adams, R. B. Bedford, E. Carter, N. J. Gower, M. F. Haddow, J. N. Harvey, M. Huwe, M. A. Cartes, S. M. Mansell, C. Mendoza, D. M. Murphy, E. C. Neeve and J. Nunn, *J. Am. Chem. Soc.*, 2012, **134**, 10333; (e) T. Hatakeyama, Y. Kondo, Y. Fujiwara, H. Takaya, S. Ito, E. Nakamura and M. Nakamura, *Chem. Commun.*, 2009, 1216; (f) R. B. Bedford, M. Huwe and M. C. Wilkinson, *Chem. Commun.*, 2009, 600.
- 9 (a) N. Nakagawa, T. Hatakeyama and M. Nakamura, *Chem. Lett.*, 2015, **44**, 486; (b) T. Hatakeyama, T. Hashimoto, K. K. A. D. S. Kathriarachchi, T. Zenmyo, H. Seike and M. Nakamura, *Angew. Chem., Int. Ed.*, 2012, **51**, 8834; (c) T. Hashimoto, T. Hatakeyama and M. Nakamura, *J. Org. Chem.*, 2011, **77**, 1168; (d) T. Hatakeyama, T. Hashimoto, Y. Kondo, Y. Fujiwara, H. Seike, H. Takaya, Y. Tamada, T. Ono and M. Nakamura, *J. Am. Chem. Soc.*, 2010, **132**, 10674.
- 10 T. L. Mako and J. A. Byers, *Inorg. Chem. Front.*, 2016, **3**, 766.
- 11 M. Jin, L. Adak and M. Nakamura, *J. Am. Chem. Soc.*, 2015, **137**, 7128.
- 12 W. Lee, J. Zhou and O. Gutierrez, *J. Am. Chem. Soc.*, 2017, **139**, 16126.
- 13 A. K. Sharma, W. M. C. Sameera, M. Jin, L. Adak, C. Okuzono, T. Iwamoto, M. Kato, M. Nakamura and K. Morokuma, *J. Am. Chem. Soc.*, 2017, **139**, 16117.
- 14 (a) L. Liu, W. Lee, M. Yuan, C. Acha, M. B. Geherty, B. Williams, O. Gutierrez, *Chem. Sci.*, 2020, **11**, 3146. A previous version of this manuscript was deposited on a preprint server ChemRxiv, DOI: 10.26434/chemrxiv.9858500.v1; (b) L. Liu, W. Lee, J. Zhou, S. Bandyopadhyay and O. Gutierrez, *Tetrahedron*, 2019, **75**, 129.
- 15 Z.-Q. Zhang, X.-Y. Meng, J. Sheng, Q. Lan and X.-S. Wang, *Org. Lett.*, 2019, **21**, 8256.
- 16 D. Leifert and A. Studer, *Angew. Chem., Int. Ed.*, 2020, **59**, 74.
- 17 (a) M. L. Neidig, S. H. Carpenter, D. J. Curran, J. C. DeMuth, V. E. Fleischauer, T. E. Iannuzzi, P. G. N. Neate, J. D. Sears and N. J. Wolford, *Acc. Chem. Res.*, 2019, **52**, 140; (b) J. D. Sears, P. G. N. Neate and M. L. Neidig, *J. Am. Chem. Soc.*, 2018, **140**, 11872; (c) L. Liu, W. Lee, M. Yuan and O. Gutierrez, *Comments Inorg. Chem.*, 2018, **38**, 210.
- 18 D. V. Avila, K. U. Ingold, J. Luszyk, W. R. Dolbier and H. Q. Pan, *J. Am. Chem. Soc.*, 1993, **115**, 1577.

